

Lawrence Berkeley National Laboratory

Lawrence Berkeley National Laboratory

Title

TENSI-VOLUMETRIC STUDIES OF CaO-CO₂ -CaCO₃ SYSTEM

Permalink

<https://escholarship.org/uc/item/2c74x73z>

Author

Shukla, Rama Kant

Publication Date

1979-12-01



Lawrence Berkeley Laboratory

UNIVERSITY OF CALIFORNIA

Materials & Molecular Research Division

TENSI-VOLUMETRIC STUDIES OF $\text{CaO-CO}_2\text{-CaCO}_3$ SYSTEM

Rama Kant Shukla
(Ph.D. thesis)

December 1979

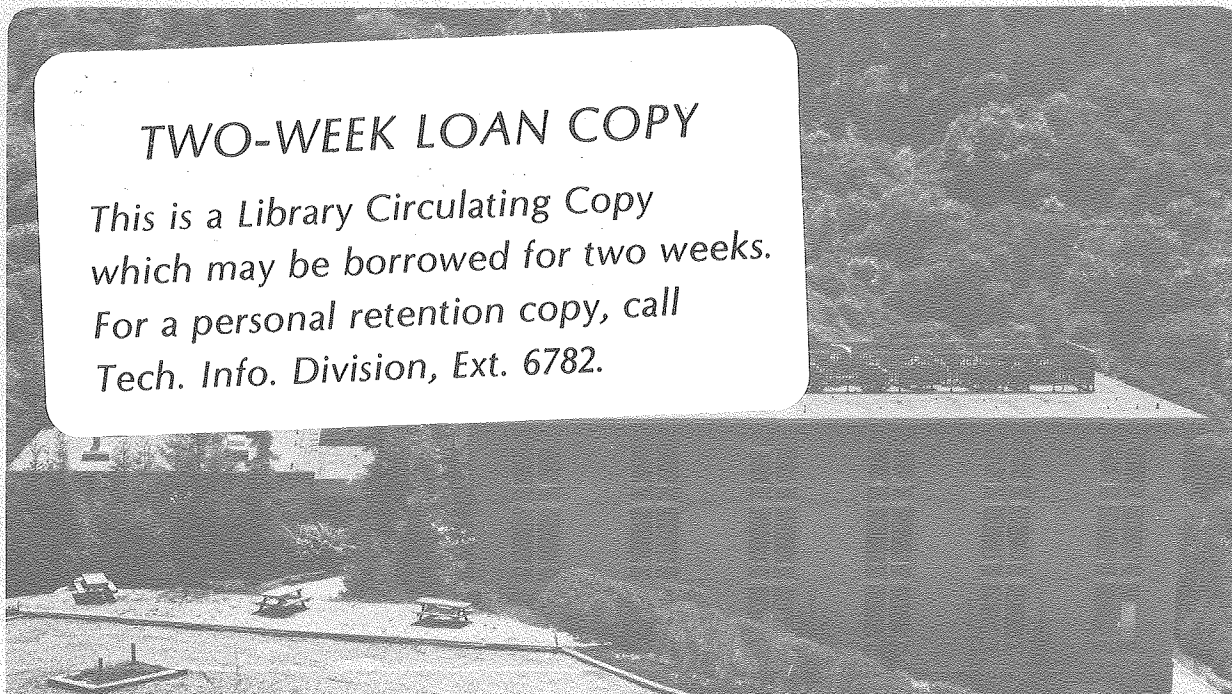
RECEIVED
LAWRENCE
BERKELEY LABORATORY

FEB 25 1980

LIBRARY AND
DOCUMENTS SECTION

TWO-WEEK LOAN COPY

*This is a Library Circulating Copy
which may be borrowed for two weeks.
For a personal retention copy, call
Tech. Info. Division, Ext. 6782.*



DISCLAIMER

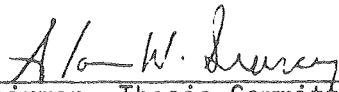
This document was prepared as an account of work sponsored by the United States Government. While this document is believed to contain correct information, neither the United States Government nor any agency thereof, nor the Regents of the University of California, nor any of their employees, makes any warranty, express or implied, or assumes any legal responsibility for the accuracy, completeness, or usefulness of any information, apparatus, product, or process disclosed, or represents that its use would not infringe privately owned rights. Reference herein to any specific commercial product, process, or service by its trade name, trademark, manufacturer, or otherwise, does not necessarily constitute or imply its endorsement, recommendation, or favoring by the United States Government or any agency thereof, or the Regents of the University of California. The views and opinions of authors expressed herein do not necessarily state or reflect those of the United States Government or any agency thereof or the Regents of the University of California.

TENSI-VOLUMETRIC STUDIES OF THE CaO-CaCO₃ SYSTEM

Rama Kant Shukla

Degree: Doctor of Philosophy
in Engineering

Major Department: Materials
Science and Mineral Engineering


Chairman, Thesis Committee

ABSTRACT

A tensi-volumetric apparatus was developed and used to study two aspects of the CaO-CO₂-CaCO₃ system, namely the thermodynamics of the CaCO₃ (calcite) phase viewed as a pseudo-binary solid solution of CaO and CO₂, and the kinetics of decomposition of CaCO₃ (calcite).

The solubility of CO₂ in the calcite (CaCO₃) phase was studied as a function of pressure and temperature. It is shown that it is possible to obtain calcite of substoichiometric compositions expressed by [CaO·(CO₂)_{1-δ}], where at the temperatures of measurement, 773°K to 1000°K, δ is a small, but measurable quantity. The composition limits of this phase increase rapidly with temperature. The extrapolated value of δ at the CaO-CaCO₃ eutectic temperature is 0.42. The defects responsible for nonstoichiometry in CaCO₃ probably are substitutional O²⁻ ions on the CO₃²⁻ sublattice. Partial molal quantities calculated for CaO and CO₂ in the calcite phase are $\Delta H_{CO_2} = -76.5 \text{ K cal mol}^{-1}$, $\Delta H_{CaO} = +35.6 \text{ K cal mol}^{-1}$, $\Delta S_{CO_2} = -56.8 \text{ eu mol}^{-1}$ and $\Delta S_{CaO} = 2.18 \text{ eu mol}^{-1}$. It was also shown that CaCO₃ forms a stable monolayer of O²⁻ ions on CO₃²⁻ surface sites as chemisorbed species prior to the decomposition.

Calcite decomposition rates were measured in the range of P/p_{eq} from 0.05 to about 0.8 and in the temperature range of 853° to 933°K. The

decomposition rate changed by about three orders of magnitude in this range of P/p_{eq} at every temperature of study. Decomposition rates of calcite powder depend on particle size, powder bed depth and compactness of samples. Measurements with single crystals of calcite suggest that at least two different processes limit the decomposition rate in different P/p_{eq} regimes. The apparent activation enthalpy, ΔH^* , for decomposition at $P/p_{eq} = 0.1$, calculated in terms of decomposition fluxes, is about 49.2 ± 1.2 K cal s mole $^{-1}$. At values of P/p_{eq} near unity, the value of ΔH^* rose to about 61.8 ± 1.8 K cal s mole $^{-1}$.

Decomposition rates for powders did not show a consistent apparent activation enthalpy over the range of P/p_{eq} studied; they varied between 65 and 80 K cal s mole $^{-1}$.

TENSI-VOLUMETRIC STUDIES OF THE CaO-CaCO₃ SYSTEM

contents

ABSTRACT	1
GENERAL INTRODUCTION	3
PART I: Solution Chemistry of CO ₂ in CaCO ₃	4
1. Introduction	4
2. Experimental	11
3. Results	31
4. Discussion	31
5. Conclusion	54
References	56
Tables	58
Appendices	61
Figure Captions	72
Figures	74
PART II: Decomposition Kinetics of Calcite	106
1. Introduction	106
2. Experimental	109
3. Results	113
4. Discussion	113
5. Conclusion	121
References	122
Figure Captions	123
Figures	125
ACKNOWLEDGMENT	144

TENSI-VOLUMETRIC STUDIES OF THE CaCO_3 - CaO - CO_2 SYSTEM

Rama K. Shukla

Materials and Molecular Research Division, Lawrence Berkeley Laboratory
and Department of Materials Science and Mineral Engineering,
University of California, Berkeley, California 94720

ABSTRACT

A tensi-volumetric apparatus was developed and used to study two aspects of the CaO - CO_2 - CaCO_3 system, namely the thermodynamics of the CaCO_3 (calcite) phase viewed as a pseudo-binary solid solution of CaO and CO_2 , and the kinetics of decomposition of CaCO_3 (calcite).

The solubility of CO_2 in the calcite (CaCO_3) phase was studied as a function of pressure and temperature. It is shown that it is possible to obtain calcite of substoichiometric compositions expressed by $[\text{CaO} \cdot (\text{CO}_2)_{1-\delta}]$, where at the temperatures of measurement, 773°K to 1000°K, δ is a small, but measurable quantity. The composition limits of this phase increase rapidly with temperature. The extrapolated value of δ at the CaO - CaCO_3 eutectic temperature is 0.42. The defects responsible for nonstoichiometry in CaCO_3 probably are substitutional O^{--} ions on the CO_3^{--} sublattice. Partial molal quantities calculated for CaO and CO_2 in the calcite phase are $\Delta H_{\text{CO}_2} = -76.5 \text{ K cal mol}^{-1}$, $\Delta H_{\text{CaO}} = +35.6 \text{ K cal mol}^{-1}$, $\Delta S_{\text{CO}_2} = -56.8 \text{ eu mol}^{-1}$ and $\Delta S_{\text{CaO}} = 21.8 \text{ eu mol}^{-1}$. It was also shown that CaCO_3 forms a stable monolayer of O^{--} ions on CO_3^{--} surface sites as chemisorbed species prior to the decomposition.

Calcite decomposition rates were measured in the range of P/P_{eq} from 0.05 to about 0.8 and in the temperature range of 853° to 933°K. The decomposition rate changed by about three orders of magnitude in this range of P/P_{eq} at every temperature of study. Decomposition rates of

calcite powder depend on particle size, powder bed depth and compactness of samples. Measurements with single crystals of calcite suggest that at least two different processes limit the decomposition rate in different P/p_{eq} regimes. The apparent activation enthalpy, ΔH^* , for decomposition at $P/p_{\text{eq}} \leq 0.1$, calculated in terms of decomposition fluxes, is about 49.2 ± 1.2 K cal s mole $^{-1}$. At values of P/p_{eq} near unity, the value of ΔH^* rose to about 61.8 ± 1.8 K cal s mole $^{-1}$.

Decomposition rates for powders did not show a consistent apparent activation enthalpy over the range of P/p_{eq} studied; they varied between 65 and 80 K cal s mole $^{-1}$.

GENERAL INTRODUCTION

Nonstoichiometry in binary inorganic solids has been well recognized in the past. It is acknowledged that the defects, which result from composition variation, play a vital role in determining various thermodynamic and kinetic properties of solid state reactions. However, a large number of binary inorganic phases are still implicitly treated as perfectly stoichiometric when the concentration of defects leading to nonstoichiometry is too small to measure experimentally.

Calcite (CaCO_3) is one example of a class of solids usually considered to be stoichiometric for all practical purposes. It seemed worthwhile to investigate whether, in fact, CaCO_3 (and by analogy, similar solids) may show measureable deviations from stoichiometry, especially at high temperatures.

A tensi-volumetric apparatus of high sensitivity is described in Part I of this thesis. This apparatus has been used to measure deviations from stoichiometry in calcite as small as 50 ppm.

During this study, it became apparent that the tensi-volumetric apparatus is also well suited for studying the effect of pressure of CO_2 on the decomposition rates of CaCO_3 . Such a kinetic study is extremely desirable since there exist at least three theories which predict different effects of pressure of CO_2 on the decomposition rates. A program to study this issue forms the subject of Part II of this thesis.

PART I

THE SOLUTION CHEMISTRY OF CO_2 IN CaCO_3 (CALCITE)

I. INTRODUCTION

It is not possible to define thermodynamically a distinction between a compound and a binary or multicomponent phase of narrow chemical composition limits. Indeed, Swalin¹ writes in his book; "There is nothing sacred in nature, contrary to the popular belief, about the need for stoichiometry." This becomes more evident on examination of phase diagrams. Thus, the definition of "stoichiometric line phase" is an operational one, which depends upon the measurability of the compositional changes within a phase under given experimental conditions.

For most phases which have small, but measurable composition ranges, the integral values of thermodynamic quantities, e.g., ΔH_f^0 , ΔG_f^0 , etc., are insensitive to exact compositions. In contrast, the partial molal thermodynamic quantities may change by many orders of magnitude over a narrow composition range. In particular, the activities of the components of a phase of narrow composition limits are usually strongly dependent on composition, and a study of the composition dependence of thermodynamic properties of such phases often involves measurement of activities as a function of composition.

Deviations from the ideal stoichiometric composition of a crystal are possible only if lattice defects are present. In a state of internal thermodynamic equilibrium, point defects are decisive. The maximum concentrations of point defects, and therefore the direction and degree of nonstoichiometry, are not an exclusive property of a given phase, but

also depend upon the thermodynamic activities of external phases in equilibrium with the nonstoichiometric compound.

The limits to the stable phase field can be best discussed with the aid of Gibbs free energy, G versus composition, X , diagrams, at constant temperature. Such a diagram is illustrated by the schematic plot in Fig. 1.

For the sake of simplicity, only three phases are considered, namely, two 'end phases' being dilute A in B and vice versa, and an intermediate phase AB of approximately equal mole fractions of A and B. The fundamental criterion for equilibrium between two phases at constant temperature and pressure (equality of chemical potential for each component in the coexisting phases) is met if a simultaneous tangent can be drawn to the free energy values of phases.²

The points of tangency determine the compositions of the coexisting phases and place a limit on the composition change possible within each phase. Thus, in Fig. 1, phase AB is stable between the composition limits defined by the two points of tangency of the curve of G for the AB phase with the curves of G for the two end phases. It is evident from this figure that the extent of nonstoichiometry is related to the (1) shape of $G(X)$ and (2) the relative positions of $G(X)$ for various competing phases. Only if the extent of solution of A in B and of B in A are negligible is the extent of nonstoichiometry in AB dependent only upon the variation of G with X for AB. Then a narrow, steep $G(X)$ curve shows that the stoichiometric phase must form with a narrow composition range. A wide, weakly sloping $G(X)$ curve indicates a large composition range (Fig. 2). Most of ordered solid phases show strong dependence of G on X ,

while for liquids and disordered alloys, G commonly varies slowly with X .

The occurrence of nonstoichiometry in binary solid phases has been a field of considerable interest in recent years. Deviations from stoichiometry ranging from parts per thousand to several atomic per cent have been measured for a large variety of binary solid phases, as discussed in the encyclopedic book by F. A. Kroger.³ However, almost all the phases studied belong to the type A_xB_y where A and B are elemental components. But systems of more than two elements can often also be treated as binary phases of type A_xB_y . In fact, the choice of components is limited only to the extent that the components can be defined so that measurement of their chemical potentials are experimentally possible.

For calcite (CaCO_3), which decomposes to give $\text{CaO}(s)$ and $\text{CO}_2(g)$, the choice of two components can be $A \equiv \text{CaO}$ and $B \equiv \text{CO}_2$. Thus, CaCO_3 can be viewed as a pseudo-binary solid solution of components CaO and CO_2 , i.e., thermodynamically, we can write



From the arguments outlined previously regarding the necessity of nonstoichiometry at all temperatures above absolute zero, one finds that $\text{CaO} \cdot \text{CO}_2$ must be described as $\text{CaO} \cdot (\text{CO}_2)_{1 \pm \delta}$, where δ may be very small compared to 1.

The nature of point defects responsible for deviations from stoichiometry is not known a priori and can only be deduced from experiments. However, the thermodynamic description of the $\text{CaO} \cdot \text{CO}_2$ solid solution can be obtained without reference to the nature of its defects. Thus, if one applies the Gibbs free energy-composition diagram approach

to this system (Fig. 3), we find that negative deviations from stoichiometry ($\text{CaO} \cdot (\text{CO}_2)_{1+\delta}$ where $\delta < 0$) is limited by the appearance of $\text{CaO}(s)$ as the competing phase (neglecting any solubility of CO_2 in the CaO end phase).

The effect of the change in pressure from 1 atm to $P_{\text{eq}}(\text{CO}_2)$ on the activity of $\text{CaO}(s)$ can be neglected. The partial pressure of CaO and its decomposition products $\text{Ca}(g) + \frac{1}{2} \text{O}_2(g)$ are very low, and the $\text{CaO} \cdot (\text{CO}_2)_{1+\delta}$ phase field limit on the CO_2 -rich side ($\delta > 0$) is fixed by the composition that equilibrates with the highest CO_2 pressure imposed in the apparatus, so long as the critical pressure of CO_2 is not exceeded.

In recent years, the effect of temperature on the composition for congruent vaporization of binary solids has been investigated,⁴ and significant departures from stoichiometry have been found. Similar arguments show that the composition of calcium carbonate for incongruent vaporization (i.e., decomposition) may change with temperature and may be significantly different from the ideal stoichiometry. This fact has been generally neglected in the decomposition studies of CaCO_3 and similar systems. It seems worthwhile to determine whether the change in stoichiometry of the CaO -rich boundary of the $\text{CaO} \cdot (\text{CO}_2)_{1+\delta}$ phase with temperature in fact, does or does not measurably influence the properties measured for calcite.

Such information seems not to have been measured, as yet, for salts of complex ions. Searcy and Meschi⁵ have shown that small departures from stoichiometry of certain metallic hydrides can lead to significant error in calculation of integral free energies, enthalpies and entropies. Furthermore, they were able to calculate the partial molal free energies,

heats and entropies of components as a function of composition from the dissociation pressure data measured as a function of composition in the single phase region. A similar approach has been used in this work to estimate thermodynamic data for the CaO-CO₂ pseudo-binary system.

Besides the purely academic interest in the nonstoichiometric CaCO₃, this study was further motivated by the following findings: (i) Decomposition of CaCO₃ in vacuum at high temperatures has been reported to lead to less than 100% of the stoichiometric weight loss, the discrepancy being as high as ~0.5% at 700°C.⁶ (ii) The CaO-CaCO₃ system has been reported to form a eutectic (of poorly defined composition) at ~1250°C.^{7,8} This circumstance suggests the possibility of high solubilities of CaCO₃ in CaO and CaO in CaCO₃ at high temperatures. (iii) CaCO₃ has been reported⁹ to give off significant amounts of CO₂ *prior* to its decomposition to CaO. Similar 'degassing' is a widely encountered phenomenon in decomposition reactions, but has been inadequately studied.¹⁰

The only known previous investigations of solubility relationships in the CaO-CO₂ system is due to Tumarev¹¹ and Zavriev.¹² Baikov and Tumarev reported, from kinetic studies, up to 2.4% solubility of CaO in CaCO₃ at 900°C, but they point out the probable inaccuracy in their data. Later study by Chuchmarev, et al.¹³ using x-ray precision lattice parameter determinations proved inconclusive. On the other hand, careful gravimetric analysis of calcite crystals by Maier and Anderson¹⁴ showed the composition to be stoichiometric within the limits of experimental accuracy, which was about 0.01%. It thus remained to be established if the deviations from stoichiometry are measurable at all at higher temperatures.

The experimental study of nonstoichiometry involves two key steps: (i) Measurement of absolute composition, and (ii) the effect of pressure and temperature on the composition. The former information requires a careful chemical analysis. The accuracy with which CaO/CO_2 ratios can be measured appears to be at best 0.01%. In such a case, the concentration of the defects, and hence smaller departures from stoichiometry have to be studied by evaluating the results of a physical measurement such as of the electrical conductivity, Seebeck effect, Hall effect, magnetic susceptibility, or variations in optical absorption. All of these measurements require a theoretical model to correlate the physical property being measured with the composition changes and are, therefore, restricted in their general applicability.

Thermogravimetric, electrochemical and tensi-volumetric methods yield activities as functions of composition. The electrochemical method requires setting up a cell with properly defined electrodes, which is difficult to do for CaCO_3 . For a study of CaCO_3 , therefore, a gravimetric or tensi-volumetric method should be most suitable. After a careful evaluation of the precision and accuracy (to be discussed later) of the two methods, the tensi-volumetric method was chosen for this study.

This method gives directly the change in composition with changes in the pressure and temperature of the sample. The method has been successfully employed to obtain data on various metallic oxides^{15,16} and hydrides.¹⁷

The tensi-volumetric measurements involve use of a manometer, a gas burette or calibrated gas reservoir, a temperature controlled environment and a gas analyzer for partial pressures analysis. This method is

especially suited for study of deviations from stoichiometry in the CaO·CO₂ phase, because it has only one component (CO₂) which has a significant partial pressure. Measurements of the pressure of CO₂ establish its activity in calcite and measurements of the changes in the pressure and volume of CO₂ determine variations in composition of the calcite phase.

Partial molal free energies, enthalpies and entropies have been ascertained from the pressure-volume measurements and the nature of defect responsible for deviations from stoichiometry has been postulated. The extreme diverse conditions for formation of calcite in various mineralogical sources suggests that the compositions may reflect the mineralogical history. Therefore, additional measurements have been made on some geological specimen of calcite to establish their CO₂ content and implications to the conditions for calcite formation in nature have been discussed.

II. EXPERIMENTAL

1. Apparatus

Figure 4 shows the layout of the apparatus for the tensi-volumetric measurements. The overall apparatus includes a manometer, gas burette, furnace with temperature sensors, mass spectrometer and vacuum line assembly. In the initial experimental set up, the sample was heated in a quartz tube, mounted horizontally in the furnace, and cooled at the two ends by water jackets between two viton 'O' rings, which also acted as vacuum seals. The 'O' rings, however, proved inefficient in holding a static vacuum when the furnace was heated to higher temperatures ($>600^{\circ}\text{C}$). Therefore, in the final design, the 'O' rings were completely eliminated by using a quartz tube with steel flanges mounted at the two ends and with Cu gaskets used as the vacuum seals. A static vacuum could be maintained at pressures below 10^{-2} torr Hg almost indefinitely with this assembly. The quartz tube was 45 cms long with an inner diameter of 45 mm and wall thickness of 2.5 mm. The tube was mounted in a series 54231 Lindberg resistance heated horizontal furnace. Temperatures were controlled by a proportional band control unit to an accuracy of $\pm 1^{\circ}\text{C}$. A zone 5 cms long in the center of the tube was found to be isothermal to within 1°C . The sample holder assembly consisted of a Pt boat approximately 5 cm x 1.25 cm x 1.25 cm, which was mounted on an alumina rod attached to the Varian Conflat[®] flange at one end of the quartz tube (Fig. 5). The alumina rod acted both as the support for the crucible and as the feed-through for the thermocouple. Chromel-Alumel thermocouples were used to measure the temperatures, which were recorded by a digital thermocouple temperature display unit. The thermocouple was shaped in such a way that its tip

could be buried directly in the specimen for accurate sample temperature determination. The other end of the quartz tube was attached to the vacuum pumps, manometer, gas burette and the mass spectrometer. A leak valve was used to isolate the mass spectrometer from the rest of the system.

The manometer was a combination of two MKS 'Baratron' 200 series electronic capacitance vacuum gauges. These manometers contain a metal diaphragm, one side of which is exposed to the gas for which the pressure is to be measured, the other side is adjacent to an electrode assembly placed in a factory sealed high vacuum reference cavity. A change in absolute pressure causes the diaphragm to deflect, which produces a capacitance change in the system. This change is detected, demodulated and converted into a DC voltage output which is linear with pressure.

The two gauges had full scale ranges of 10^{-3} to 10 torrs and 10^{-1} to 10^3 torrs respectively. These gauges were provided with calibrated outputs, which the manufacturer claimed to have an accuracy of 1% of each reading and to have a response time of 11 to 33 m sec. The calibration of the gauges was checked periodically with a McLeod gauge attached to the system. The maximum error was found to be $\sim .007$ torr at a total pressure of 6.200 torr, corresponding to an accuracy of better than 0.1%.

The signal output of the manometers was displayed on a $4 \frac{1}{2}$ digit panel meter. A switching circuit was used to change from the low pressure manometer (10 torr full scale) to the higher pressure manometer (1000 torr full scale) so that only one display unit was necessary for the pressure readout. The signal from the manometers was also connected to a linear chart recorder so that pressures were recorded graphically as

a function of time. This pressure-time recording proved extremely useful in establishing the asymptotic approach to a certain pressure, when the rate of pressure change became extremely slow in some experiments. The pressure record was also useful for correcting for the linear pressure rise due to small leaks, when present, during the experiments.

The gas burette (Fig. 6) consisted of a series of bulbs with calibrated volumes of approximately 50, 200 and 725 cc capacity. The volume of the capillary tubing between the inlet 2-way stop cock and the fiducial mark was calibrated and added to the total volume of the bulbs to get corrected total volumes. The pressure in the burette was read by a mercury manometer, with an accuracy of ± 0.5 torr.

A mercury diffusion pump backed by a mechanical pump was used to evacuate the system. During the experiments, pumps were valved off to provide a closed system with a static vacuum.

An EIA Quadrupole Residual Gas Analyzer (RGA) (a kind of mass spectrometer), series Quad 250 was used to measure the gas compositions. This gas analyzer is equipped with a 14 stage, Be-Cu electron multiplier which has a gain $>10^6$. The gas analyzer, which was attached to the system through a leak valve was pumped upon by a Titanium vac-ion pump so that the pressure in the gas analyzer could be kept $<10^{-6}$ torr, regardless of the ambient pressures in the furnace chamber. The only significant impurities in the CO_2 gas were N_2 and H_2O . The gas analyzer was calibrated for these gases to obtain the partial pressure of CO_2 in the system.

2. Calibration of the Gas Burette

Prior to the assembly of the bulbs in the gas burette, each bulb was calibrated by measuring the mass of H₂O it could hold, using a Mettlers microbalance, and calculating the volume by using the density of H₂O at room temperature.

3. Calibration of Apparatus Volume

The number of moles of gaseous CO₂ in an isothermal system can be obtained from the gas law

$$n_{\text{CO}_2} = \frac{P_{\text{CO}_2} V}{RT}$$

Because part of the system is at high temperature (500-800°C) while part of it is at room temperature, the effect of non-isothermal conditions on the CO₂ content of the system must be evaluated. For this purpose, the system can be considered to consist of a hot chamber of volume V₁ at T₁°K (taken to be the furnace temperature in the hot zone), coupled with a reservoir of volume V₂ at T₂°K, taken to be room temperature (Fig. 7). When the system is in a steady state, the pressure read by the manometer is the ambient pressure P_A, which can, to the first approximation, be written as

$$P_A = \frac{(n_1 + n_2) RT_2}{V_A} \quad (1)$$

where n₁ and n₂ are the number of moles of gases in the two chambers at temperatures T₁ and T₂ respectively, V_A is the *effective* volume which will make equation (1) hold true at the hot zone temperature T₁. V_A is a function of the furnace temperature T_F (≡ T₁). The volume calibration then requires measuring V_A as a function of T_F, the furnace temperature. This involves using (1) in slightly different form:

$$V_A = \frac{n RT_2}{P_A}$$

where $n = n_1 + n_2$ = total # moles of gases in the system. For constant T_1 and T_2 , as Δn moles of gas is added (or subtracted) from the system, a pressure change of ΔP_A results. Then, V_A is obtained from

$$V_A = \frac{\Delta n RT_2}{\Delta P_A} \quad (2)$$

Equation (2) was utilized to obtain the effective volume V_A at different furnace temperatures. However, analytic expressions for V_A can be derived using appropriate assumptions as shown below:

(i) Molecular flow region (flux balance)

Referring to Fig. 7, if pressures in chambers 1 and 2 are low enough for Knudsen flow conditions to hold, the steady state condition requires fluxes to the left and right be equal, i.e.,

$$j_1 = j_2 \quad (3)$$

where j_1 is the flux of molecules from the furnace (chamber 1) to the reservoir (chamber 2) and j_2 is the opposite flux. Then from the kinetic theory of gases, one gets from equation (3).

$$\frac{P_1}{\sqrt{T_1}} = \frac{P_2}{\sqrt{T_2}} \quad (4)$$

where P_1 and P_2 are the pressures in the chambers 1 and 2, respectively, (since the pressure gauge is connected to the chamber 2, $P_2 \equiv P_A$).

Applying the ideal gas law to chambers 1 and 2, gives

$$P_i = \frac{n_i R T_i}{V_i}, \quad i = 1, 2 \quad (5)$$

combining equations (4) and (5), gives

$$P_1 = \sqrt{\frac{T_1}{T_2}} \frac{n_2 R T_2}{V_2} \quad (6)$$

also,

$$n = \sum n_i = \sum_{i=1,2} \frac{P_i V_i}{R T_i}$$

Substituting for P_1 from equation 6 in above, gives

$$n = \frac{P_2 V_2}{R T_2} + \frac{V_1}{R T_1} \sqrt{\frac{T_1}{T_2}} \frac{n_2 R T_2}{V_2}$$

or, using equation 5, gives

$$n = \frac{P_2 V_2}{R T_2} + \frac{V_1}{R T_1} \sqrt{\frac{T_1}{T_2}} P_2$$

Rearranging above gives,

$$P_2 = \frac{(n_1 + n_2) R T_2}{V_2 \left[1 + \frac{V_1}{V_2} \sqrt{\frac{T_2}{T_1}} \right]} \quad (7)$$

comparing this with equation (1) ($P_2 \equiv P_A$), we see that

$$V_A = V_2 \left[1 + \frac{V_1}{V_2} \sqrt{\frac{T_2}{T_1}} \right] \quad (8)$$

which is the desired expression for the effective volume V_A as a function of T_1 (assuming V_1 , V_2 and T_2 are kept constant).

(ii) Hydrodynamic flow region (pressure balance)

Under hydrodynamic flow conditions, the steady state condition for the system becomes

$$P_1 = P_2 \equiv P_A$$

but,

$$P_2 = \frac{(n_1 + n_2) R T_2}{V_A}$$

or,

$$P_2 V_A = \left(\frac{P_1 V_1}{R T_1} + \frac{P_2 V_2}{R T_2} \right) R T_2$$

dividing by P_2 on both sides ($P_2 \equiv P_1$), and rearranging, we obtain

$$V_A = V_2 \left[1 + \frac{V_2}{V_1} \left(\frac{T_2}{T_1} \right) \right]. \quad (9)$$

Equations (8) and (9) are similar, $\sqrt{T_2/T_1}$ in (8) is replaced by T_2/T_1 , in (9).

The effective volume of the system was obtained experimentally for different furnace temperatures by introducing known amounts of CO_2 (Δn) from the gas burette, observing the change in pressure (ΔP_A) and using equation (2). Using the measured values of V_A for furnace at two different temperatures, namely $T_1 = T_2$ (room temperature) and $T_1 \gg T_2$ (highest possible T_F) two sets of values of V_1 and V_2 were derived by solving equations (8) and (9).

The calibration curves that result for both equations are shown in Fig. 8. The experimental values are reported on the same plot. Both theoretical curves are within the error bars of the experimental values. Calculation of the mean free path, λ , for Knudsen flow by CO_2 gives $\lambda \cong 2$ cms at a pressure of 10 m torr and $T = 500^\circ\text{C}$. Thus, it appears that for $P > 10$ m torr, which is the range usually employed in this

study, equation (9) should apply. It was used in calculating V_A as a function of the furnace temperature, T_F . The merit of using a theoretical value of V_A becomes apparent in correcting for changes in room temperature during the experiment and especially in correcting the measurements of non-isothermal experiments, to be described later.

Using the theoretical values of effective volume, blank runs were made to ascertain the extent of adsorption of CO_2 by the walls of the system. The amount absorbed was found to be $<10^{-6}$ moles of CO_2 at 298°K and $<10^{-7}$ moles of CO_2 at 900°K . These quantities are negligible at all temperatures of interest.

4. Pressure, Temperature Calibration

The manufacturer's calibration of the electronic manometers were shown by comparison with a McLeod gauge to be within 0.1% of the reading at all times.

The thermocouple was calibrated against an NBS standard Pt-Pt/Rh thermocouple at 500, 650 and 800°C , a range which includes all temperatures used in this study. The thermocouple read 500.5°C , 650.4°C and 799.9°C , showing an accuracy of better than 0.1%. Since the thermocouple was placed in direct contact with the samples during experiments, no other temperature correction was deemed necessary.

As a check for the temperature scale calibration, an in-situ, second law determination of the heat and entropy of decomposition of CaCO_3 was made with the apparatus. The CaCO_3 was first decomposed in the closed system, and then resulting CaO partially recarbonated by introducing $P_{\text{CO}_2} > P_{\text{eq}}$. The equilibrium pressure for decomposition, P_{eq} , was taken to be the mean of the asymptotic limits of the pressures obtained in the

decomposition and recarbonation runs, which were found to be within 10% of each other at every test temperature.

Figure 9 shows a plot of $\ln P_{eq}$ as a function of $1/T$. For comparison, the accepted equilibrium decomposition pressure data for calcite¹⁸ has been plotted in the same figure. From the experimental plot, the second law heat of decomposition is calculated to be, $\Delta H_d^\circ = 40.87 \text{ kcal mole}^{-1}$, in the temperature range 600°C to 700°C. This agrees very well with the accepted value,¹⁸ $\Delta H_d^\circ = 40.83 \text{ kcal mole}^{-1}$.

The agreement is not as good, however, for the entropy of decomposition, which was determined to be $\Delta S_d^\circ = 34.91 \text{ eu mole}^{-1}$, compared with the reference value¹⁸ $\Delta S_d^\circ = 36.37 \text{ eu mole}^{-1}$. This is a discrepancy of $1.46 \text{ eu mole}^{-1}$ for the value of ΔS_d° . Since the thermocouple was calibrated to an accuracy of 0.1%, the discrepancy cannot be explained by any error in the temperature calibration. The entropies of CaCO_3 (calcite) and CaO at 298°C are uncertain by 0.2 eu for each.³⁰ This means that the literature value of ΔS_d° is uncertain by $.4 \text{ eu mole}^{-1}$, which is not large enough to explain the discrepancy.

The thermodynamic and kinetic values of enthalpies and entropies obtained in this work are therefore derived by using the experimentally determined P_{eq} for calcite decomposition, where needed, and not the previously accepted values,¹⁸ since it is not clear that the thermodynamically calculated values should be preferred to the direct measurements.

5. Calibration of the Gas Analyzer

Known amounts of CO_2 and N_2 and of CO_2 and H_2O were introduced into the system using the gas burette (Fig. 4). The background pressure in the gas analyzer was below 10^{-8} torr in all runs. The leak valve was

opened to let gases from the system into the gas analyzer until the pressure inside rose to $\sim 10^{-7}$ torr. The leak rate was then adjusted to maintain a constant pressure near 10^{-7} torr during the mass scan. Masses were scanned from mass 0 to 50, a range which includes all the peaks for CO_2 , N_2 and H_2O .

The ion species were identified by introducing pure CO_2 , N_2 and H_2O respectively. The electron voltage could not be reduced below 20 ev, which is above the appearance potential for CO^+ (mass 28) from CO_2 . This fact complicated the calibration measurements because N_2^+ (A.P. = 15.5 ev) has the same mass as CO^+ (see Table I for major ion fragments and their A.P. for CO_2 , N_2 and H_2O). In order to obtain consistent results, the electron voltage was adjusted to maximize the intensity of mass 44 (CO_2^+), which seemed to maximize the intensities for mass 28 ($\text{N}_2^+ + \text{CO}^+$) and 18 (H_2O^+) also. Apparently, focussing of all the ions was optimum at about the same electron energy.

The ratio of CO_2 to, say, N_2 was changed in known amounts by using the gas burette and the ratio of intensities for mass 44 (CO_2^+) to that for mass 28 (CO^+ and N_2^+) was plotted as a function of % N_2 (Fig. 10). The same procedure was repeated for CO_2 and H_2O (Fig. 11). The calibration curves thus obtained were found to be relatively insensitive to the emission current, ion energy and the actual pressure in the gas analyzer. The consistency of the calibration curves was checked periodically and they were found to remain consistent.

6. Isothermal Experiments

Two kinds of samples of calcite were used for this study. Calcite single crystals (Iceland spar) obtained from Chihuahua, Mexico were used

first (see Appendix I for a spectrographic analysis). A crystal was hand crushed to yield particles of the order of one micron linear dimensions. Surface areas were measured by the BET method. The method and the apparatus for surface area measurements have been described elsewhere.⁵ Scanning electron microscope observations showed the spread in particle size to be significant, as expected for hand crushed specimen (see Fig. 12).

The powdered calcite was also analyzed by x-ray diffraction for the sake of complete characterization. The sample was placed in an aluminum holder and irradiated in a Picker x-ray diffractometer using Cu K α radiation, at 14ma, 40kV, 2° 2 θ /min, τ = 3 sec and 200 cps. Scans were made from 2 θ = 28° to 70°, which covers the major peaks for calcite, aragonite, Ca(OH)₂ and CaO (Appendix II).

The second source of calcite powder was Baker-analyzed, high purity CaCO₃ (see Appendix III for characteristics).

In a typical isothermal experiment, the Pt boat was loaded with a sample that weighed 1 to 5 gms and the thermocouple junction was positioned to rest in the center of the sample. The furnace chamber was evacuated. The vacuum was maintained at $\sim 10^{-6}$ torr for about 12 hours with the furnace heated to about 200°C, to desorb gases from the walls and sample surfaces.

The valve to the vacuum pump was then closed. If no significant desorption was observed, indicating a clean system, CO₂ from the gas burette was added to a fixed pressure (typically ~ 5 torrs), higher than the CO₂ decomposition pressure at any temperature of subsequent heating.

On reaching the desired temperature, the pressure of CO_2 was adjusted to some specific initial value and the sample was left to equilibrate isothermally. Equilibrium conditions were considered established when the rate of pressure rise fell below 1 m torr per hour (which is the background pressure rise in a clean, baked system under the best leak-free conditions), over several hours. Typically, this equilibrium was insured by leaving the system at constant T and P up to 12 hours.

Next, a known amount of CO_2 was extracted from the system by opening it to the gas burette. The sudden drop of CO_2 pressure in the reaction chamber was partially reversed by release of CO_2 by the calcite. The final pressure was recorded when no further pressure rise was observed. The amount of CO_2 released by the sample was calculated by using equations described above to calculate the change in the number of moles of CO_2 in the gaseous phase in the system and comparing it with the amount added from the gas burette.

Experiments were carried out with samples of different particle size to estimate the effect of surface adsorption/desorption. With large crystals (~1cm x 1cm x 0.5cm), the time to reach equilibrium was so long in the practical temperature range, below 1000°K that the errors in final equilibrium pressures were high. Hence, most of the study was done with powdered calcite.

To ensure equilibrium conditions, experiments were also carried out in the reverse direction, i.e., by starting from a lower P_{CO_2} and increasing it by addition of known amounts of CO_2 .

The change in composition, ΔX_{CO_2} in going from pressure P_1 to P_2 was calculated from

$$\Delta X_{\text{CO}_2} \text{ (in mole \%)} = \pm \left[\frac{P_B V_B}{RT_A} - \frac{|\Delta P| V_A}{RT_A} \right] \frac{100}{n_{\text{CaCO}_3}}$$

where,

P_B = CO_2 pressure in the gas burette in torrs

V_B = volume of gas burette in cc

T_A = ambient, room temperature ($^{\circ}\text{K}$)

ΔP = $P_2 - P_1$ in torr

V_A = effective volume in cc

n_{CaCO_3} = # moles of CaCO_3 in the sample.

A + sign is used on the right hand side of equation when $P_2 > P_1$; a- sign for $P_2 < P_1$.

7. Non-isothermal Experiment

The isothermal experiments described above were restricted to a narrow temperature range because of the experimental difficulty in maintaining a static vacuum system leak-free at high temperatures over a prolonged time period, because of the exponential rise in decomposition pressure with temperature and because of the inherent inaccuracy involved in utilizing the gas burette (see discussion of accuracy in the discussion section). A non-isothermal method completely eliminates use of a gas burette, which was the main source of error. The method involves measuring P_{CO_2} in equilibrium with CaCO_3 phase in a closed system as the temperature changes. These changes in pressure and temperature lead to a unique change in composition. Useful thermodynamic data can be obtained by this method as discussed below.

(i) Theory

Consider heating some fixed amount of CaCO_3 in a closed system under an imposed pressure of CO_2 , ($P_{\text{CO}_2} > P_{\text{eq}}$). Then, in a general thermodynamic sense, the composition of CaCO_3 at a given P and T , is uniquely determined according to the phase rule. This can be written formally as

$$P = P(X, T) \quad (10)$$

where P is the imposed pressure of CO_2 , T is the temperature of the sample ($\equiv T_F$) and X is the mole fraction of CO_2 in the CaCO_3 phase.

Differentiating equation 10, we get

$$dP = \left(\frac{\partial P}{\partial X} \right)_T dX + \left(\frac{\partial P}{\partial T} \right)_X dT \quad (11)$$

However, P in the system, from experimental consideration, is given by

$$P = \frac{n RT_A}{V_A}$$

where V_A is the effective volume as discussed before. Differentiation gives

$$dP = \frac{RT_A}{V_A} dn + n RT_A d \left(\frac{1}{V_A} \right) \quad (12)$$

which relates the differential changes in pressure to changes in the amount of gas in the system, and changes in the effective volume as T_F changes. Now, dn is related to the change in composition in a closed system by

$$dn = -dX n_{\text{CaCO}_3} \quad (13)$$

where n_{CaCO_3} is the number of moles of CaCO_3 in the system.

Combining equations (11), (12) and (13), yields

$$\frac{RT_A}{V_A} dn - \frac{n RT_A}{V_A^2} dV_A = - \left(\frac{\partial P}{\partial X} \right)_T \frac{dn}{n_{CaCO_3}} + \left(\frac{\partial P}{\partial T} \right)_X dT$$

which on rearranging gives,

$$\left[1 + \alpha \left(\frac{\partial P}{\partial X} \right)_T \right] \frac{dn}{dt} = \frac{n}{V_A} \frac{dV_A}{dT} + \frac{V_A}{RT_A} \left(\frac{\partial P}{\partial T} \right)_X \quad (14)$$

where

$$\alpha \equiv \frac{V_A}{RT_A} \frac{1}{n_{CaCO_3}} \quad (15)$$

i.e. α is a constant for a given amount of n_{CaCO_3} , if room temperature T_A is constant. Now, from equation 8, we see that

$$\frac{dV_A}{dT} \equiv \frac{dV_A}{dT_1} = - \frac{V_1 T_2}{T_1^2} \quad (16)$$

where V_1 = volume of hot zone at temperature $T_1 \equiv T$,

T_2 = ambient temperature $\equiv T_A$.

also, P_{CO_2} is related to $\overline{\Delta G}_{CO_2}(X,T)$ by

$$P_{CO_2} = P_{CO_2}^\circ \exp \left[\frac{\overline{\Delta G}_{CO_2}^\circ}{RT} \right] \quad (17)$$

when $\overline{\Delta H}_{CO_2}^\circ$ and $\overline{\Delta S}_{CO_2}^\circ$ are assumed to be temperature independent,

differentiation of both sides of equation 17 with respect to temperature yields

$$\left(\frac{\partial P}{\partial T}\right)_X = - \frac{P \overline{\Delta H_{CO_2}}(x)}{RT^2} \quad (18)$$

combining equations (16), (18) with equation (14), we get

$$\left[1 + \alpha \left(\frac{\partial P}{\partial X}\right)_T\right] \frac{dn}{dt} = - \frac{nV_1 T_A}{V_A T^2} - \frac{V_A P}{RT_A} \frac{\overline{\Delta H_{CO_2}}(x)}{RT^2}, \text{ and, since } n = \frac{P V_A}{RT_A}, \therefore$$

$$\left[1 + \alpha \left(\frac{\partial P}{\partial X}\right)_T\right] \frac{d \ln n}{d T/T} = - \frac{V_1 T_A}{V_A} - \frac{\overline{\Delta H_{CO_2}}(x)}{R} \quad (19)$$

equation (19) has two unknowns, namely $(\partial P/\partial X)_T$ and $\overline{\Delta H_{CO_2}}(x)$. To solve for these, one can start at a given X_0 (i.e., specified P_0, T_0) and heat (or cool) two different samples, differing in $\alpha(n_{CaCO_3})$. This procedure leads to two different values of $\frac{d \ln n}{d T/T}$, which can be used to solve equation (19) for the two unknowns, algebraically.

The theory suggests that this method will lead to measurement of $(\partial P/\partial X)_T$ and $\overline{\Delta H_{CO_2}}(x)$ as a function of composition, and it appears to be a valuable method for obtaining thermodynamic information by means of the tensi-volumetric apparatus.

Success with the non-isothermal experiments depends upon being able to measure $\frac{d \ln n}{d T/T}$ accurately at the initial compositions for the two different samples. The differences in two slopes can be maximized by making α_1/α_2 as large as possible, i.e., by doing the experiment with as much difference in the amounts of $CaCO_3$ as possible.

(ii) Experimental method for non-isothermal experiments

About 0.17 gms. of $CaCO_3$ powder (Baker analyzed) was loaded into the furnace, the system was baked at $300^\circ C$ for ~12 hrs. A CO_2 pressure of

about 4 torrs was imposed upon the sample, which was then heated to 900°K. The pressure was readjusted to ~7.0 torrs and system was left to equilibrate (~10 hrs). Starting from these initial conditions of P and T, the temperature was reduced in steps of about 50°C and the pressure was recorded for each temperature after it had stopped changing. The amount of CO₂ in the system was calculated using equation (1) and ln n was plotted against T. A similar set of measurements at increasing temperatures was then made to determine if the measured composition changes were reversible. A similar set of heating and cooling experiments were performed for another sample which weighed about 2 gms. Limiting slopes of the data, $\frac{d \ln n}{dt}$ were obtained at the initial P_o, T_o and equation (19) was solved algebraically.

8. Experiments on CaCO₃ Minerals

Experiments were undertaken to establish the differences in CO₂ content of calcite obtained from different geological sources. These experiments were motivated by the preliminary observation that on heating a ground specimen of Iceland Spar calcite, CO₂ was evolved in measurable amounts when the specimen was heated under pressures of CO₂ greater than the decomposition pressure. In a typical run, a calcite specimen, hand ground and dried in a vacuum oven at 75°C for ~1 week was placed in the furnace and heated to 100°C in the closed system in vacuum. The gases released were analyzed by the residual mass analyzer (RGA) and then the system was pumped (~12 hrs) at 100°C to remove any trace amounts of H₂O impurity, which was checked by RGA. A CO₂ back pressure was then imposed and sample was heated to 900°K, with the P_{CO₂} kept above P_{eq} at all temperatures. The gaseous atmosphere in the furnace was analyzed again using the RGA and the amount of gases desorbed was calculated. The

surface area of powder was measured using a Quantachrom BET surface area analyzer which was found to be consistent with 1-5 μ m particle size obtained by SEM examination (Fig. 13). The surface area of granular CaCO₃ of uniform mesh size (=14), which was used in the experiment, was obtained by photographing the particles at low magnification and estimating the mean grain size over several grains (see Fig. 14). This surface area measurement was made in order to determine whether or not the CO₂ loss during heating might arise from desorption from the surface of CaCO₃ samples rather than from the bulk composition change, to be discussed later.

CaCO₃ samples were also prepared by grinding them in CCl₄ to avoid any contact with CO₂ and H₂O in air, and the same procedure was repeated with these samples to check the difference due to exposure of powder to air. No difference in CO₂ adsorption/release was found between the samples powdered in air or under CCl₄.

9. Determination of Absolute Compositions

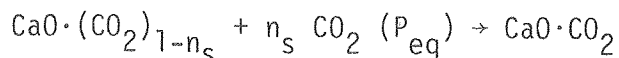
In all the experiments involving compositional changes discussed previously, the absolute composition is unknown and only relative changes in composition were measured. For example, in isothermal experiments, $\Delta X_{\text{CO}_2} = X - X^*$ was measured as a function of P_{CO_2} , where X^* is the composition at a reference pressure, not known a priori.

In order to complete the thermodynamic description of non-stoichiometric calcite, it becomes important to know the absolute value of δ in CaO·(CO₂)_{1 \pm δ} as accurately as possible. A series of CaCO₃ specimen, both 'Iceland Spar' and 'Baker-analyzed' reagent were analyzed for Ca and C content by standard chemical analysis techniques. The ratio of Ca

to C was found to be stoichiometric within the experimental accuracy (see Table II). A survey of the literature showed that previous analysis of CaCO_3 have shown it to be of stoichiometric composition to within 0.01%, and this result was accepted as characteristic of CaCO_3 .

A test of the total calibration of the tensi-volumetric apparatus was obtained by decomposing small weighed amounts of calcite powder (Baker analyzed-reagent grade) at 700°C in the apparatus used in this work. Correcting for the amount of CO_2 evolved during 'degassing', the total amount of CO_2 evolved was found to be 99.45% of the theoretical amount based upon stoichiometry. No release of CO_2 was detected on further heating of the product CaO up to 950°C , indicating negligible solubility of CO_2 in CaO . This result, coupled with the previous chemical analysis was taken to mean that the 0.55% discrepancy in the amount of CO_2 released reflects a systematic error of 0.55% in the volume calibration of the apparatus. Thus, the calibrated volume was corrected by 0.55% at all temperatures.

Since CaCO_3 is stoichiometric within 0.01% at lower temperatures ($\sim 300^\circ\text{C}$), the absolute compositions can be determined by measuring the amount of CO_2 absorbed when the sample is equilibrated at a higher temperature under $P_{\text{CO}_2} = P_{\text{eq}}$ and cooled to a lower temperature (300°C). The equation describing this process can be written as:



where n_s is the difference between the number of moles of CaO and CO_2 in calcite when it is saturated with CaO . The amount of CO_2 absorbed in this process gives the composition of calcite at the reference pressure = P_{eq} at any temperature.

Experiments to determine the phase boundary composition of calcite were performed both with granular samples and with Baker analyzed powder. In a typical run, CaCO_3 was placed in the furnace and the system was baked under vacuum at 300°C . The vacuum pump valves were closed to isolate the system, and the sample was heated to a high temperature usually about 700°C under an imposed P_{CO_2} equal to the equilibrium pressure of CO_2 at the final temperature. After the system had equilibrated at constant temperature and pressure ($= P_{\text{eq}}$). The sample was cooled to 300°C slowly (a typically, cooling rate was about 50°C per hour). At 300°C , the final pressure was recorded and the amount of CO_2 absorbed was calculated using the equation

$$\Delta n_{\text{CO}_2} = \frac{P_f V_f}{RT_A^f} - \frac{P_i V_i}{RT_A^i} \quad (20)$$

where P_f , V_f , T_A^f are the final pressure, effective volume and ambient temperature respectively, and P_i , V_i , T_A^i are values at the initial furnace temperature.

In one run, a sample was cooled from 700°C with $P_{\text{CO}_2} = P_{\text{eq}}$ at 700°C to 300°C in four steps of $\Delta T = 100^\circ\text{C}$ in each step. The amount of CO_2 absorbed was calculated for each step and absorption in the final step ($400^\circ\text{C} \rightarrow 300^\circ\text{C}$) was found to be negligible.

The experiments to determine the extent of nonstoichiometry at the CaO-CaCO_3 phase boundary were performed for several temperatures between 500°C and 750°C . The assumption in all these experiments was that the phase width of calcite at 300°C is negligible. The validity of this assumption will be discussed in a later section.

III. RESULTS AND DISCUSSION

1. Sensitivity and Accuracy of the Tensi-volumetric Method

The tensi-volumetric apparatus was used in this study to determine from changes in the pressure of known quantities of gas, the corresponding compositional changes in the solid phase. For very small compositional changes at low pressures, this method has some distinct advantages over a thermogravimetric apparatus in which the solid compositional changes are determined from changes in the weight of the sample.

The minimum relative change in composition of CaCO_3 , $\Delta x_{\text{CO}_2}^{\text{min}}$, which can be measured by the apparatus is $\frac{\Delta n_{\text{min}}}{n_{\text{CaCO}_3}}$, where Δn_{min} is the minimum measurable change in the CO_2 content in the gas phase and n_{CaCO_3} is the number of moles of calcium carbonate. Thus, for a given Δn_{min} , $\Delta x_{\text{CO}_2}^{\text{min}}$ can be made smaller by increasing n_{CaCO_3} , i.e., by using larger amounts of sample. This size effect is opposite to that for a microbalance, for which the sensitivity decreases with increased sample size. However, sample size is limited to a certain extent by the necessity of keeping the sample isothermal for which smaller samples are desirable. The sensitivity of the tensi-volumetric apparatus can also be increased by decreasing Δn_{min} by decreasing the overall volume of the apparatus. For the apparatus used in this study, n_{CaCO_3} was typically ~ 0.05 moles. Using the calibrated volume of the apparatus, $\Delta x_{\text{CO}_2}^{\text{min}}$ is calculated to be $\sim 10^{-6}$ per mole of CaCO_3 , at $T = 900^\circ\text{K}$. This sensitivity is more than an order of magnitude better than conventional microbalances and is comparable with the best electrochemical measurements of shifts in composition; and the electrochemical method is not suitable for a poorly conducting phase like CaCO_3 .

The accuracy of the measurements depends upon the accuracy with which the variables V, P and T can be measured. The largest source of error was found to be introduced by the use of a mercury manometer to measure the pressure in the gas burette. In isothermal experiments with the gas burette, typical accuracy was $\pm 1\%$ of n_{CO_2} in the burette. The pressure and temperature measurements in the furnace chamber are accurate to $\pm 0.1\%$. Thus, non-isothermal experiments which do not involve the gas burette are an order of magnitude better in accuracy.

The overall conclusion then is, that at low pressures, the tensi-volumetric method is a precision, high accuracy method for measurement of the compositional changes in the sample, being superior to gravimetric method and comparable to electrochemical method in precision. However, when CaCO_3 is used as the sample, the exponential rise in decomposition pressure with temperature makes the measurement of small changes in composition difficult with the system described here, at temperatures greater than 670°C because the use of a higher pressure range monometer reduces the sensitivity by two orders of magnitude, to the value $\Delta x_{\text{CO}_2}^{\text{min}} = 10^{-4}$ mole/mole CaCO_3 . Such a problem will not occur if one were to measure, say, the solution of CO_2 in CaO phase at high temperatures. In fact, the precision of $\Delta x_{\text{min}} = 10^{-6}$ moles/mole CaO at $T > 600^\circ\text{C}$ probably makes this technique superior to any other method of studying the solubility of CO_2 in CaO at high temperatures. It is hoped that it will be found useful in studying the solubility of CO_2 in the metastable CaO produced by vacuum decomposition of CaCO_3 , which seems to dissolve up to 15 mole% CO_2 at 700°C .⁶

2. Solubility of CO₂ in CaCO₃: bulk vs. surface effects

The release of CO₂ by calcite prior to decomposition may be due to a change in bulk composition of the calcite phase and/or to a change in the surface composition. A simple calculation permits estimation of the number of monolayers of CO₂ that must be released from the surface in order to account for the measured changes in ΔX_{CO_2} .

Assume the CaCO₃ surface to be planar and chemisorption of CO₂ to occur only on one type of lattice site (cationic or anionic). Using the lattice parameters of calcite, we then calculate that the number of chemisorption sites/area $\approx 5 \times 10^{14}$ per cm². Therefore, the number of moles of CO₂ per monolayer per m²,

$$n_m = 8.2 \times 10^{-6} \text{ moles per m}^2$$

If Δn_{CO_2} is the number of moles of CO₂ released or absorbed from the sample surface, then the corresponding number of monolayers, n , is

$$n = \frac{\Delta n_{\text{CO}_2}}{\omega \sigma (8.2 \times 10^{-6})} \text{ monolayers} \quad (21)$$

where ω is wt. of sample in gms and σ is specific surface area in m² gm⁻¹.

Table III gives a list of samples studied and a correlation of ΔX_{CO_2} with the equivalent surface coverage. It is seen that for high surface area calcite ($\sigma = 0.67 \text{ m}^2 \text{ g}^{-1}$), changes in the quantity of CO₂ chemisorbed can not be ruled out as the source of the measured changes in CO₂ content because the surface coverage is calculated to vary from ~0.63 to 2.7 monolayers. However, for the granular samples ($\sigma = 10^{-3} \text{ m}^2 \text{ g}^{-1}$) a calculated value close to $n = 300$ monolayers is required to account for the observed change in ΔX_{CO_2} in the

sample. This implausible result rules out changes in surface coverage as the main source of the observed changes in CO_2 content of calcite.

However, ΔX_{CO_2} for the powdered sample is larger than that for the granular sample, suggesting that desorption is partially responsible for the observed evolution of CO_2 on heating powdered calcite. The surface effect can be accounted for quantitatively as will be done in the next section.

3. Isothermal Experiments

Figures 15-20 show plots of ΔX_{CO_2} vs. P_{CO_2} at four different temperatures and for different sources of calcite (note the difference in scales for different isotherms). The data in Fig. 15 was obtained at 773°K for hand ground sample of calcite ($\sigma = 0.25 \text{ m}^2 \text{ g}^{-1}$). The experiment was done in a cyclical pattern, by establishing a high pressure (0.8 torr-Hg) and lowering it in successive steps to 0.075 torr. Then the direction of pressure change was reversed. This overall cycle was repeated a few times. The experimental points have been marked with numbers to show the order in which they were generated. The order is important because the errors in measuring the compositional shifts are cumulative.

This plot shows that the initial, relatively large changes in composition as P_{CO_2} decreased, are not reversed when P_{CO_2} is increased. This large, initial composition shift could be accounted for by an irreversible desorption of about 0.4 monolayer of CO_2 from the particle surfaces. It may be that at the temperatures and pressures of this study, a stable CaCO_3 surface consists largely of Ca^{++} and O^{--} ions rather than Ca^{++} and CO_3^{--} ions.

On further cycling, the composition shifts are smaller, but reproducible within the error limits.

To avoid crowding on figures, the P - ΔX isotherm at T = 773°K for 'Baker Analyzed' calcite powder ($\sigma = 0.67 \text{ m}^2 \text{ g}^{-1}$) is reported in Fig. 16. For this material, the surface area is higher and initial irreversible CO₂ loss is even greater, as would be expected if the loss of CO₂ from the surface is responsible for this effect. The initial, overall composition shift corresponds to ~0.3 monolayer of surface-oxide formation.

The reversible part of this plot is in reasonable agreement with that in Fig. 15. A similar experiment with granular CaCO₃ ($\sigma = 10^{-3} \text{ m}^2 \text{ g}^{-1}$) at 773°K failed to show any measurable shifts in composition within a large scatter in data. For this sample, the surface area is too low to contribute a significant irreversible desorption, and presumably diffusion of CO₂ in CaCO₃ at 773°K is too slow to make study of shifts in bulk composition possible.

P- ΔX isotherms at 900°K are reported in Figs. 17 and 18, for calcite powder and granular calcite, respectively. There is some irreversibility for the powder (Fig. 17) but, as expected, not for granular sample (Fig. 18). The overall composition shift is larger at 900°K than at 773°K, suggesting that the phase width of CaCO₃ increases with temperature.

Figures 19 and 20 are P- ΔX plots for granular calcite, at 973°K and 1000°K, respectively. These plots show the same general behavior found for the lower temperature isotherms.

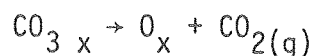
On comparison of all P- ΔX isotherms, it becomes evident that the shifts in composition, ΔX_{CO_2} is non-linear with pressure of CO₂. Also, the compositions at all temperatures seem to approach a saturation value

asymptotically at higher pressures of CO_2 .

Another feature which is evident in $P-\Delta X$ isotherms is that it is possible to reduce the pressure below the equilibrium decomposition pressure by as much as 20% without leading to decomposition, with reversible changes in composition. In this region calcium carbonate is metastable with respect to formation of CaO and CO_2 , suggesting a barrier to the nucleation of the oxide phase. For example, at 900°K ($P_{\text{eq}}^{\text{expt.}} = 3.9$ torrs), the pressure of CO_2 could be reduced to 3.2 torrs without observing any decomposition, with continuity in $P-\Delta X_{\text{CO}_2}$ plot. Further reductions in pressure lead to decomposition at extremely slow rates, as shown in Fig. 18, where the composition shifted with time, with pressure approaching P_{eq} slowly. The minima in $P-\Delta X_{\text{CO}_2}$ were taken as the limit of metastability.

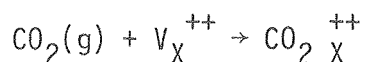
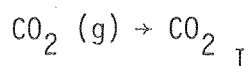
4. Point-defects Modelling

As mentioned in the introduction of Part I of this thesis, point defects are decisive in defining nonstoichiometry in solid phases. The equilibrium concentrations of various defects in a binary phase are controlled by the defect formation energy and entropy, and the condition for charge neutrality. The simplest type of defect which will lead to nonstoichiometry in the $\text{CaO}\cdot\text{CO}_2$ phase, compatible with the energetics and charge neutrality is $\text{O}^{\cdot\cdot}$ ions on $\text{CO}_3^{\cdot\cdot}$ ion sublattice. The two other common defects, namely Schottky and Frenkel defects¹⁹ do not lead to nonstoichiometry. The equation describing the formation of $\text{O}^{\cdot\cdot}$ defects on $\text{CO}_3^{\cdot\cdot}$ sites, following Kröger-Vink notation²⁰ is



where X represents anionic sites in the crystal. This defect reaction would lead to a negative deviation from stoichiometry, making calcite a CaO-rich phase.

Positive deviations from stoichiometry, i.e., occurrence of $\delta > 0$ in the formula $\text{CaO} \cdot (\text{CO}_2)_{1+\delta}$ are possible by the following defect reactions:



where I, M and X represent the interstitial, cationic and anionic sites respectively, and V is a vacancy. None of these three is likely to be present at a readily measurable concentration. Of the three, CO_2 interstitials are likely to be most important.

Formally, one can look upon substitution of O^{--} for CO_3^{--} on an anionic site and CO_2 on interstitial sites as being an example of the general case of a defect compound of type $\text{AB}_{1+\delta}$, for which the defects are B component on interstitial sites and vacancies on B sites. Physically, a vacancy on a B site for $\text{CaO} \cdot \text{CO}_2$ corresponds to the occurrence of O^{--} ions on the CO_3^{--} sublattice. The symbols for these defects (following Kröger³) are B_i and V_B , respectively. The general theory for deviations from stoichiometry for such a system was put forward by Wagner, who showed on the basis of statistical mechanics that²¹

$$\delta = 2 X_{B_i}^{\circ} \sinh [\ln(a_B/a_B^{\circ})] \quad (22)$$

where δ is the deviation from stoichiometry leading to $\text{AB}_{1+\delta}$, $X_{B_i}^{\circ}$ is the

mole fraction of interstitial defects of B at the stoichiometric composition and a_B is the activity of B- component, quantities referring to ideal composition ($\delta=0$) being denoted by a degree superscript.

A plot of $\ln a_B/a_B^\circ$ vs. δ , according to equation (22) yields an antisymmetrical curve with the inflection point at the origin ($\delta=0$), as shown in Fig. 21. The part of plot exhibiting $\delta<0$ is concave upwards, with the $\delta>0$ part being concave downwards. The value of X_{Bi}° comes as a scale factor in this plot, and if it is extremely small, which one expects for $\text{CaO}\cdot\text{CO}_2$ on the basis of energy involved in putting CO_2 molecules interstitially, the inflection point will not be seen unless a_B ($\equiv P_{\text{CO}_2}$) becomes very large.

The experimental isotherms (Figs. 15-20) seem to indicate that only the concave upward part of the general curve of Fig. 21 has been obtained. To obtain $\delta>0$, P_{CO_2} will probably have to be enormous compared to the experimental pressures. It therefore seems reasonable to assume $B_i \sim 0$ and consider the deviations from stoichiometry to be a measure of O^{--} ions concentration in CaCO_3 lattice. The general behavior of $P-\Delta X_{\text{CO}_2}$ isotherms can thus be interpreted as being due to an increase in the O^{--} ion concentration as P_{CO_2} is lowered, until a saturation value is reached and CaO nucleates. In general, the formula $\text{CaO}\cdot(\text{CO}_2)_{1+\delta}$, then, only the range with the negative sign before δ is likely to be measurable.

With this interpretation, we can assume that the higher pressure part of the $P-\Delta X$ experimental isotherm tends asymptotically to the stoichiometric composition, which enables us to define the exact compositions from the relative deviations in composition. However, since only the concave upward part of the general curve has been obtained, determination

of the exact location of the inflexion point ($\delta=0$) is not possible a-priori. An alternate method, therefore, was used to determine the exact compositions. This method involves measurement of deviations δ , at the CaO-CaCO₃ phase boundary. The theory developed in the next section enables one to interpret the significance of δ_s .

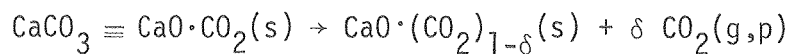
5. Phase Width and Solubility Limits of CaO(CO₂)_{1- δ}

Let us assume that the only significant defect responsible for deviations from stoichiometry is substitutional O²⁻ on the anionic sublattice. Then, the nonstoichiometric phase CaO·(CO₂)_{1- δ} ($\delta>0$) corresponds to



i.e., δ is the number of moles of O²⁻ ions when the total number of anionic sites is one mole.

Consider now the reaction at temperature T:



the free energy change for this reaction is,

$$\Delta G(\text{P}, \delta) = \sum G_{\text{products}} - \sum G_{\text{reactant}}$$

$$\text{i.e., } \Delta G(\text{P}, \delta) = \delta RT \ln \frac{a_{\text{CO}_2}}{a_{\text{CO}_2}^\circ} + \Delta G_{\text{CaO} \cdot (\text{CO}_2)_{1-\delta}} - \Delta G_{\text{CaO} \cdot \text{CO}_2} \quad (23)$$

where the ΔG 's correspond to the free energy of formation of each reactant or product from CaO and CO₂ in their standard states, which are CaO_(s) at 1 atm pressure and CO_{2(g)} at 1 atm at the reaction temperature T°K. The

effect on the activity of $\text{CaO} \cdot \text{CO}_2$ from variations in pressure of CO_2 between 0 and 1 atm will be very small, and is therefore, neglected in the treatment.

We can now write

$$\Delta G = \Delta G_{\text{CaO} \cdot (\text{CO}_2)_{1-\delta}} - \Delta G_{\text{CaO} \cdot \text{CO}_2} \quad (24)$$

where ΔG is the excess free energy of the nonstoichiometric phase over that of stoichiometric composition. This excess free energy arises from three contributions, (i) the enthalpy of defect formation (ΔH), (ii) the change in entropy due to changes in vibrational states around defects (ΔS^{th}), and (iii) the change in entropy due to configurational disorder on the sublattice (ΔS^{conf}), which will be assumed to reflect random mixing of O^{2-} and CO_3^{2-} . The division of entropy change into configurational and thermal components is arbitrary to the extent that if disorder on the sublattice does not correspond to random mixing, the difference in ideal and non-ideal mixing can be incorporated into ΔS^{th} term. With the assumption made

$$\begin{aligned} \Delta G &= \Delta H - T \Delta S^{\text{th}} - T \Delta S^{\text{conf}} \\ &= \Delta G^{\text{th}} - T \Delta S^{\text{conf}} \end{aligned} \quad (25)$$

Now, ΔS^{conf} , when the total number of mixing sites is one mole, is given by²²

$$\Delta S^{\text{conf}} = -R[\delta \ln \delta + (1-\delta) \ln (1-\delta)] \quad (26)$$

The enthalpy and thermal entropy of defect formation can be combined to give ΔG^{th} , the thermal free energy of mixing, i.e.,

$$\Delta H - T \Delta S^{th} = \Delta G^{th} \quad (27)$$

ΔG^{th} can be written in terms of partial molal quantities as,

$$\Delta G^{th} = \overline{\Delta G}_{CaO}^{th} + (1-\delta) \overline{\Delta G}_{CO_2}^{th} - \overline{\Delta G}_{CaO}^{th'} - \overline{\Delta G}_{CO_2}^{th'} \quad (28)$$

where the first two terms on the right hand side of the equation are partial molal thermal free energies of the components in the nonstoichiometric phase, and the latter two terms (primed) are for the stoichiometric phase. For a low concentration of defects, such as found in the $CaCO_3$ phase, these quantities can be assumed to be composition-independent, i.e., no association of defects occurs³ and hence, we can write

$$\overline{\Delta G}_i^{th} = \overline{\Delta G}_i^{th'}, \text{ where } i=CaO \text{ or } CO_2$$

hence, equation (28) becomes

$$\Delta G^{th} = -\delta \overline{\Delta G}_{CO_2}^{th} \quad (29)$$

Using equations (23), (24), (25), (26) and (29), we get

$$\Delta G(\delta, P) = RT[\delta \ln \delta + (1-\delta) \ln (1-\delta)] - \delta \overline{\Delta G}_{CO_2}^{th} + \delta RT \ln P/P^\circ \quad (30)$$

The equilibrium value of δ at a given pressure P is the value which minimizes $\Delta G(\delta, P)$. This condition gives, using equation (30)

$$\left[\frac{\partial \Delta G(\delta, P)}{\partial \delta} \right]_{P, T} = 0 = RT [1 + \ln \delta - 1 - \ln(1-\delta)] - \overline{\Delta G}_{CO_2}^{th} + RT \ln P/P^\circ$$

or, simplifying, we get

$$\frac{\delta}{1-\delta} = \exp \left[\frac{\overline{\Delta G}_{CO_2}^{th}}{RT} \right] \frac{1}{P/P^\circ} \quad (31)$$

but when $\delta \ll 1$, δ can be neglected in the denominator, so that,

$$\delta = \exp \left[\frac{\overline{\Delta G}_{CO_2}^{th}}{RT} \right] \frac{1}{P/P^\circ} \quad (32)$$

This equation predicts that the extent of nonstoichiometry at any given temperature is inversely proportional to the pressure of CO_2 . This prediction can be verified on the experimental isotherms, as will be shown later. However, another useful quantity that can be obtained from equation 32 is the value of δ_s , the saturation value of δ at CaO-CaCO₃ phase boundary. This value is obtained by putting $P = P_{eq}$ equation (32)

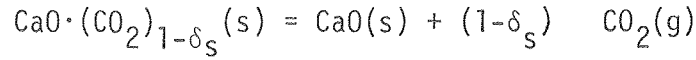
$$\delta_s = \exp \left[\frac{\overline{\Delta G}_{CO_2}^{th}}{RT} \right] \frac{P^\circ}{P_{eq}}$$

but $P_{eq}/P^\circ = \exp(-\Delta G_d^\circ/RT)$, where ΔG_d° is the standard free energy of decomposition of CaCO₃. Substituting for P_{eq}/P° in the above equation gives

$$\delta_s = \exp \left[\frac{\overline{\Delta G}_{CO_2}^{th} + \Delta G_d^\circ}{RT} \right] \quad (33)$$

Equation (33) can also be derived independently by considering the equilibrium condition at CaO-CaCO₃ phase boundary, (see appendix IV).

Now, consider the reaction



The enthalpy change for this reaction is ΔH_d , the integral heat of decomposition, which is also the negative of the integral heat of formation of $\text{CaO} \cdot (\text{CO}_2)_{1-\delta_s}$. This integral heat can be written as a sum of partial molal enthalpies of the components, i.e.,

$$\Delta H_d = -\Delta H_f = - \left[\overline{\Delta H}_{\text{CaO}} + (1-\delta_s) \overline{\Delta H}_{\text{CO}_2} \right] \quad (34)$$

since $\delta_s \ll 1$ in the experimental range, it can be neglected to obtain

$$\Delta H_d \cong - \overline{\Delta H}_{\text{CaO}} - \overline{\Delta H}_{\text{CO}_2}$$

or,

$$\overline{\Delta H}_{\text{CO}_2} + \Delta H_d = -\overline{\Delta H}_{\text{CaO}} \quad (35)$$

Similarly, for the entropy,

$$\begin{aligned} \Delta S_d &= -\Delta S_f = - \Delta S^{\text{th}} - \Delta S^{\text{conf}} \\ &= -\overline{\Delta S}_{\text{CaO}}^{\text{th}} - (1-\delta_s) \overline{\Delta S}_{\text{CO}_2}^{\text{th}} + RT \left[\delta \ln \delta + (1-\delta) \ln(1-\delta) \right] \end{aligned}$$

for $\delta_s \ll 1$, taking the limit of $\delta \rightarrow 0$,

$$\Delta S_d \cong -\overline{\Delta S}_{\text{CaO}}^{\text{th}} - \overline{\Delta S}_{\text{CO}_2}^{\text{th}}$$

or,

$$\Delta S_d + \overline{\Delta S}_{\text{CO}_2}^{\text{th}} = -\overline{\Delta S}_{\text{CaO}}^{\text{th}} \quad (36)$$

using equations (35) and (36), gives

$$\Delta G_d + \overline{\Delta G}_{\text{CO}_2}^{\text{th}} = -\overline{\Delta G}_{\text{CaO}}^{\text{th}} \quad (37)$$

hence, equation (33) becomes

$$\delta_s = \exp \left[\frac{-\overline{\Delta G}_{\text{CaO}}^{\text{th}}}{RT} \right] \quad (38)$$

or,

$$\delta_s = \exp \left[\frac{-\overline{\Delta H}_{\text{CaO}}}{RT} \right] \exp \left[\frac{\overline{\Delta S}_{\text{CaO}}^{\text{th}}}{R} \right] \quad (39)$$

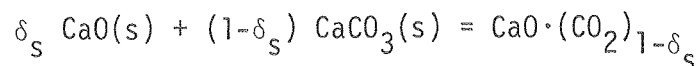
Thus, we see that an experimental plot of $\ln \delta_s$ vs. $1/T$ will be a straight line, the slope being $-\overline{\Delta H}_{\text{CaO}}^\circ/R$ and the intercept at $T = \infty$ being $\overline{\Delta S}_{\text{CaO}}^{\text{th}}/R$.

It is interesting to note that equation (39) can also be derived by taking CaO and CaCO₃ to be two components rather than CaO and CO₂. Then, CaO·(CO₂)_{1-δ} can be viewed as a solid solution of CaO_(s) in CaCO_{3(s)}. This approach is justified because we have assumed implicitly in derivation of equation (39) that the CO₂/CaO ratio in the CaCO₃ phase can never exceed 1. Then, solution thermodynamics can be used with CaO and CaCO₃ taken as the two components. At the CaO - CaCO₃ phase boundary, equilibrium requires the activity of CaO to be the same in both phases, i.e.,

$$a_{\text{CaO}} \text{ in CaO(s)} = a_{\text{CaO}} \text{ in CaO} \cdot (\text{CO}_2)_{1-\delta_s}$$

Neglecting any solubility of CO₂ in the CaO end phase, a_{CaO} in CaO(s) is unity while its activity as a dilute solute in CaCO₃ is $r_{\text{CaO}} X_{\text{CaO}}$, where r_{CaO} is the Henry's law coefficient and X_{CaO} is its solubility (δ_s).

That is, for the reaction



$$r_{\text{CaO}}^{\delta_s} = 1, \text{ or } \delta_s = \frac{1}{r_{\text{CaO}}}$$

and r_{CaO} , the activity coefficient of solute for a dilute solution is given by¹

$$r_{\text{CaO}} = \exp \frac{\overline{\Delta G}_{\text{CaO}}^{\text{th}}}{RT} \quad (40)$$

which then leads to the same result as equation (39). However, $\overline{\Delta G}_{\text{CaO}}^{\text{th}}$ in equation (40) is the partial molal quantity when CaCO_3 is considered as the second component, while equation (39) was derived with respect to CO_2 as the second component. It is shown in Appendix V that the partial molal thermodynamic quantities for a component A in a solid solution $\text{AB}_{1-\delta}$ are the same whether AB or B is considered as the second component. From this relation, the identity of equations (39) and (40) is established.

Figure 22 is an experimental plot of $\ln \delta_s$ vs. $1/T$ for a calcite powder. The plot is found to be, in fact, linear at higher temperatures, but not at lower temperatures. The low temperature results also depend upon whether the value of δ_s was obtained by cooling or heating the sample. In the heating run (obtained by starting at 300°K and heating the sample under imposed $P_{\text{CO}_2} = P_{\text{eq}}$ for the higher, final temperature), δ_s is found to be higher than the value obtained by linear extrapolation of the high temperature data.

This anomaly can be explained on consideration of surface chemisorption of CO_2 ; the high, anomalous δs value obtained corresponds closely to one monolayer coverage of the carbonate with oxide, in the initial heating run. Subsequent cycling of the sample temperature (experimental points are marked by numbers to show the order in which they were obtained) shows that the anomalous values of δs at lower temperature are also dependent upon previous cycling of the specimen. This fact again suggests that chemisorption is partially irreversible as well as dependent upon the pressure of CO_2 .

The irreversible surface effect is not seen in Fig. 23, which was obtained for granular calcite of low surface areas. The plot in Fig. 23 is fairly linear over the whole temperature range, verifying the theory presented above and also substantiating the assumption of the nature of defect responsible for the nonstoichiometric behavior of calcite.

It was concluded above that δs obtained from the reversible changes in composition in the experiments (Figs. 22,23) are measures of the O^{--} ion concentration in the CaCO_3 lattice. This assumption should be justified. The experimental points were obtained by a slow cooling (heating) of samples from high temperature T and pressure P_{eq}^T (300°C , P_{eq}^T) to 300°C ($T^\circ\text{K}$). The value of δs thus obtained was based upon the assumption that δs at 300°C is zero. Extrapolation of plot in Fig. 23 to 300°C gives $\delta s = 2.1 \times 10^{-10}$ at 300°C , which is negligible compared to δs at higher temperatures. Hence, no significant error is introduced in the measurement of δs at higher temperatures by assuming zero phase width at 300°C .

A least squares fit through experimental points in Fig. 23 gives the following values:

$$\overline{\Delta H}_{\text{CaO}} = 35.6 \text{ K cal. mole}^{-1}$$

$$\overline{\Delta S}_{\text{CaO}}^{\text{th}} = 21.8 \text{ cal. } ^{\circ}\text{K}^{-1} \text{ mole}^{-1}$$

using equation (35) and (36), and using the values for $\Delta H^{\circ}_{\text{d}}$ and $\Delta S^{\circ}_{\text{d}}$ obtained previously (page 31) we get

$$\overline{\Delta H}_{\text{CO}_2} = -76.47 \text{ K cal. mole}^{-1}$$

$$\overline{\Delta S}_{\text{CO}_2}^{\text{th}} = -56.8 \text{ cal. } ^{\circ}\text{K}^{-1} \text{ mole}^{-1}$$

6. Activity vs. Composition Isotherms: determination of exact compositions

We have derived, for $\text{CaO} \cdot (\text{CO}_2)_{1-\delta}$, in a previous section, the following equation (32):

$$\delta (P, T) = \exp \left[\frac{\overline{\Delta G}^{\circ \text{th}}_{\text{CO}_2}}{RT} \right] \frac{P^{\circ}}{P}$$

In the isothermal experiments discussed previously we measured ΔX_{CO_2} , the relative change in composition which results from changing the CO_2 pressure from a reference pressure P^* to the pressure P . This corresponds to

$$\Delta X_{\text{CO}_2} = - (\delta^* - \delta) \tag{45}$$

which, on using equation (32), gives

$$\begin{aligned} \Delta X_{\text{CO}_2}(P^*, P) &= P^{\circ} \exp \left[\frac{\overline{\Delta G}^{\circ \text{th}}_{\text{CO}_2}}{RT} \right] \left[\frac{1}{P^*} - \frac{1}{P} \right] \\ &= A \left[\frac{1}{P^*} - \frac{1}{P} \right] \end{aligned} \tag{46}$$

where $A = P^{\circ} \exp(\overline{\Delta G}^{\circ \text{th}}_{\text{CO}_2} / RT)$ is constant at a given temperature. Thus,

theory suggests $\Delta X_{CO_2}(P^*, P)$ to be inversely proportional to $\Delta(1/P)$ ($\equiv 1/P^* - 1/P$).

Figure 24 shows plots of $\log \Delta X$ vs $\log \Delta 1/P$ at several temperatures. They are, as predicted by the theory, linear within experimental accuracy. The least squares lines through experimental points for different temperatures give slopes ranging from 0.80 to 1.03, with an average slope of 0.95 ± 0.2 . Thus, it is concluded that within the experimental accuracy, the $P - \Delta X$ plots show an inverse pressure dependence as predicted by equation (32).

This fact enables calculation of exact compositions because according to equation (45),

$$\Delta X_{CO_2} = -(\delta^* - \delta)$$

and $\delta = A/P^*$, where $A = P^\circ \exp \left[\frac{\overline{\Delta G}_{CO_2}^{th}}{RT} \right]$.

Using value of $\overline{\Delta G}_{CO_2}^{th}$ obtained in the previous section, a value of δ^* was calculated for different temperatures and reference pressures. The $P - \Delta X_{CO_2}$ isotherms of Figs. 15 to 20 were replotted in terms of absolute compositions in Figs. 25-28, where the theoretical curves obtained by using equation (32) are also drawn. Only the reversible part of the isotherms have been replotted. Reasonable agreement is found between the theoretical curves and experimental data.

7. Partial Phase Diagram for the CaO-CaCO₃ System

Wyllie and Tuttle^{26,27} reported that a eutectic is formed in the CaO-Co₂ system at 1240°C with eutectic composition at $X_{CO_2} = 0.48$. The same eutectic has been reported by Smyth and Adams⁷ also at 1240°C, but they report the eutectic composition to be $X_{CO_2} \cong 0.25$.

The possibility that CaCO_3 may dissolve considerable CaO was not mentioned in either of the studies mentioned above. In fact, the phase diagram by Wyllie and Tuttle shows CaCO_3 to be a line phase throughout the temperature range. Extrapolation of the solubility limits found in the present study shows that at 900°C , $\delta_s = 1.2\%$. This value is in fair agreement with Tumarev's¹¹ value of $\delta_s = 2.1\%$ at 900°C , the only value previously reported for the solubility of CaO in CaCO_3 .

Extrapolating the solubility limits found at lower temperatures in this study to the eutectic temperature gives $\delta_s (1240^\circ\text{C}) = 0.42$. Thus, there is probably a very large departure from stoichiometry at the eutectic temperature.

In order to generate the phase diagram for the CaO-CaCO_3 binary system, one needs to know not only the solution limit of CaO in CaCO_3 , but also the solution limit of CO_2 in the CaO phase.

All experiments on the solubility of CO_2 in CaO(s) using the tensi-volumetric apparatus failed to show any measurable solution range for the CaO phase at 1000°K or below. The only other study of the solubility of CaCO_3 in CaO , that of Tumarev, et al.,¹¹ reports the solubility of CaCO_3 in CaO to be 4.2% at 1173°K , but Tumarev, et al., expressed doubts about the accuracy of their results.

Using the calculated values of δ_s at higher temperatures, the phase diagram for CaO-CO_2 system by Wyllie and Tuttle²⁶ has been modified in Fig. 29 to include the phase width of calcite. Since the extrapolated solubility of CaO in CaCO_3 is close to 42% at the eutectic temperature, the eutectic composition of Wyllie and Tuttle ($X_{\text{CO}_2} = 0.48$) does not seem to be correct. Smyth and Adam's value ($X_{\text{CO}_2} = 0.25$) is in better

agreement and therefore has been used in Fig. 29.

8. Non-isothermal Experiments

The amounts of calcite used in two different samples were 0.179 gms and 2.274 gms, respectively. These values give a ratio $\alpha_1/\alpha_2 = 12.7$ in Eq. 19, which requires α_1/α_2 to be large for successful results. The initial conditions used were (i) $P_0 = 7.0$ torr, $T_0 = 900^\circ\text{K}$, and (ii) $P_0 = 5.78$ torr, $T_0 = 900^\circ\text{K}$.

Figures 30 and 31 show the plots of $\ln N_{\text{CO}_2}$ vs. T obtained for both samples. It is obvious from these plots that the slopes $d \ln N/dT$ for the two samples are not different enough within the experimental accuracy limits, to warrant solution of Eq. 19. The reason this method failed at pressures used as initial conditions becomes obvious on examining the P - ΔX isotherm at 900°K (Fig. 18), which shows that $(\partial P/\partial X)_{900^\circ\text{K}}$ at $P = 7.0$ and $P = 5.78$ torrs is large enough to mask the effect of making α_1/α_2 no greater than 13.

Another experiment was done with the initial conditions being $T_0 = 973^\circ\text{K}$ and $P_0 = 25$ torrs. The result is plotted in Fig. 32. Again, there was no discernable difference in the slopes for two samples. It therefore seems that non-isothermal method fails when $(\partial P/\partial X)_T$ becomes very large, which was usually the case for the $\text{CaO}\cdot\text{CO}_2$ system, until the pressures are close to P_{eq} (Figs. 15 to 20).

The non-isothermal method is an intriguing method for studying nonstoichiometry, because it provides an independent measure of $\overline{\Delta H}$ for the gaseous component. This method would be a most useful approach for those systems where the static-vacuum, isothermal type experiments are not possible (especially at high temperatures, where static vacuum conditions are hard to achieve). The derivation of Eq. 19, which forms the basis for

this method is general, therefore Eq. 19 should apply to any binary system which vaporizes incongruently to yield only one significant gas phase component.

9. Studies on CaCO₃ Minerals

Calcite occurs in nature as sedimentary deposits formed by marine activity in and near oceans; as igneous rocks and as metamorphic rocks; as stalagmites and stalactites in caverns, etc. These different sources of CaCO₃ form at different pressures (activity of CO₂) and temperatures. It therefore seemed possible that they have significant differences in compositions. From the phase diagram generated in this study (Fig. 29), it is evident that calcite formed at low temperatures (<1000°K) and low pressures will be closely stoichiometric. The high pressures possible in metamorphic rocks formation might conceivably give rise to $\delta > 0$ in CaO·(CO₂)_{1+ δ} by forcing CO₂ to dissolve interstitially. Temperatures higher than 1000°K will favor formation of CaO·(CO₂)_{1- δ} with significant deviations from stoichiometry near eutectic temperatures, according to Fig. 29.

Table III shows that every specimen examined, except the metamorphic rock, gave $\Delta X_{\text{CO}_2} \sim 10^{-4}$ per mole of CaCO₃ before the pressure of CO₂ reached the decomposition limit at 773°K. This CO₂ release correlated closely with a surface monolayer decomposition and hence, determination of deviations from stoichiometry in the parent samples is not possible.

However, metamorphic calcite gave ΔX_{CO_2} about an order of magnitude larger than all other specimen, which corresponded to a surface decomposition of >4 monolayers. It is thus possible, that metamorphic rock has

a higher CO_2 content than all other samples studied. Chemical analysis gave a CaO/CO_2 molar ratio of 1.02 ± 0.01 (Table II), which is also larger than the CaO/CO_2 ratio for all other samples. (But the probable error in the chemical analysis is large enough to justify a quantitative deduction about the composition of the samples.)

Spectrographic analysis of metamorphic calcite (Appendix I) showed significant amounts of Mg (.63 mole%). Solution of MgCO_3 in CaCO_3 would alter the equilibrium decomposition pressure and this could also be the factor responsible for the evolution of CO_2 in amounts larger than other samples of calcite.

Two more explanations are possible for large CO_2 desorption observed on heating metamorphic calcite: (i) It reflects an excess of CO_2 , i.e. $\delta > 0$ in $\text{CaO} \cdot (\text{CO}_2)_{1+\delta}$ and which would be possible if P_{CO_2} during calcite formation is enormously large. Since the enthalpy and entropy changes associated with interstitial CO_2 defects in calcite is not known, quantitative correlations with this prediction are not possible. (ii) It reflects an infinitesimal decomposition of calcite, if conditions of formations were such that metamorphic calcite had a significant substoichiometric composition ($\delta < 0$) frozen in due to rapid cooling. In such a case, heating calcite of such a nature places it in the 2-phase field ($\text{CaO}-\text{CaCO}_3$) at lower temperatures as compared to equilibrium composition calcite. The reaction $\text{CO}_3^{--} \rightarrow \text{O}^{--} + \text{CO}_2(\text{g})$ at sites adjacent to Mg^{++} ions in the calcite phase seems to be the most probable reason for the high CO_2 evolution from the metamorphic rock sample.

It will be desirable to obtain calcite quenched from the eutectic temperature in the presence of CaO and to measure its composition as a

check of the analysis presented in this work. Calcite crystallizing from a high temperature melt ($T > 2000^\circ\text{K}$) will not show significant departure from stoichiometry because the maximum melting point of CaCO_3 phase seems to occur at composition very close to stoichiometry (Fig. 29), which is generally the case for binary solid phases.²⁸

IV. CONCLUSIONS

The tensi-volumetric method is found to be well suited for studying nonstoichiometry in binary solid phases of narrow composition range when only one component is volatile. This method is especially suited for a study of the $\text{CaO} \cdot (\text{CO}_2)_{1-\delta}$ system for which deviations from stoichiometry as small as $\delta = 4 \times 10^{-5}$ have been measured.

The defect responsible for departure from stoichiometry appears to be O^{--} ions on the CO_3^{--} sublattice of calcite. A thermodynamic analysis of substantial defects on sublattices predicts the saturation value of degree of nonstoichiometry to be exponentially dependent upon temperature.

Calcite is very closely stoichiometric at low temperatures. The departure from stoichiometry is less than .1% at $T=1000^\circ\text{K}$, but increases (as predicted) exponentially with temperature and reaches 42% at the CaO-CaCO_3 eutectic temperature (1240°C).

The thermodynamic analysis also suggests that isothermal change in composition is inversely proportional to the CO_2 activity.

The solution of O^{--} in CO_3^{--} sublattice occurs with large changes in partial molal heats and entropies for the components, indicating strong interactions, even for dilute solution. The values for partial molal enthalpies are $\overline{\Delta H}_{\text{CaO}} = 35.6 \text{ Kcals mole}^{-1}$, $\overline{\Delta H}_{\text{CO}_2} = -76.5 \text{ Kcals mole}^{-1}$. Partial molal entropies are $\overline{\Delta S}_{\text{CaO}} = 21.8 \text{ eu mole}^{-1}$ and $\overline{\Delta S}_{\text{CO}_2} = -56.8 \text{ eu mole}^{-1}$.

CaCO_3 seems to form a stable monolayer (or less) of O^{--} on its surface, giving rise to appreciable CO_2 desorption prior to decomposition. For powder specimens this irreversible surface effect releases more CO_2 at temperatures below 1000°K than are released and resorbed by bulk compositional changes.

Variations in CO_2 contents of CaCO_3 specimens from several mineralogical sources were too small to measure by the sensitive apparatus used in this study, except for a sample of metamorphic rock. This specimen released a significantly higher quantity of CO_2 , but the CO_2 release may have been a consequence of conversion of CO_3^{--} near dissolved Mg^{++} to $\text{O}^{--} + \text{CO}_2$.

REFERENCES

1. R. A. Swalin, Thermodynamics of Solids, 2nd ed., p. 319, John Wiley and Sons, New York (1973).
2. E. A. Guggenheim, Thermodynamics, North-Holland Publishing Co., Amsterdam, 1949.
3. F. A. Kröger, The Chemistry of Imperfect Crystals, Vol. 2, 2nd ed., North-Holland Publishing Co., Amsterdam (1974).
4. James A. Roberts, Jr., High Temperature Mass Spectrometry, Ph.D. Thesis, University of California, Berkeley, 1974.
5. A. W. Searcy and D. J. Meschi, in Thermodynamics of Nuclear Materials International Atomic Energy Agency, Proceedings series, Vienna (1962).
6. Jay D. Ewing, Effect of CO₂ on the Oxide Decomposition Products of Calcite, M.S. Thesis, University of California, Lawrence Berkeley Laboratory (1978).
7. F. H. Smyth and L. H. Adams, J. Am. Chem. Soc., 45, 1167 (1923).
8. E. H. Baker, J. Chem. Soc., pp. 464-70 (1962).
9. J. Zawadzki, et al., Trans. Faraday Soc., 34 951 (1938).
10. D. Young, Decomposition of Solids, Pergamon Press, New York (1966).
11. A. A. Baikov and A. C. Tumarev, Dokl. Akad. Nauk SSSR 4 565 (1937).
12. D. Zavriev, XPOΦXO (Russian) 40, 543, 726 (1908), and 41, 34 (1909).
13. C. K. Chuchmarev, et al., Dokl. Akad. Nauk SSSR 91 1115 (1953).
14. C. G. Maier and C. T. Anderson, Jour. Am. Chem. Soc., 56, 513 (1934).
15. N. G. Schmahl, Z. Electrochem, 47, 821 (1941).
16. W. Biltz and H. Muller, Z. Anorg. Allg. Chem. 163, 257 (1927).
17. G. G. Libowitz and R. P. Gibb, Jr., J. Phys. Chem., 61, 793 (1957).

18. K. H. Stern and E. L. Weise, NBS Report No. NSRDS-NB530 (1969).
19. G. G. Libowitz, in Treatise on Solid State Chem., Vol. 1, Ch. 6, Ed. B. Hannay, Plenum Press, NY (1975).
20. F. A. Kroger, et al., Philips Research Reports, 14, 557 (1959).
21. C. Wagner and W. Schottky, Z. Physik, Chem., B, 11, 163 (1930).
22. R. A. Swalin, Thermodynamics of Solids, 2nd ed., P. 263, John Wiley and Sons, New York (1973).
23. Surface Chem., Somorjai, John Wiley & Sons.
24. A. W. Searcy in Chemical and Mechanical Behavior of Inorganic Solids, Wiley Interscience, New York (1970).
25. C. Kittel, Introduction to Solid State Physics, 5 ed., John Wiley and Sons, New York (1976).
26. P. J. Wyllie and O. F. Tuttle, Jour. Petrol, 1 [1], pp. 1-46 (1960).
27. P. J. Wyllie, Jour. Am. Cer. Soc., 50 [1], 43 (1967).
28. R. F. Brebrick, in Progress in Solid State Chem., Ch. 5, Vol. 3, Ed. H. Reiss, Pergamon Press, New York (1967).
29. A. Waddington, Advances in Inor. and Rad. Chem., 1 204 (1959).
30. K. K. Kelly and E. G. King, Bureau of Mines, Bull. 592 (1961).

Table I. Major Ion Fragments and Their Appearance Potentials CO₂, N₂ and H₂O

Species	Fragment (in the order of decreasing importance)	Mass A.M.U.	A.P.*
CO ₂	CO ₂ ⁺	44	13.79
	CO ⁺	28	18.5
	O ⁺	16	19.7±0.4
N ₂	N ₂ ⁺	28	15.55
	N ⁺	14	23.0-24.6
H ₂ O	H ₂ O ⁺	18	12.61
	OH ⁺	17	18.0
	O ⁺	16	18.9±0.5

* Taken from "Electron Impact Phenomena," F. H. Field and J. L. Franklin, Academic Press Inc., NY, 1957.

Table II. Ca/C ratio for Different Sources of Calcite

Sample	Ca wt. %	C wt. %	CaO/CO ₂ molar ratio
Baker analyzed powder	40.02	12.00	0.988 ± 0.01
Single crystal #1	39.94	11.94	1.002 ± 0.01
Single crystal #2	40.12	12.07	0.996 ± 0.01
Single crystal #3	40.05	12.01	0.999 ± 0.01
Granular #14 mesh crystals	39.95	11.99	1.001 ± 0.01
Metamorphic* calcite	39.69	11.70	1.02 ± 0.01

* Small residue obtained on dissolving in HCl.

Table III. Correlation of Amount of CO₂ Released with Fraction of Surface Layer Desorption

Sample	Preparation Technique	Heat Treatment	Specific Surface Area m ² g ⁻¹	Number of Monolayers Corresponding to Observed Desorption	ΔX_{CO_2} moles CO ₂ /Mole CaCO ₃
Iceland spar	Hand ground in CCl ₄	Heated to 784°K in vacuum	0.42	0.67	2x10 ⁻⁴
Iceland spar	Hand ground in air	Heated to 750°K in vacuum	0.25	1.35	3.3x10 ⁻⁴
Baker analyzed Calcite	-	Heated to 770°K in vacuum	0.67	0.74	4.2x10 ⁻⁴
Baker analyzed Calcite	-	Heated to 873°K under imposed P _{CO₂} = 2.0 torrs	0.67	2.7	1.6x10 ⁻³
Iceland spar	Granular mesh #14 size	Heated to 873°K under imposed P _{CO₂} = 2.0 torrs	0.001	330	2.0x10 ⁻⁴
Metamorphic rock	Ground in CCl ₄	Heated to 774°K in vacuum	0.35	4.5	1.7x10 ⁻³

APPENDIX I

1. Semiquantitative spectrographic analysis for Iceland Spar

Element	Percent (reported as oxide)		
	Sample #1	Sample #2	Sample #3
Ca	Principal element	Principal element	Principal element
Sr	.003	.008	<.003
Mg	.05	.015	.025
Ba	-	-	-
Na	-	-	-
K	-	-	-
Fe	-	-	.003
Cu	.001	<.001	<.001
Si	.02	<.008	0.025
Mn	-	.002	-
Al	.002	.001	.003

2. Semiquantitative analysis of metamorphic calcite

Element	Percent (reported as oxide)
Ca	Principal constituent
Si	1.5
Mg	0.15
Al	.04
Fe	.04
Ti	.008
Cr	.002
Sr	.002
Mn	.002
Ba	.002
Cu	<.001

APPENDIX II

Calcite (CaCO_3) JCPDS* Number 5-0586

d	I/I ₁	2θ (CuKα)
3.86	12	23.0
3.035	100	29.4
2.845	3	31.4
2.495	14	36.0
2.285	18	39.4
2.095	18	43.2
1.927	5	47.1
1.913	17	47.5
1.875	17	48.5
1.626	4	56.5
1.604	8	57.4

Calcium oxide (CaO) JCPDS Number 4-0777

d	I/I ₁	2θ (CuKα)
2.778	34	32.2
2.405	100	37.4
1.701	45	53.9
1.451	10	64.1
1.390	5	67.3
1.203	4	79.9
1.1036	4	88.5
1.0755	9	91.5

Calcium hydroxide (Ca(OH)_2) JCPDS Number 4-0733

d	I/I ₁	2θ (CuKα)
4.90	74	18.1
3.112	27	28.6
2.628	100	34.1
1.927	42	47.1

APPENDIX II (Continued)

Calcium hydroxide ($\text{Ca}(\text{OH})_2$) JCPDS* Number 4-0733

1.796	36	50.8
1.687	21	54.3
1.484	13	62.5
1.449	13	64.2

Argonite (CaCO_3) JCPDS* Number 24-0025

d	I/I ₁	2θ (CuKα)
3.396	100	26.2
1.976	77	45.9
3.273	58	27.2
2.700	50	33.1
2.372	39	37.9
1.881	34	48.4
1.814	34	50.2
1.742	32	52.5
2.106	28	42.9

* Joint Committee on Powder Diffraction Standards

APPENDIX III

Characteristics of 'Baker analyzed' Calcite Powder

1. Surface area = $0.67 \text{ m}^2 \text{ g}^{-1}$
2. Particle size = 3-5 μm
3. Spectrographic semi-quantitative analysis

Element	Percent (reported as oxide)
Ba	0.002
Pb	0.0005
Fe	<0.0005
Mg	0.001
Sr	0.005
K	0.008
Na	0.006
Si	-
Ca	major constituent

4. Particle shape: rhombohedral (See Fig. 13)
5. Ca/C ratio (by combustion and wet chemical analysis)

$$\text{Ca/C} = 3.2965 \text{ (theoretical stoichiometric ratio} = 3.337)$$

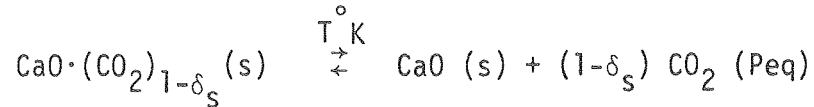
$$\% \text{ deviation from stoichiometry} = 1.2 \pm 1\%$$

APPENDIX IV

Alternate derivation of Equation V (33):

$$\delta_s = \exp \left[\frac{\Delta G_d^\circ + \overline{\Delta G}_{CO_2}^{th}}{RT} \right] \quad \text{IV -(1)}$$

Consider the decomposition reaction



At equilibrium, $\Delta G = 0$ for the above reaction. Writing ΔG as the difference in free energies of the products and reactant, we have

$$0 = \Delta G = (1-\delta_s) RT \ln a_{CO_2}(eq)/a_{CO_2}^\circ - \Delta G_f \quad \text{IV -(2)}$$

where ΔG_f refers to the free energy of formation of $CaO \cdot (CO_2)_{1-\delta_s}$ from $CaO (s)$ and $CO_2 (g)$ in their standard states. Writing ΔG_f in terms of the partial molal free energies of the components, we get

$$\Delta G_f = \overline{\Delta G}_{CaO} + (1-\delta_s) \overline{\Delta G}_{CO_2} \quad \text{IV -(3)}$$

since the decomposition reaction occurs at the $CaO - CaCO_3$ phase boundary, the activity of CaO is equal in $CaO (s)$ and $CaO \cdot (CO_2)_{1-\delta_s}$, giving $\overline{\Delta G}_{CaO} = 0$. $\overline{\Delta G}_{CO_2}$ can be divided into thermal and configurational parts. Thus, IV -(3) becomes

$$\Delta G_f = (1-\delta_s) \Delta G_{CO_2} = (1-\delta_s) \left[\overline{\Delta G}_{CO_2}^{conf} + \overline{\Delta G}_{CO_2}^{th} \right] \quad \text{IV -(4)}$$

$\overline{\Delta G}_{CO_2}^{conf}$ can be calculated from the configurational free energy of mixing of CO_3^{--} and O^{--} ions on the anionic sublattice, which is

$$\Delta G_{\text{conf}} = RT \left[n_{\text{CO}_3^{--}} \ln \frac{n_{\text{CO}_3^{--}}}{n_{\text{O}^{--}} + n_{\text{CO}_3^{--}}} + n_{\text{O}^{--}} \ln \frac{n_{\text{O}^{--}}}{n_{\text{O}^{--}} + n_{\text{CO}_3^{--}}} \right] \quad \text{IV -(5)}$$

where $n_{\text{O}^{--}}$ and $n_{\text{CO}_3^{--}}$ are the number of moles of O^{--} and CO_3^{--} ions respectively, the total number of anionic sites being $(n_{\text{O}^{--}} + n_{\text{CO}_3^{--}})$. The number of moles of components, n_{CaO} and n_{CO_2} are related to $n_{\text{O}^{--}}$ and $n_{\text{CO}_3^{--}}$ by

$$n_{\text{CO}_3^{--}} = n_{\text{CO}_2}$$

$$n_{\text{O}^{--}} = n_{\text{CaO}} - n_{\text{CO}_2}$$

from which we get $n_{\text{CaO}} = n_{\text{O}^{--}} + n_{\text{CO}_3^{--}}$. Rewriting Eq. (5) in terms of new variables, n_{CaO} and n_{CO_2} , we get

$$\Delta G_{\text{conf}} = RT \left[n_{\text{CO}_2} \ln \frac{n_{\text{CO}_2}}{n_{\text{CaO}}} + (n_{\text{CaO}} - n_{\text{CO}_2}) \ln \frac{n_{\text{CaO}} - n_{\text{CO}_2}}{n_{\text{CaO}}} \right] \quad \text{IV -(6)}$$

Differentiating IV -(6) with respect to n_{CO_2} , keeping n_{CaO} , T, P constant and simplifying, we get

$$\bar{\Delta G}_{\text{CO}_2}^{\text{conf}} = \left. \frac{\partial \Delta G_{\text{conf}}}{\partial n_{\text{CO}_2}} \right|_{n_{\text{CaO}}, T, P}$$

or,

$$\bar{\Delta G}_{\text{CO}_2}^{\text{conf}} = RT \ln \frac{n_{\text{CO}_2}}{n_{\text{CaO}} - n_{\text{CO}_2}} \quad \text{IV -(7)}$$

substituting $n_{\text{CO}_2} = 1 - \delta_s$, $n_{\text{CaO}} - n_{\text{CO}_2} = n_{\text{O}} = \delta_s$,

we get,

$$\overline{\Delta G}_{\text{CO}_2}^{\text{conf}} = RT \ln \frac{1 - \delta_s}{\delta_s} = -RT \ln \frac{\delta_s}{1 - \delta_s}. \quad \text{IV - (8)}$$

Hence, using equations (2), (4) and (8), we get

$$\Delta G = 0 = (1 - \delta_s) RT \ln \frac{a_{\text{CO}_2(\text{eq})}}{a_{\text{CO}_2}^\circ} - (1 - \delta_s) \overline{\Delta G}_{\text{CO}_2}^{\text{th}} + (1 - \delta_s) RT \ln \frac{\delta_s}{1 - \delta_s}$$

simplifying this equation, we get

$$RT \ln \frac{\delta_s}{1 - \delta_s} = -RT \ln \frac{a_{\text{CO}_2(\text{eq})}}{a_{\text{CO}_2}^\circ} + \overline{\Delta G}_{\text{CO}_2}^{\text{th}} \quad \text{IV - (9)}$$

However, the standard free energy of decomposition, ΔG_d is equal to $\Delta G_d^\circ = -RT \ln \frac{a_{\text{CO}_2(\text{eq})}}{a_{\text{CO}_2}^\circ}$; substituting it in equation (9), we get

$$RT \ln \left[\frac{\delta_s}{1 - \delta_s} \right] = \Delta G_d^\circ + \overline{\Delta G}_{\text{CO}_2}^{\text{th}}$$

and since $\delta_s \ll 1$, we get

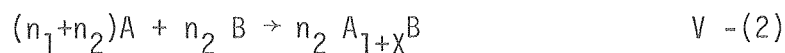
$$\delta_s \cong \exp \left[\frac{\Delta G_d^\circ + \overline{\Delta G}_{\text{CO}_2}^{\text{th}}}{RT} \right]$$

which is the same as equation (33) in the text, which was derived using the condition of minimization of the free energy of nonstoichiometric $\text{CaO} \cdot \text{CO}_2$, while the above derivation is based upon condition of equilibrium at the phase boundary.

APPENDIX V

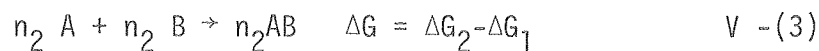
Proof of the assertion that $\overline{\Delta G}_A$ in $A_{1+\chi}B$ is independent of the choice of the second component (B or AB):

Formation of $A_{1+\chi}B$ can be described by two reaction involving components A and B, or A and AB:



Suppose the free energy changes accompanying reaction V-1 and V-2 are ΔG_1 , and ΔG_2 , respectively.

Subtracting (1) from (2) gives



however, from V-3, we see that the reaction corresponds to formation of AB from A and B, hence

$$\Delta G_2 - \Delta G_1 = n_2 \Delta G_f \quad V-(4)$$

where ΔG_f is the Gibbs free energy of formation of AB from A and B, per mole of AB.

Now, for reaction V-1, $\overline{\Delta G}_A$, by definition, is

$$\overline{\Delta G}_A = \left. \frac{\partial \Delta G_1}{\partial n_1} \right|_{n_2, T, P} \quad V-(5)$$

but $\Delta G_1 = \Delta G_2 - n_2 \Delta G_f$ according to V-(4).

Hence, V -(5) becomes

$$\begin{aligned} \overline{\Delta G}_A &= \frac{\partial [\Delta G_2 - n_2 \Delta G_f]}{\partial n_1} \Bigg|_{n_2, T, P} \\ &= \frac{\partial \Delta G_2}{\partial n_1} \Bigg|_{n_2, T, P} - \frac{\partial n_2 \Delta G_f}{\partial n_1} \Bigg|_{n_2, T, P} \end{aligned} \quad V -(6)$$

the second term on the R.H.S. of equation (6) is zero, as $n_2 \Delta G_f$ is independent of n_1 . Hence,

$$\overline{\Delta G}_A = \frac{\partial \Delta G_2}{\partial n_1} \Bigg|_{n_2, T, P} \quad V -(7)$$

But, since n_2 is constant in the partial differential on the right hand side of equation 7,

$$\frac{\partial n_1}{\partial n_1} \Bigg|_{n_2} \equiv \frac{\partial (n_1 + n_2)}{\partial (n_1 + n_2)} \Bigg|_{n_2}, \text{ giving}$$

$$\overline{\Delta G}_A = \frac{\partial \Delta G_2}{\partial (n_1 + n_2)} \Bigg|_{n_2, T, P} \quad V -(8)$$

Now, considering equation V -(2), the partial molal Gibbs free energy of A, $\overline{\Delta G}'_A$ (where the primed superscript shows that this partial molal value is with respect to B as the second component) is

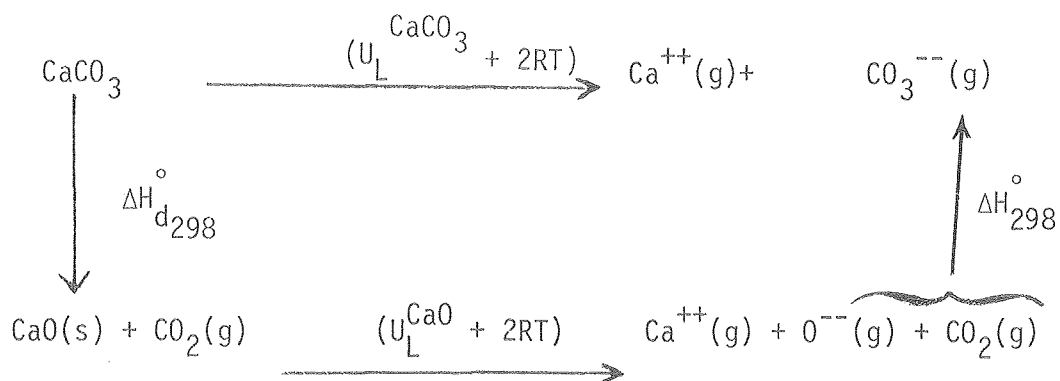
$$\overline{\Delta G}'_A = \frac{\partial \Delta G_2}{\partial (n_1 + n_2)} \Bigg|_{n_2, T, P} \quad V-(9)$$

Comparing equations (8) and (9), we obtain $\overline{\Delta G}_A = \overline{\Delta G}'_A$, i.e., the partial molal free energy of A is the same, whether B or AB is chosen as the second component.

APPENDIX VI

Calculation of the enthalpy of formation of $\text{CO}_3^{--}(\text{g})$ from $\text{CO}_2(\text{g})$ and $\text{O}^{--}(\text{g})$

Consider a Born-Haber cycle:



where U_L = lattice energy

ΔH_d° = enthalpy of decomposition

ΔH_{298}° = enthalpy of formation of $\text{CO}_3^{--}(\text{g})$ from $\text{CO}_2(\text{g})$ and $\text{O}^{--}(\text{g})$.

Thus, we get

$$U_L(\text{CaCO}_3) + 2RT = \Delta H_{d298}^\circ + U_L(\text{CaO}) + 2RT + \Delta H_{298}^\circ$$

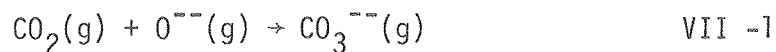
hence,
$$\Delta H_{298}^\circ = -U_L^{\text{CaO}} + U_L^{\text{CaCO}_3} - \Delta H_{d298}^\circ$$

Following values are used:

Quantity	Value K Cals mole ⁻¹	Reference
$U_L(\text{CaO})$	828	(29)
$U_L(\text{CaCO}_3)$	701	(29)
$U_L(\text{CaCO}_3)$	714	(29)
ΔH_{d298}°	42.61	(18)

which gives $\Delta H_{298}^\circ = -169.6$ or -156.6 K Cals mole⁻¹.

Thus, ΔH° for the reaction



is $\Delta H_{298}^\circ = -163.1 \pm 6.5 \text{ K Cals mole}^{-1}$, taking the average of the two possible values estimated above. The enthalpy change at a temperature other than 298°K can be estimated, if we assume gases to be ideal and write for reaction VII-1,

$$\begin{aligned} \Delta C_p &= \Delta C_v - R = C_p(\text{CO}_3^{--}(\text{g})) - C_p(\text{O}^{--}(\text{g})) - C_p(\text{CO}_2(\text{g})) + R \\ &\cong 6R - 3/2 R - 5/2 R - R \\ &\cong -R \end{aligned}$$

hence, $\Delta H_T^\circ = \Delta H_{298}^\circ - R (T-298)$

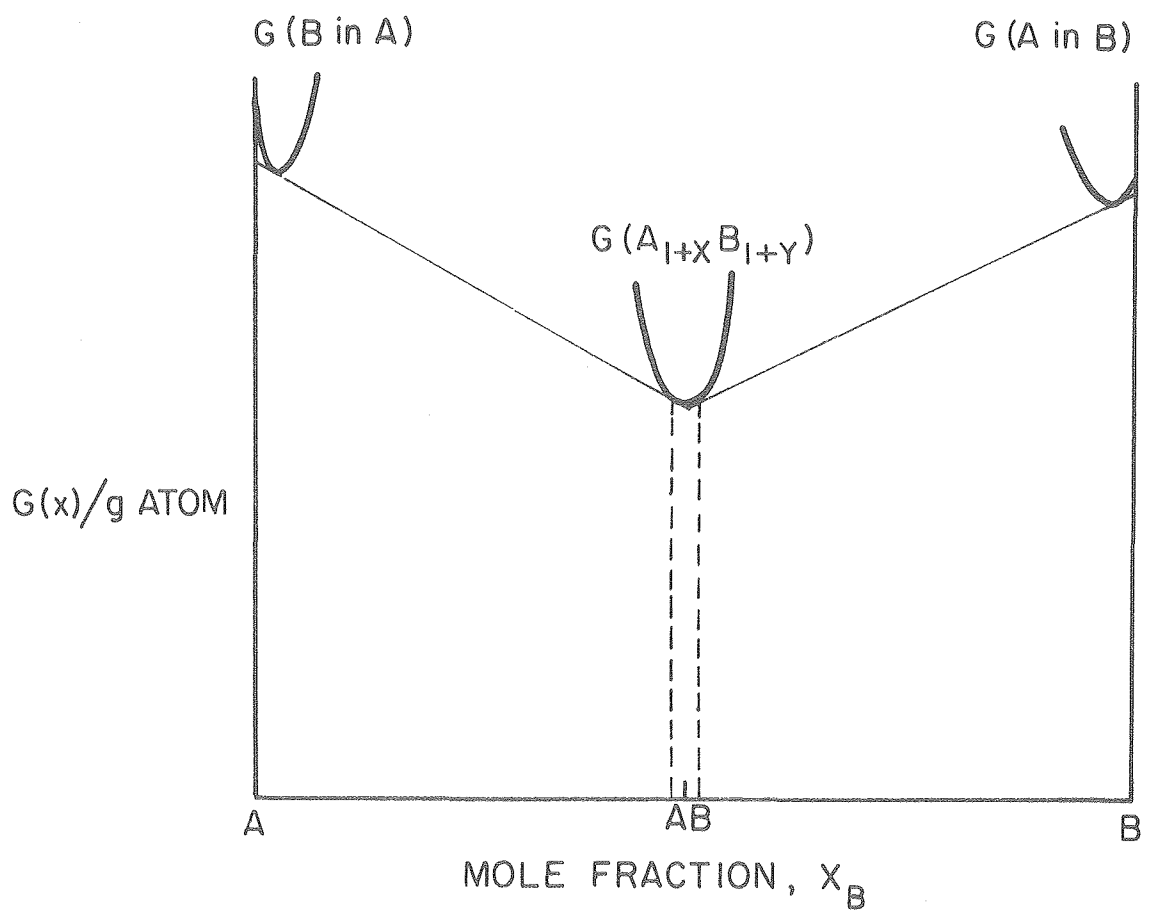
e.g. at $T = 900^\circ\text{K}$,

$$\Delta H_{900}^\circ \cong -164.2 \pm 6.5 \text{ K Cals mole}^{-1}$$

FIGURE CAPTIONS

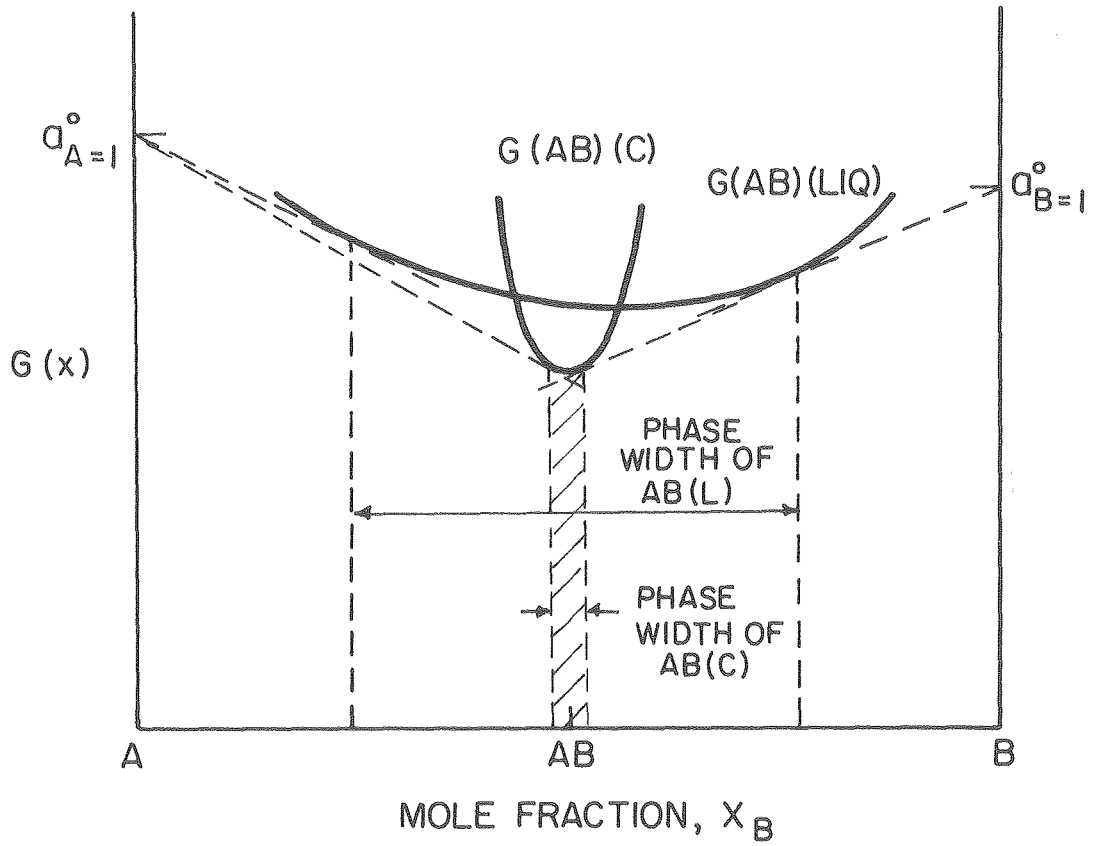
- Fig. 1. Schematic Gibbs free energy vs. composition diagram for a two component system exhibiting only one intermediate phase.
- Fig. 2. Schematic Gibbs free energy vs. composition diagram for a two component system A-B, illustrating phase field width of AB(c) and AB(l), as determined by tangency rule.
- Fig. 3. Schematic plot of Gibbs free energy G of $\text{CaO} \cdot (\text{CO}_2)_{1+\delta}$ vs. composition illustrating phase boundary, as determined by CaO of unit activity.
- Fig. 4. Layout of tensi-volumetric apparatus.
- Fig. 5. Detailed diagram of furnace, quartz tube and specimen holder assembly.
- Fig. 6. Diagram of gas burette assembly.
- Fig. 7. Schematic representation of tensi-volumetric apparatus as a two-temperature zones system for volume calibration. j_1 and j_2 are molecular fluxes in the direction of arrows indicated.
- Fig. 8. Effective volume as a function of furnace temperature — theoretical curves and experimental points.
- Fig. 9. Equilibrium CO_2 pressure vs. temperature plot for calcite decomposition.
- Fig. 10. RGA calibration data for CO_2/N_2 mixtures.
- Fig. 11. RGA calibration data for $\text{CO}_2/\text{H}_2\text{O}$ mixtures.
- Fig. 12. Scanning electron micrograph of hand crushed Iceland spar crystals.
- Fig. 13. Scanning electron micrograph of 'Baker analyzed' calcite powder.

- Fig. 14. Optical micrograph of granular calcite. Background grid size is $1/8'' \times 1/8''$.
- Fig. 15. Pressure, P_{CO_2} vs. change in CO_2 content, ΔX_{CO_2} of calcite at 773°K for hand-ground sample.
- Fig. 16. P_{CO_2} vs. ΔX_{CO_2} for 'Baker analyzed' calcite powder at 773°K .
- Fig. 17. P_{CO_2} vs. ΔX_{CO_2} for 'Baker analyzed' calcite powder at 900°K .
- Fig. 18. P_{CO_2} vs. ΔX_{CO_2} for granular calcite at 900°K .
- Fig. 19. P_{CO_2} vs. ΔX_{CO_2} for granular calcite at 973°K .
- Fig. 20. P_{CO_2} vs. ΔX_{CO_2} for granular calcite at 1000°K .
- Fig. 21. Dependence of deviation from stoichiometry, δ , upon the activity of component B, according to equation 22 in the text.
- Fig. 22. Dependence of phase-boundary value, δ_s , upon temperature for 'Baker analyzed' calcite powder.
- Fig. 23. Arrhenius plot of δ_s vs. $1/T$ for different samples of calcite of low surface area.
- Fig. 24. Log-log plot of total absolute change in concentration of CO_2 , ΔX_{CO_2} vs. total absolute change in inverse of P_{CO_2} , $\Delta 1/P$.
- Figs. 25-28. Plots showing deviation from stoichiometry, ΔX_{CO_2} vs. P_{CO_2} as predicted by equation 32 in the text, and experimental points obtained. 0 on composition axis corresponds to the stoichiometric value.
- Fig. 29. Partial phase diagram of CaO-CaCO_3 system, showing extrapolated values of non-stoichiometry at higher temperatures.
- Figs. 30-32. Plots of $\ln n_{\text{CO}_2}$ vs. furnace temperature T_F for two different samples used in non-isothermal experiment, with various initial condition of P_o, T_o .



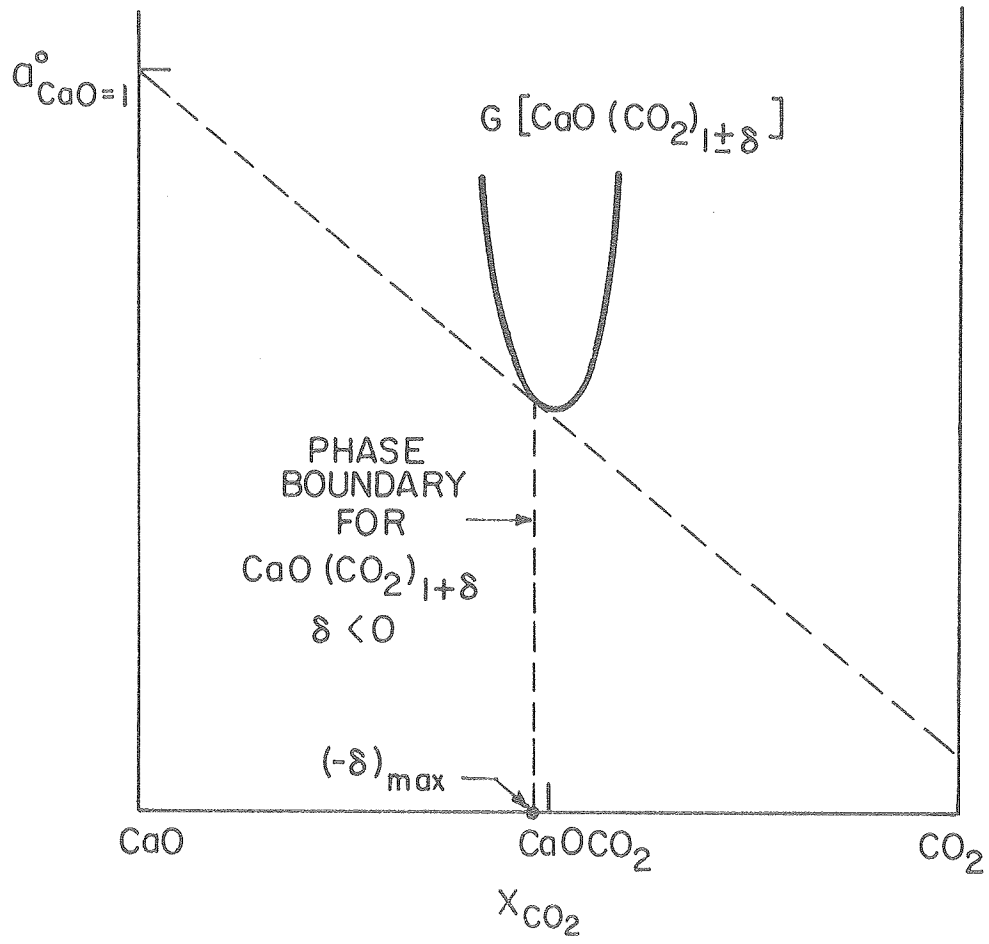
XBL 797-6694

Fig. 1



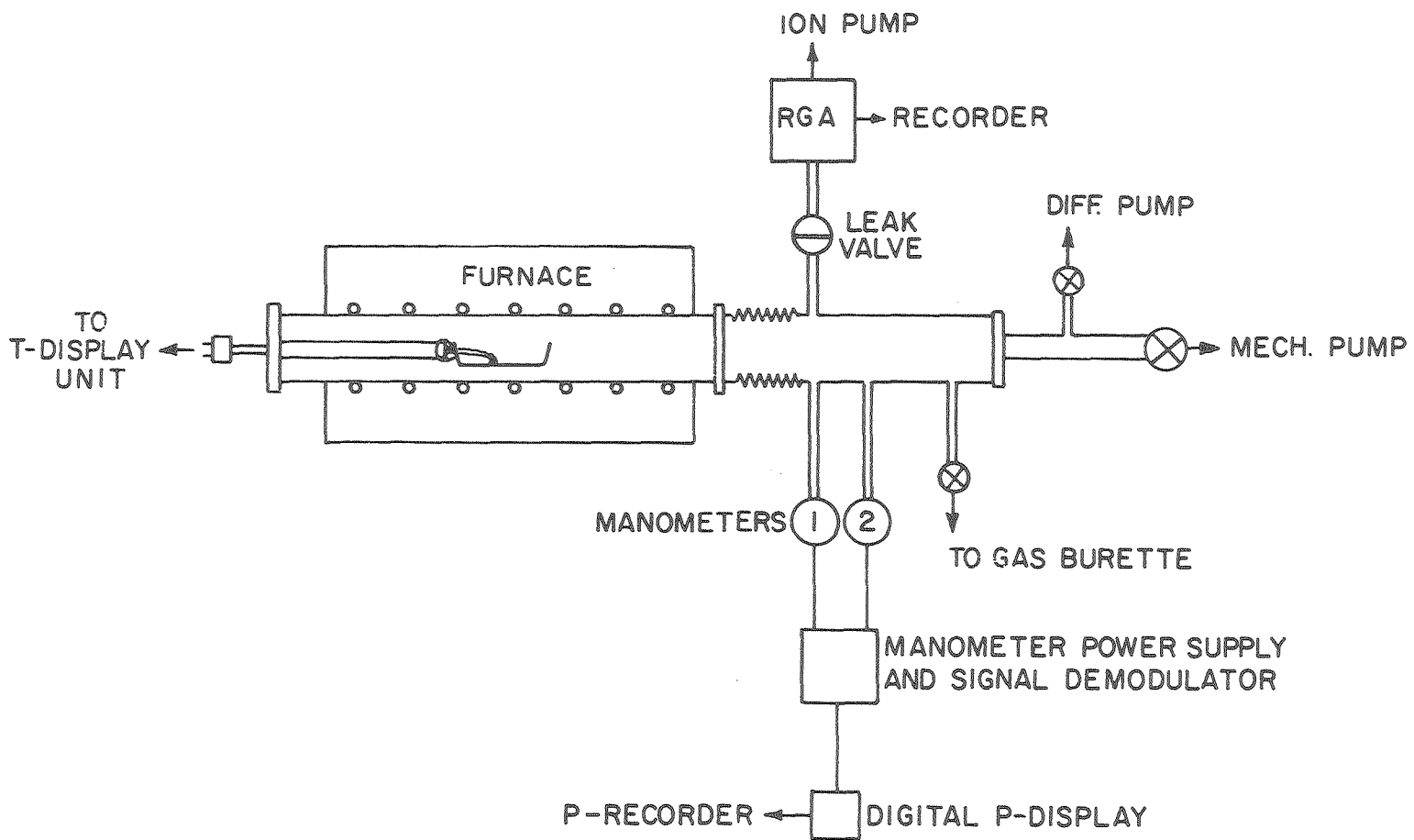
XBL 797-6695

Fig. 2



XBL797-6696

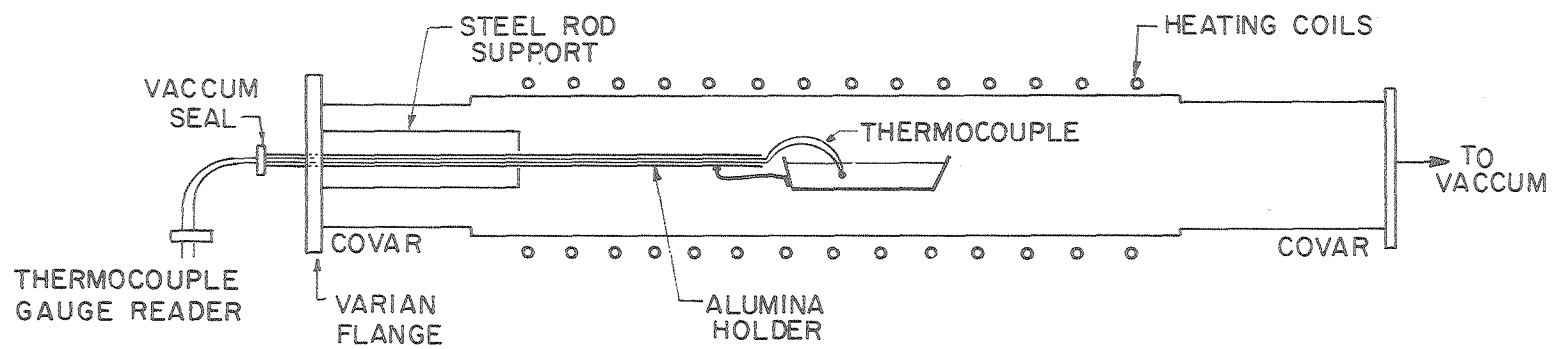
Fig. 3



-77-

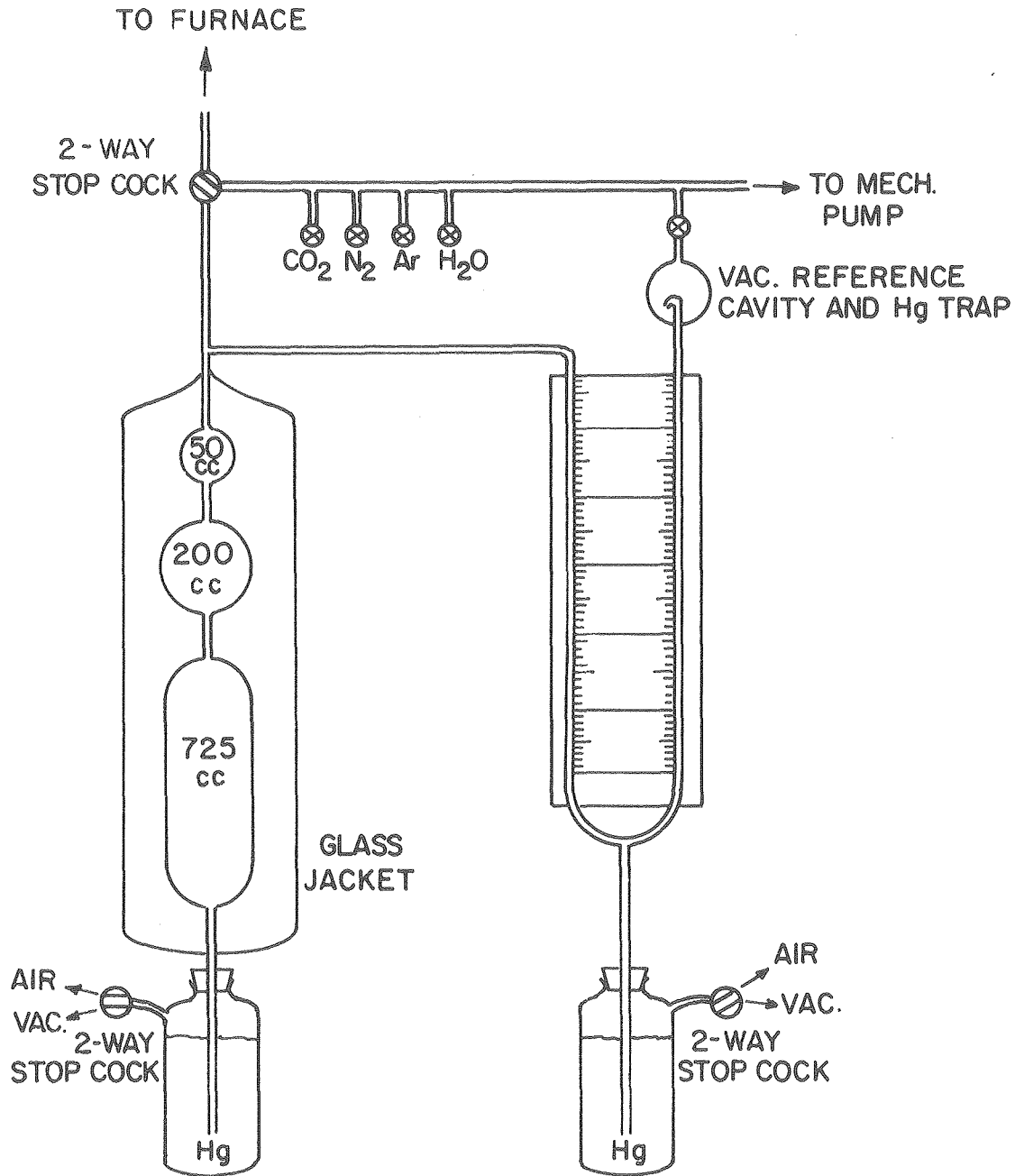
XBL 797-6508

Fig. 4



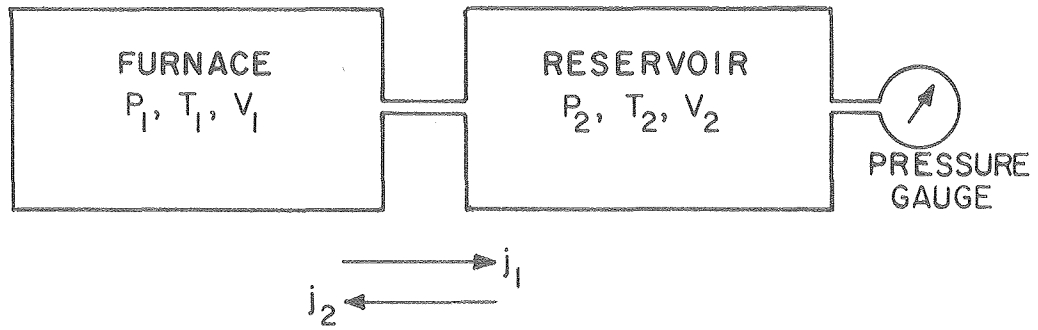
XBL 797-6509

Fig. 5



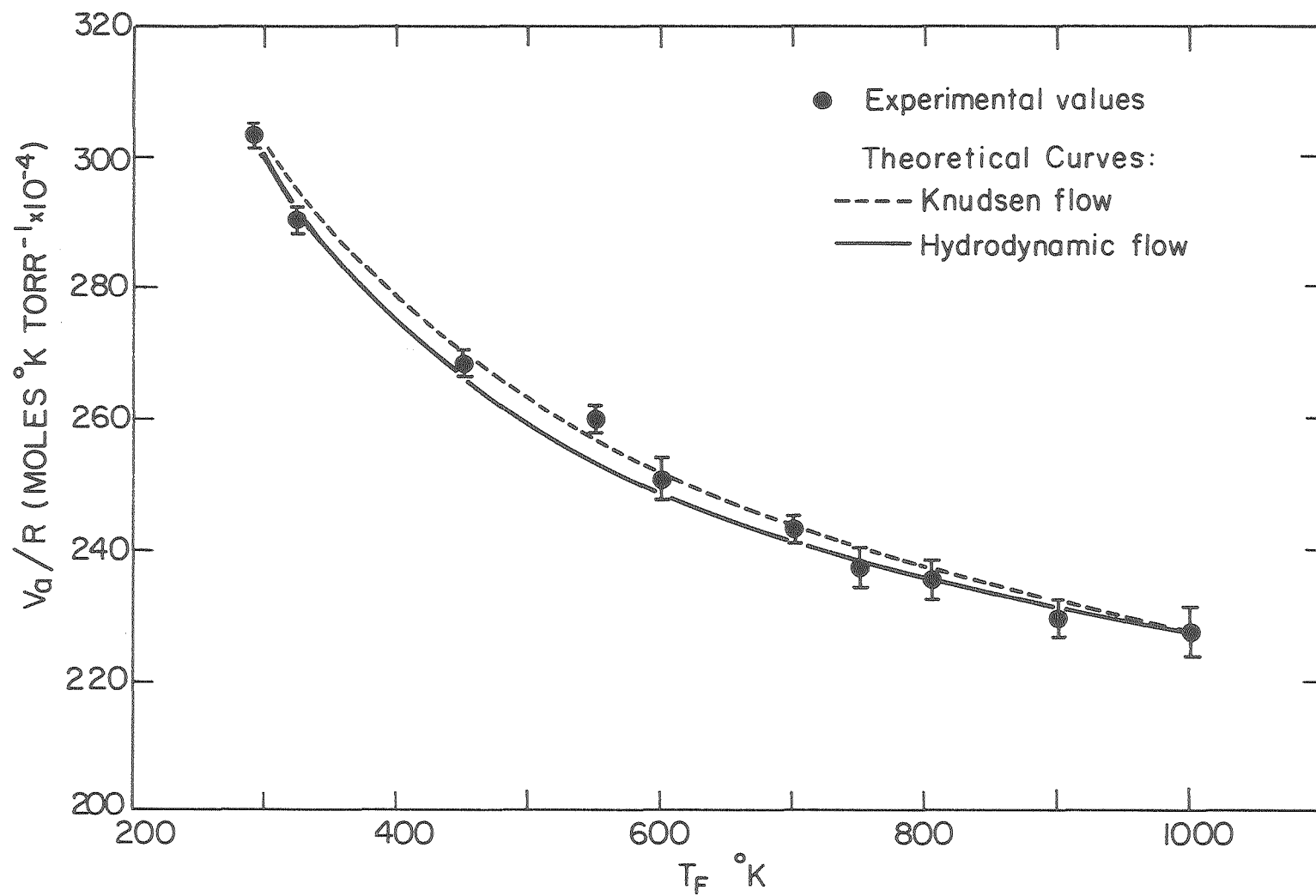
XBL 797 - 6510

Fig. 6



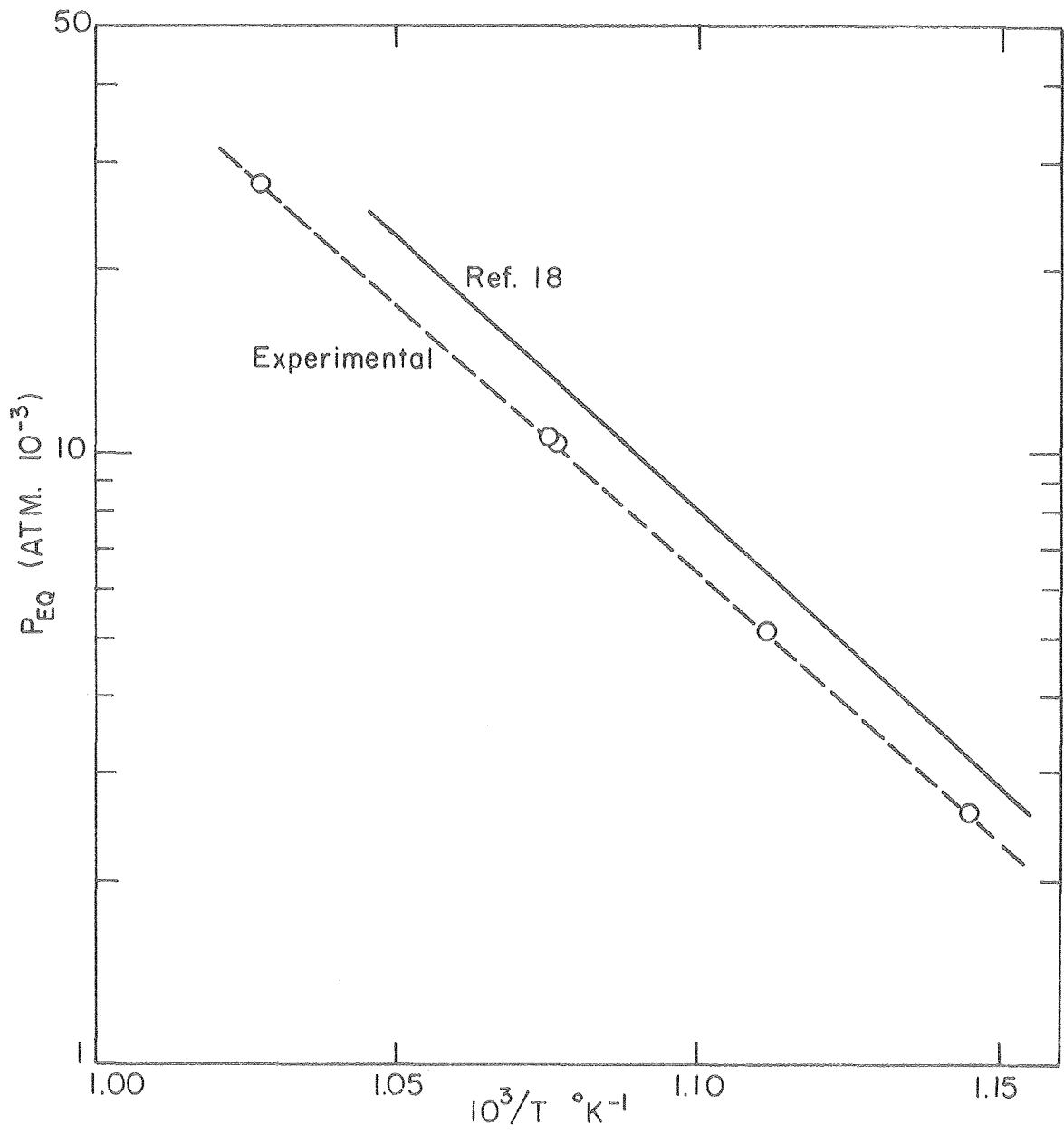
XBL 797-6511

Fig. 7



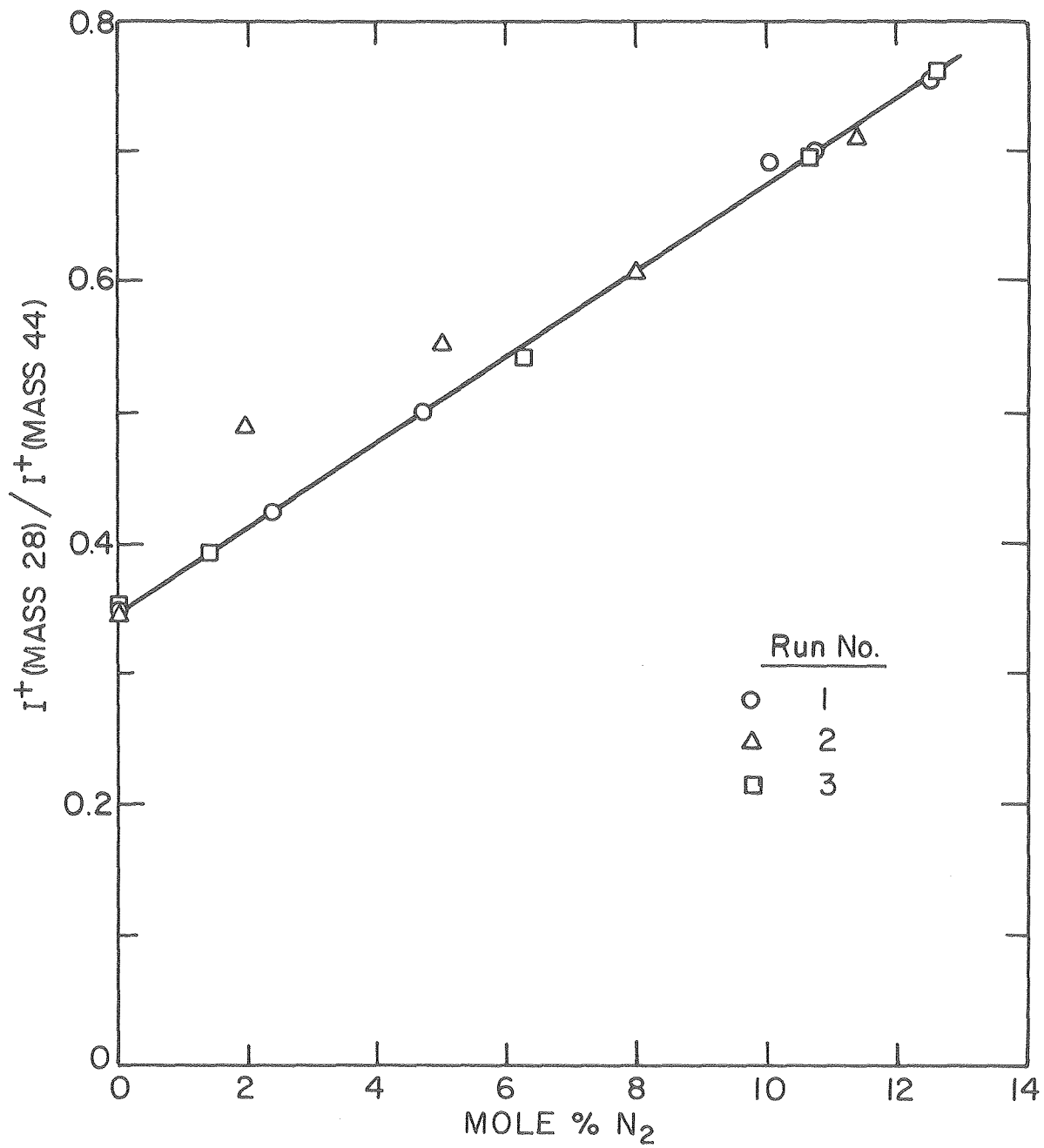
XBL 797-6512

Fig. 8



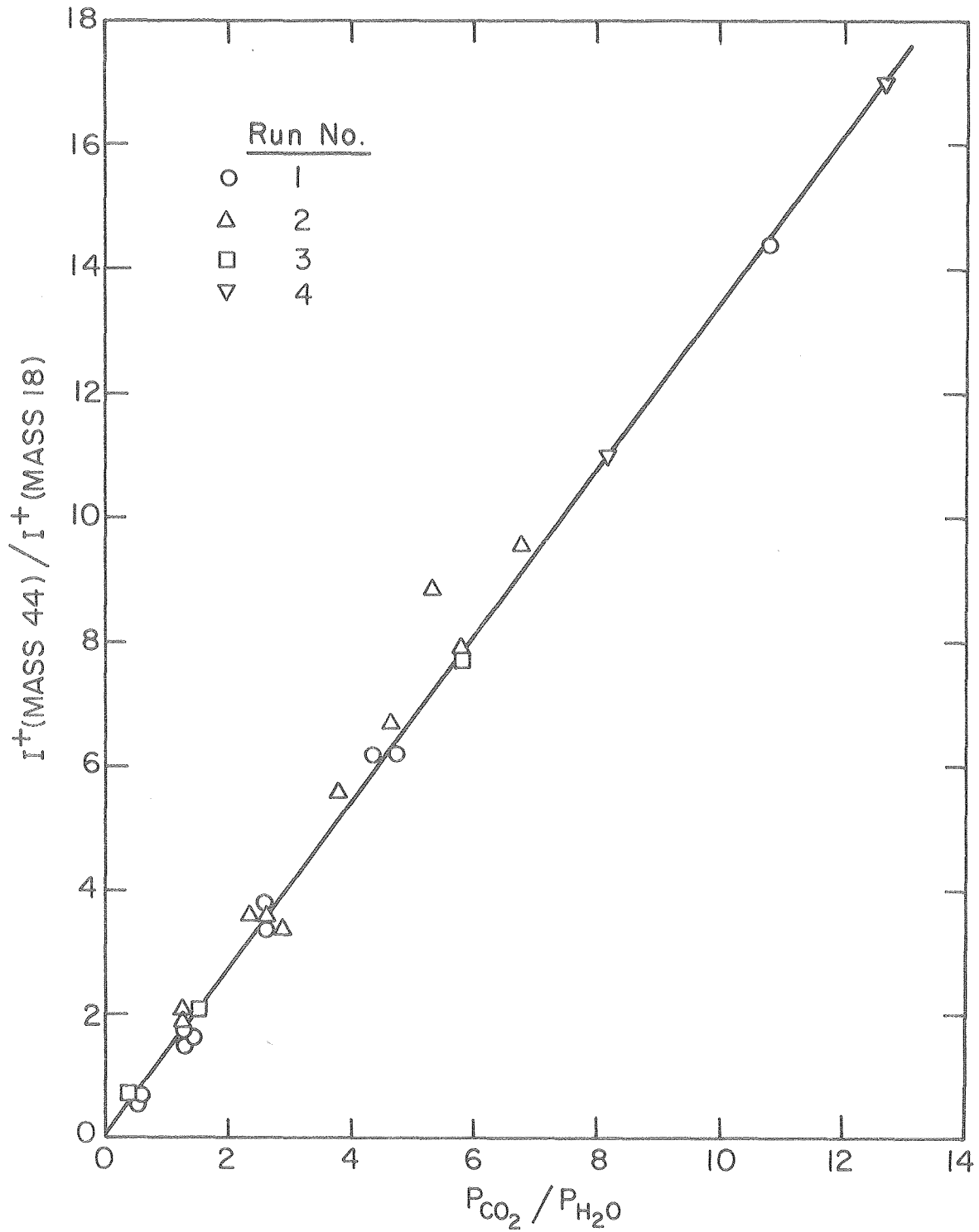
XBL797-6513

Fig. 9



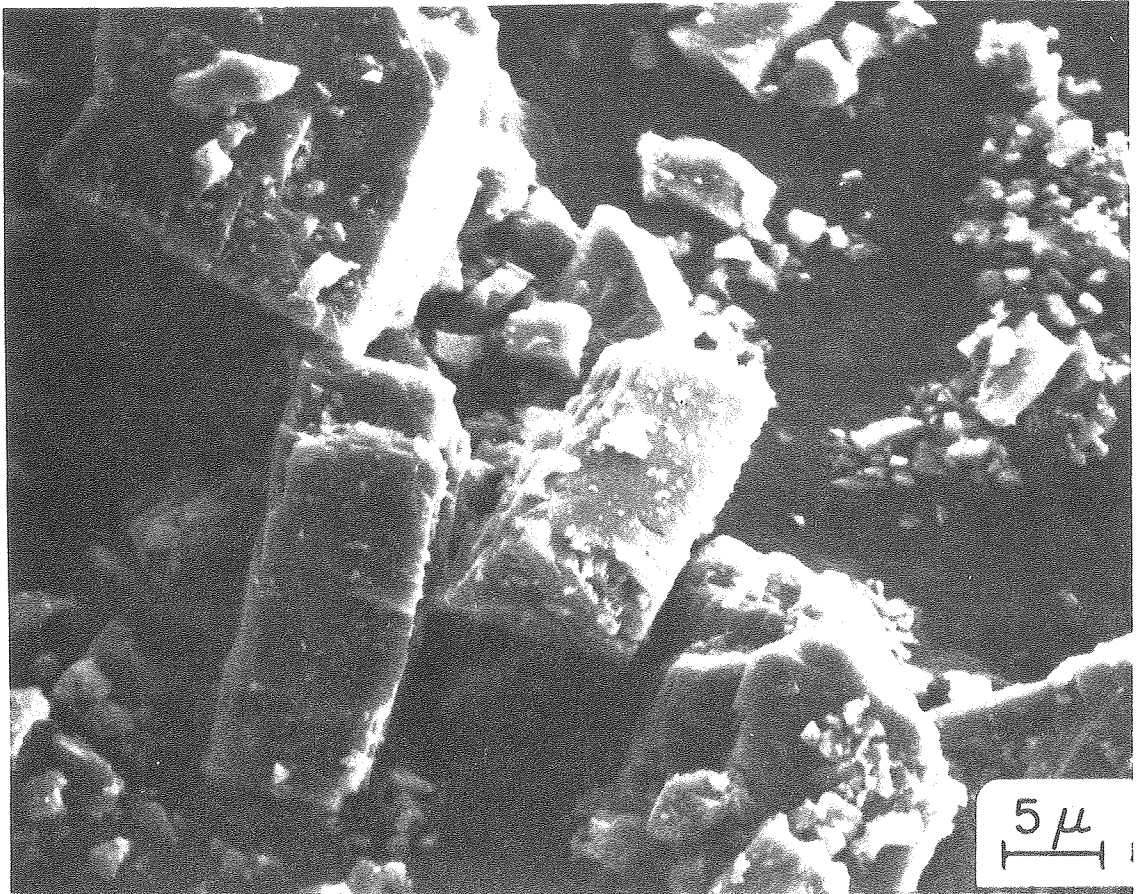
XBL797-6514

Fig. 10



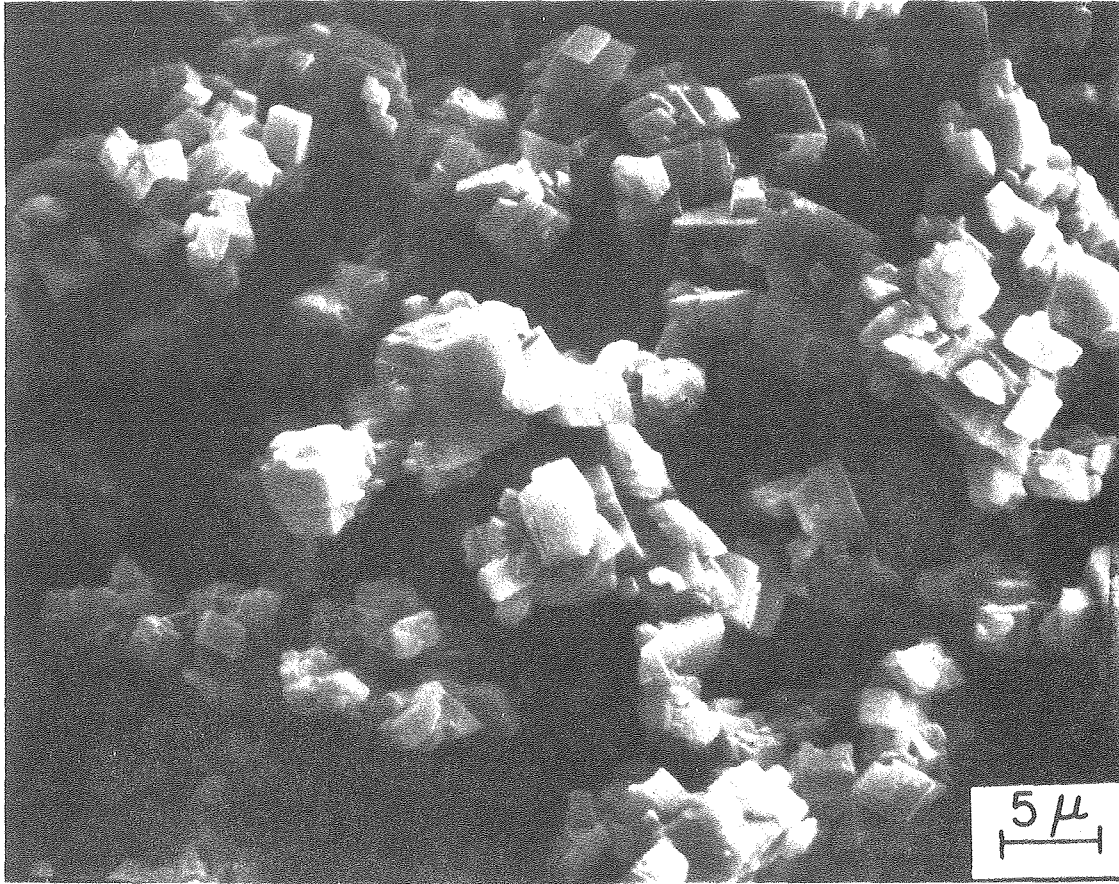
XBL797-6515

Fig. 11



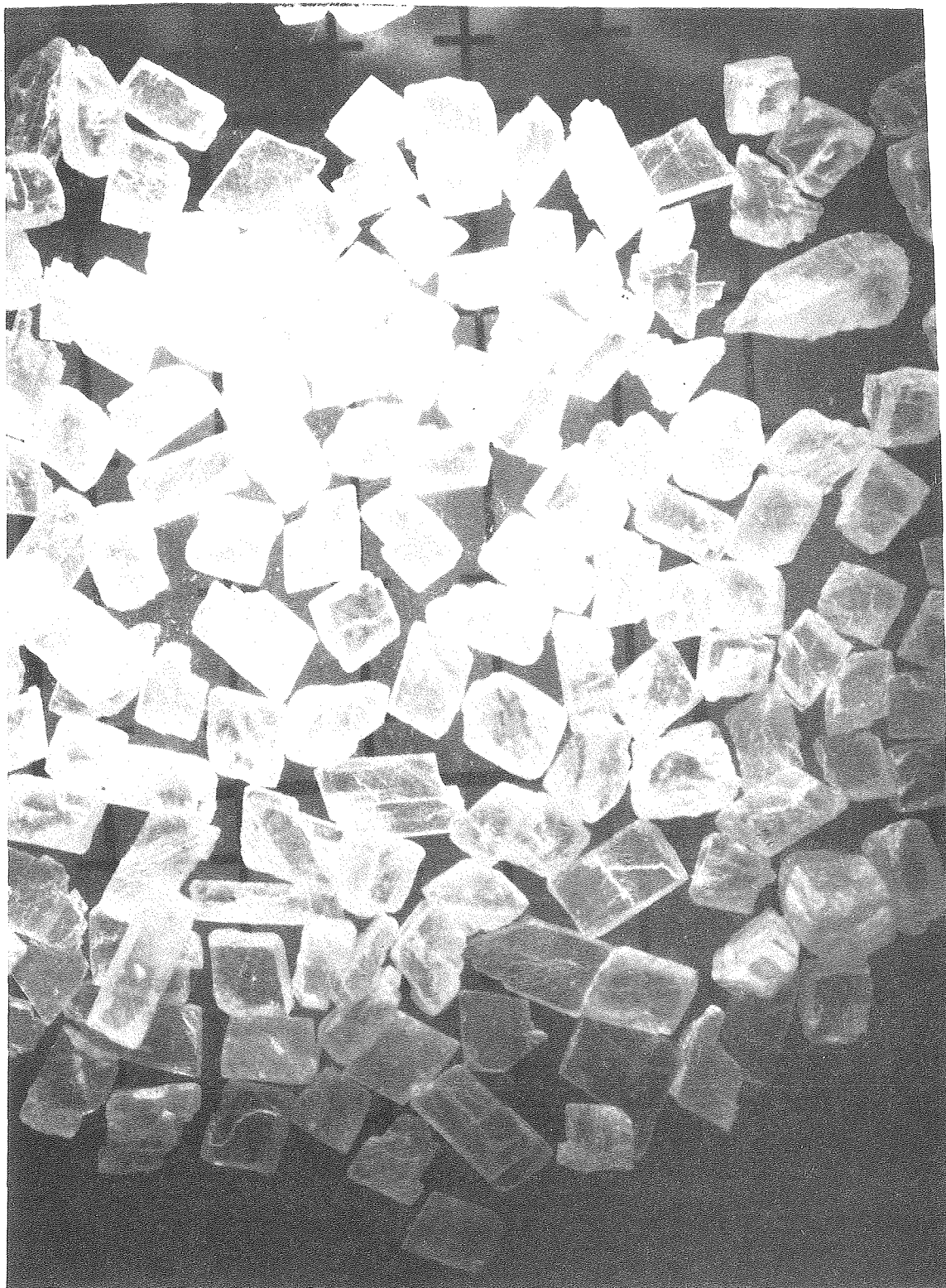
XBB798-10987

Fig. 12



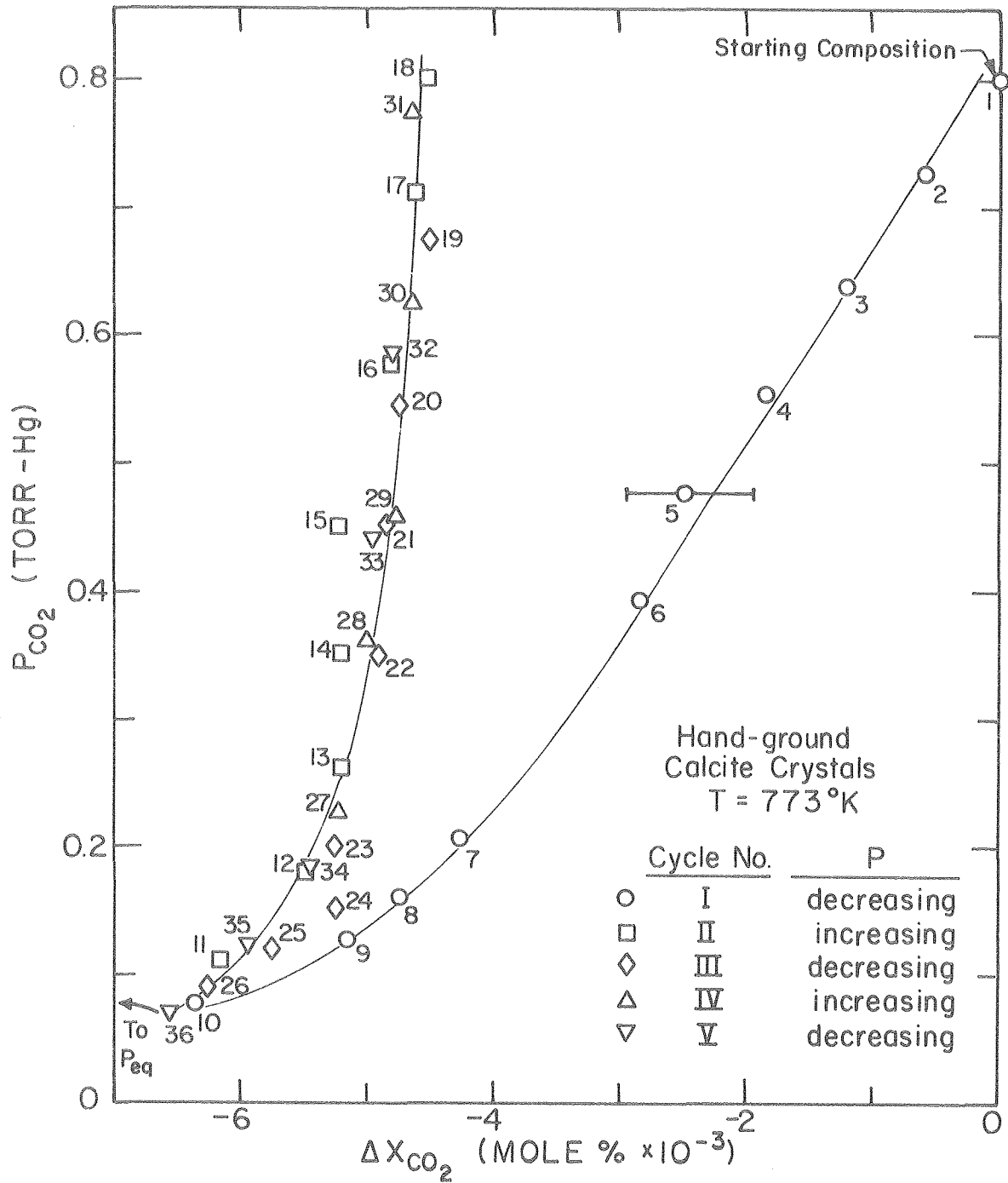
XBB798-10988

Fig. 13



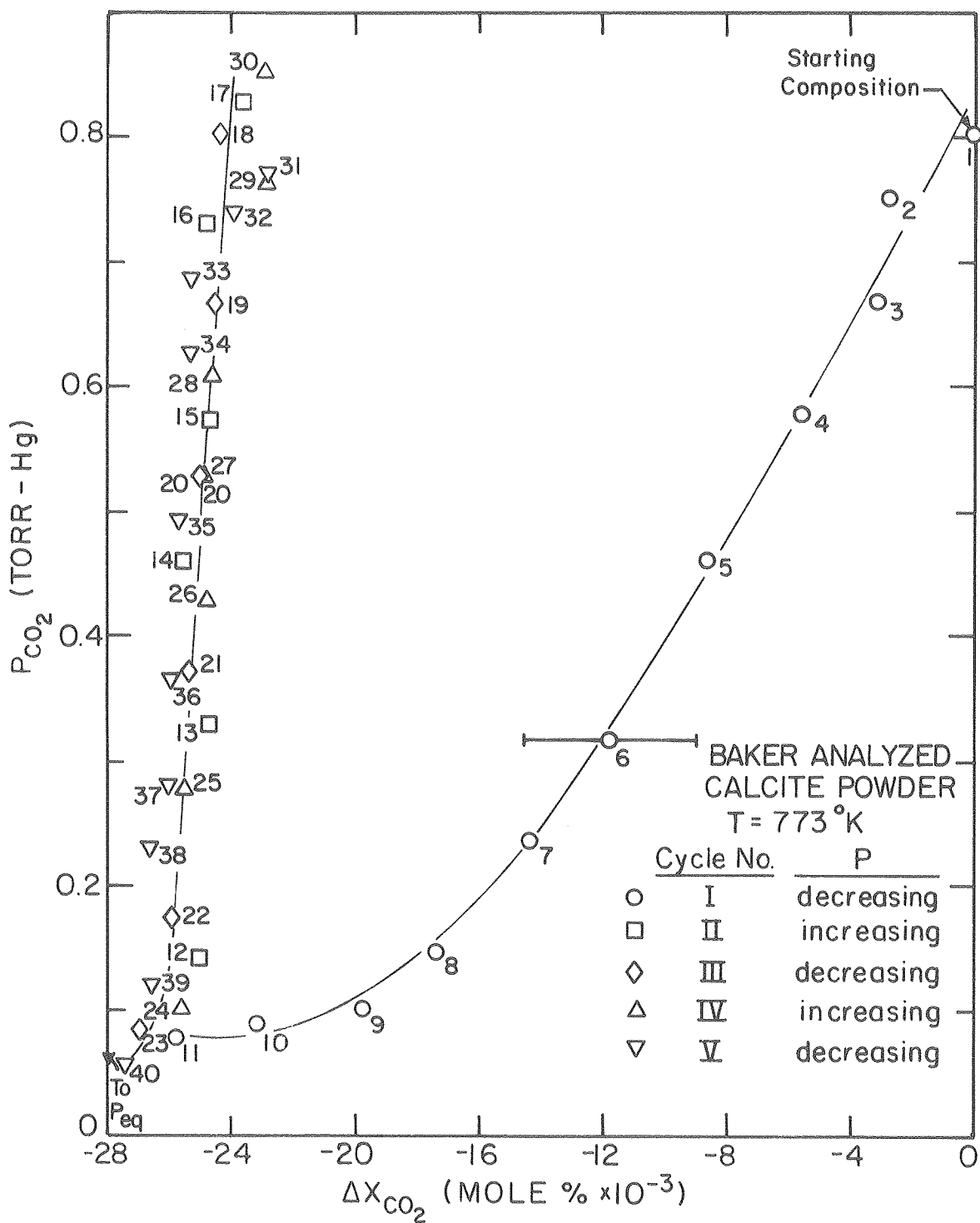
XBB798-10989

Fig. 14



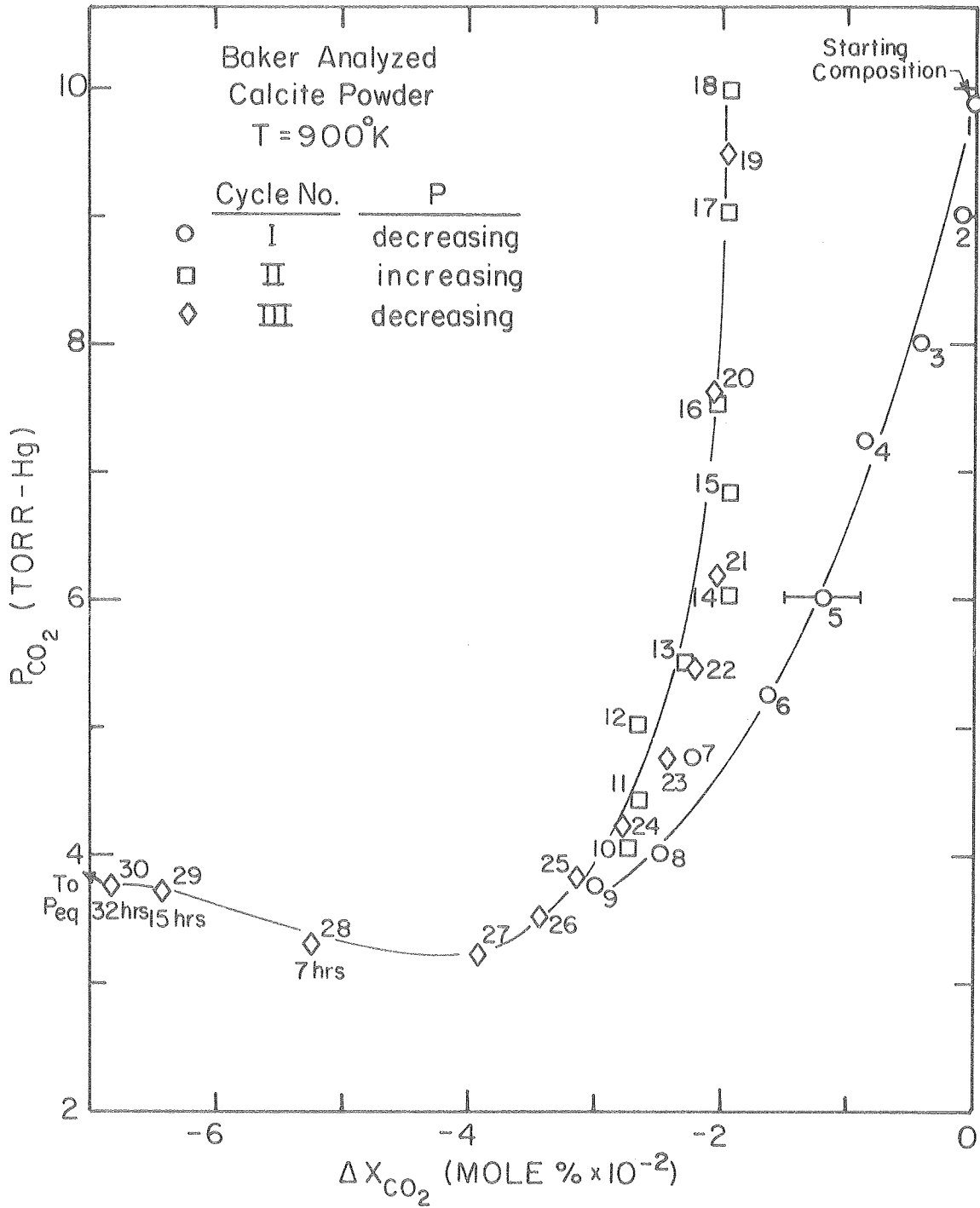
XBL 797-6516

Fig. 15



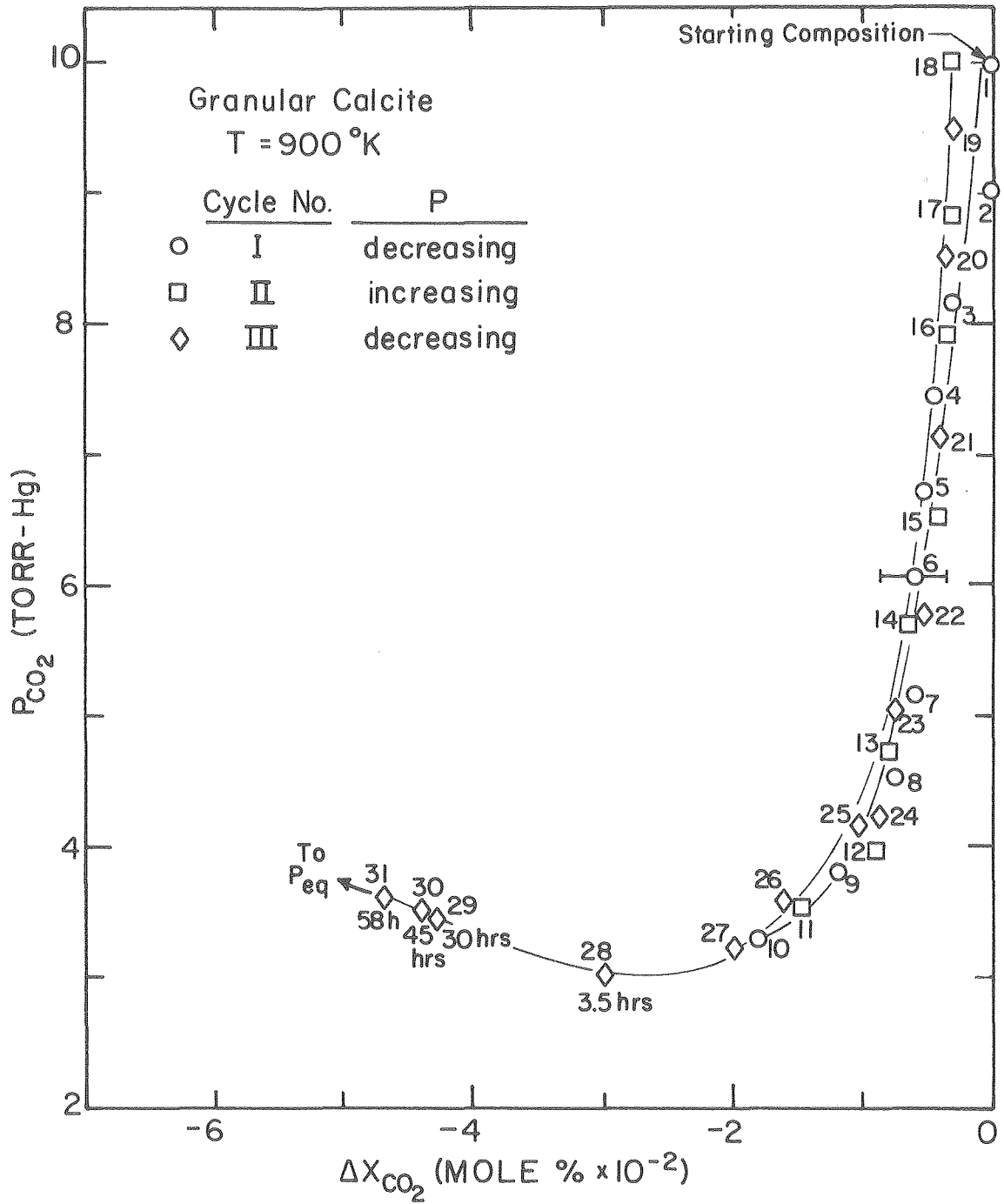
XBL797-6517

Fig. 16



XBL797-6518

Fig. 17



XBL 797-6519

Fig. 18

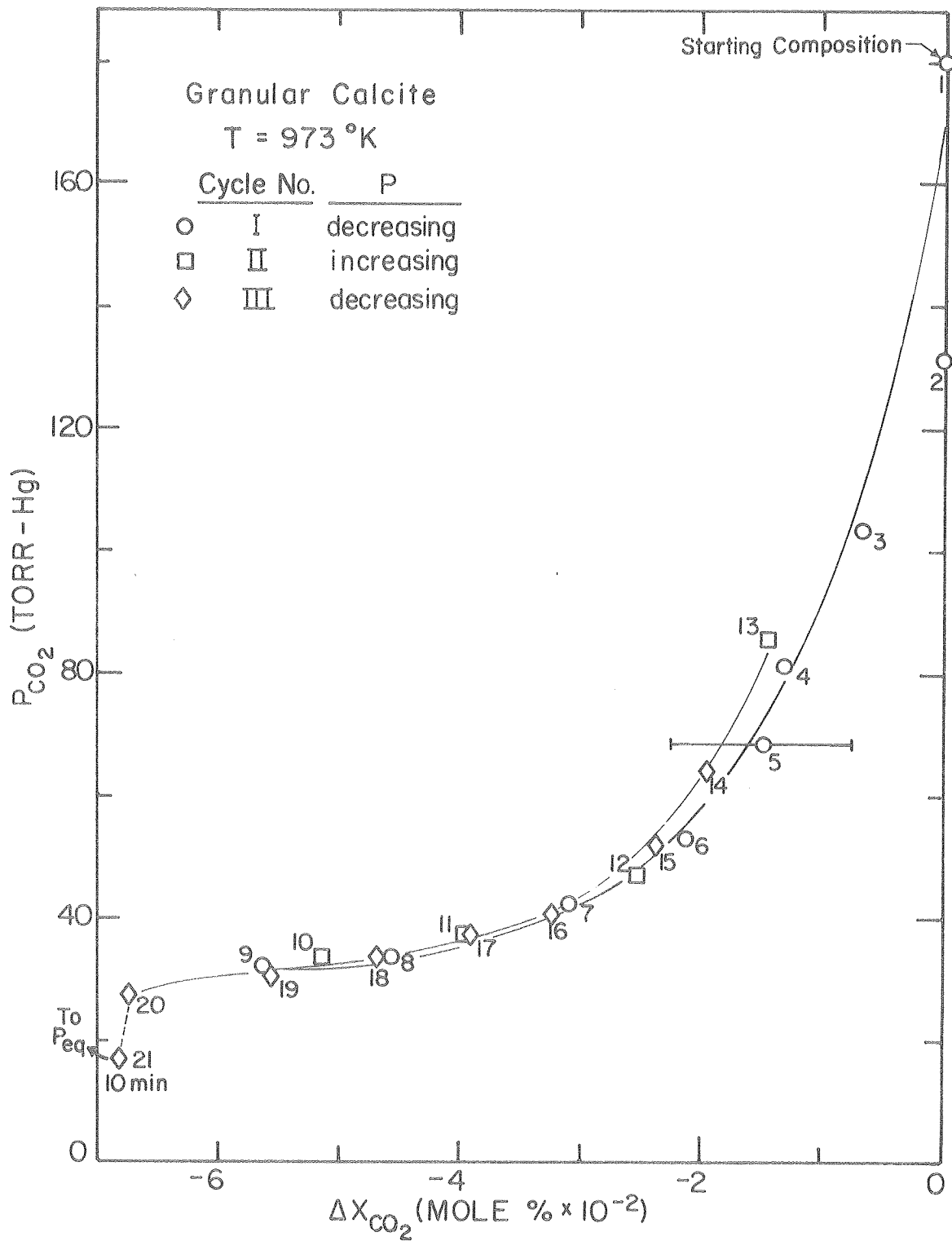
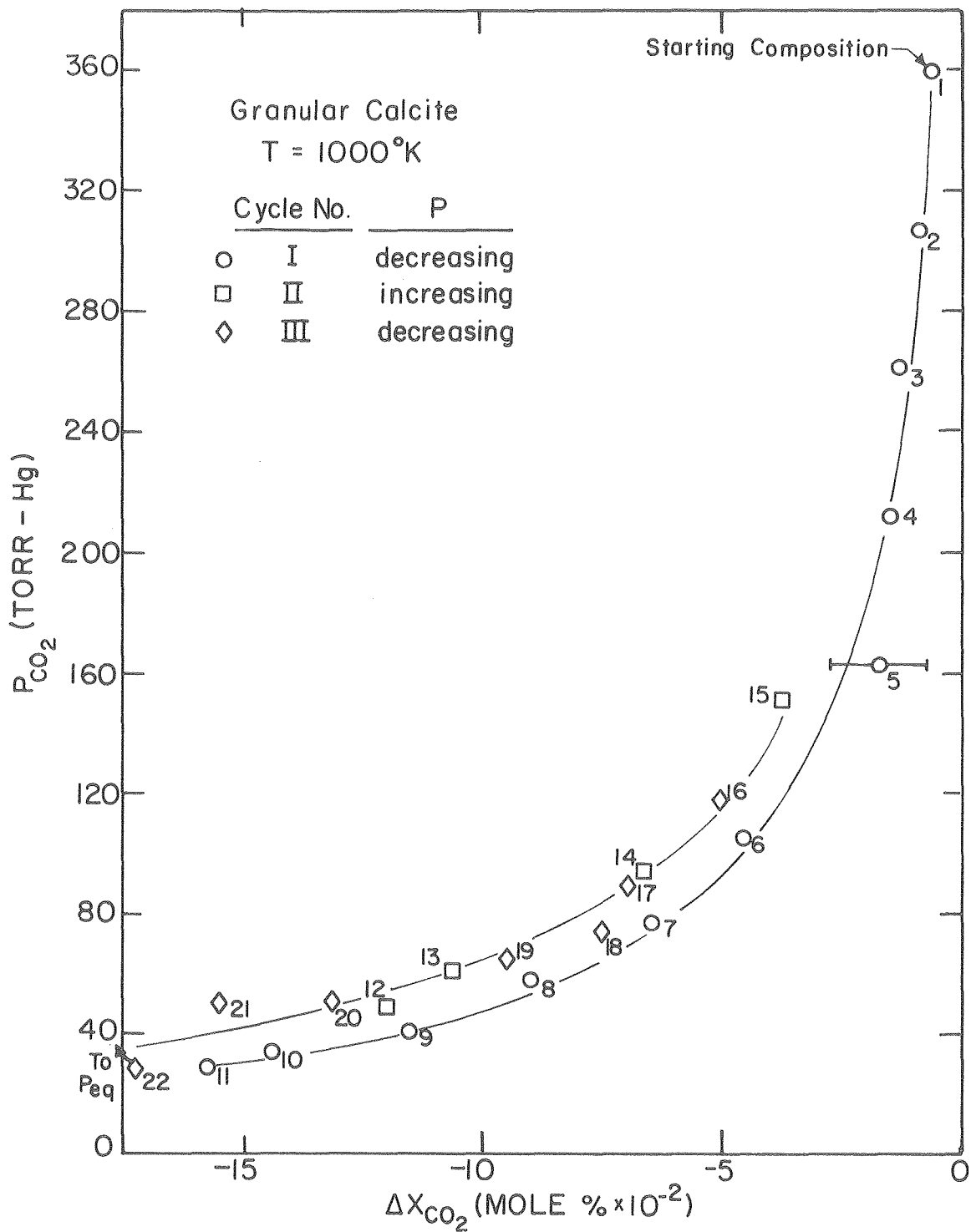
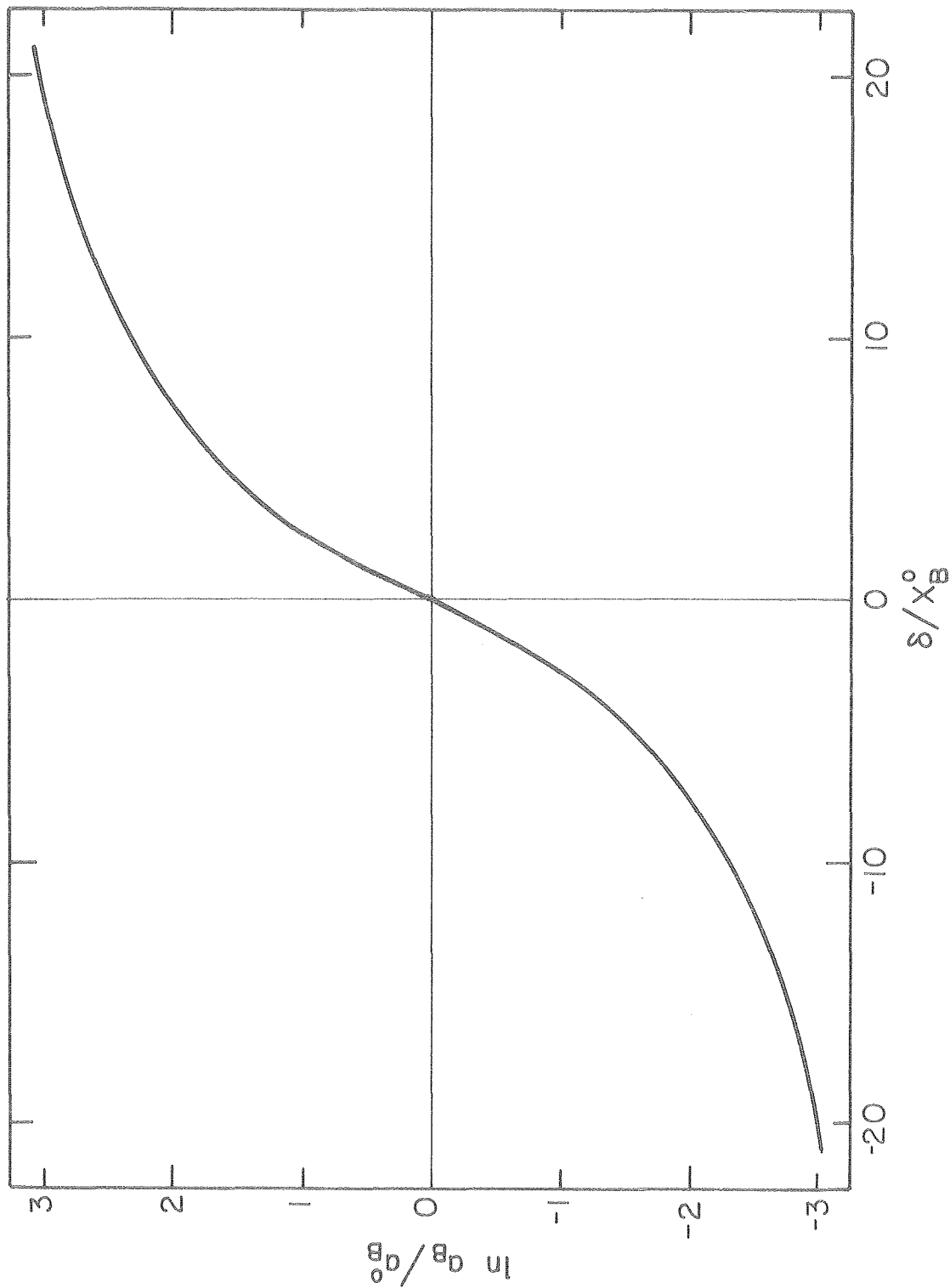


Fig. 19



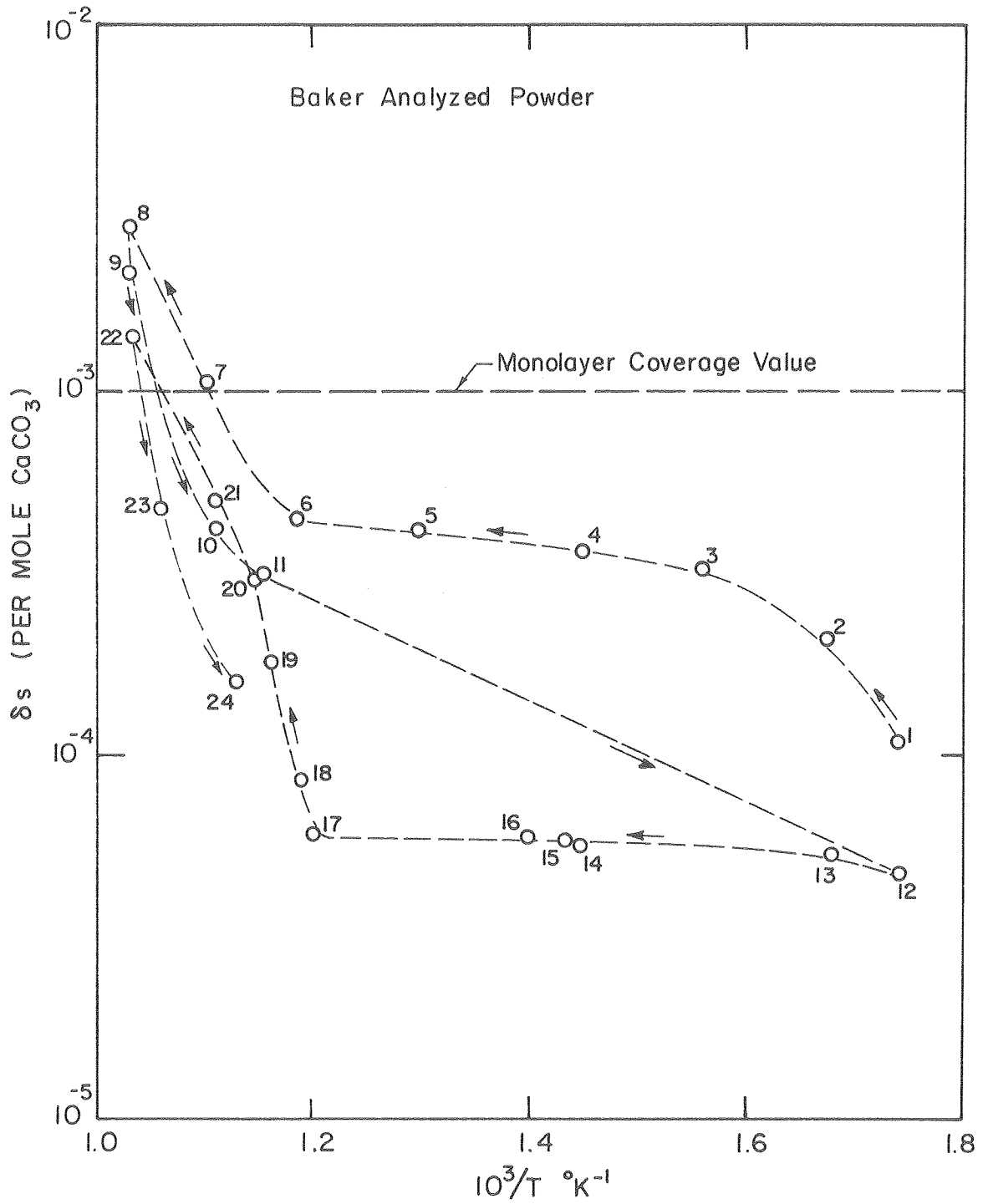
XBL 797-6521

Fig. 20



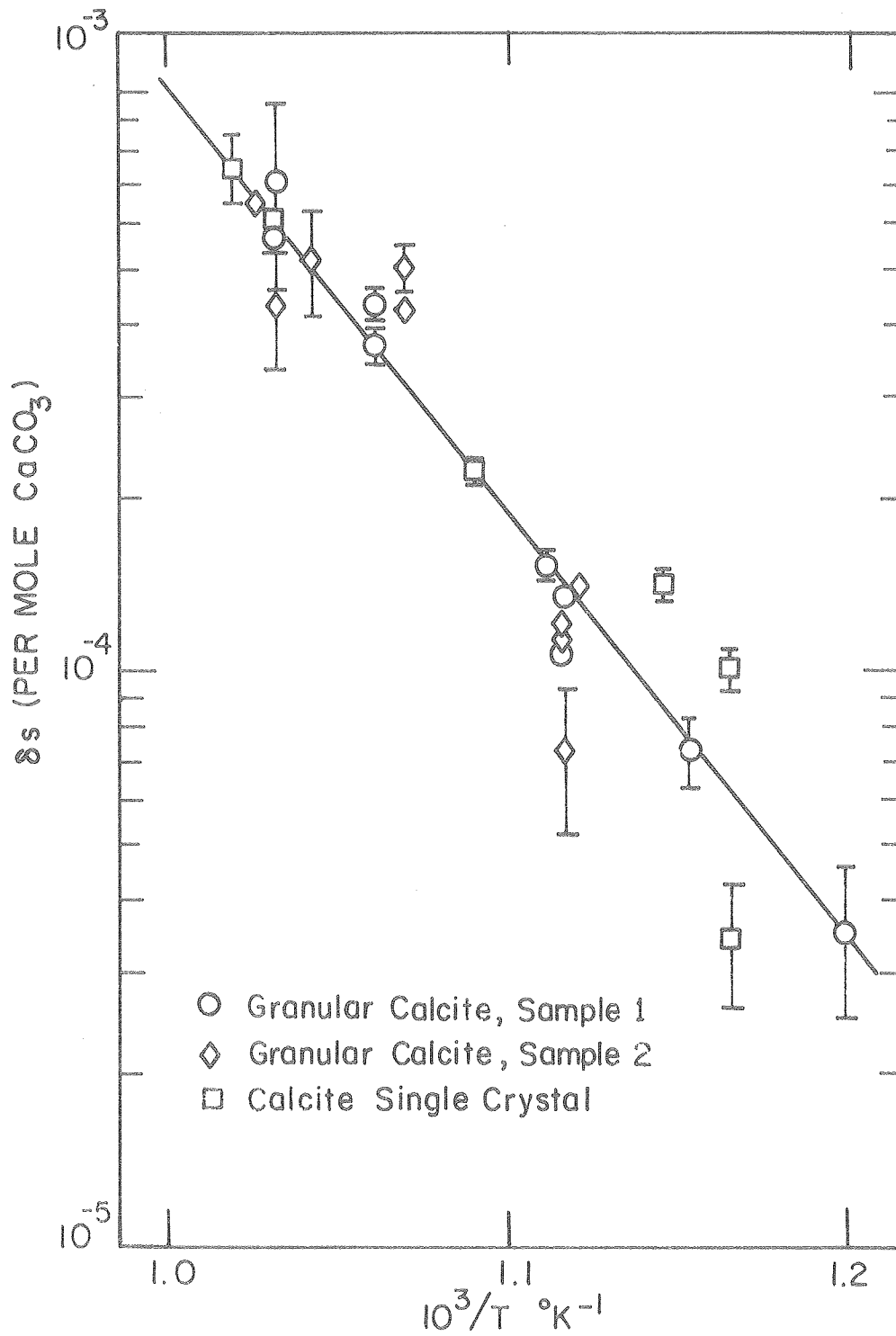
XBL 797-6522

Fig. 21



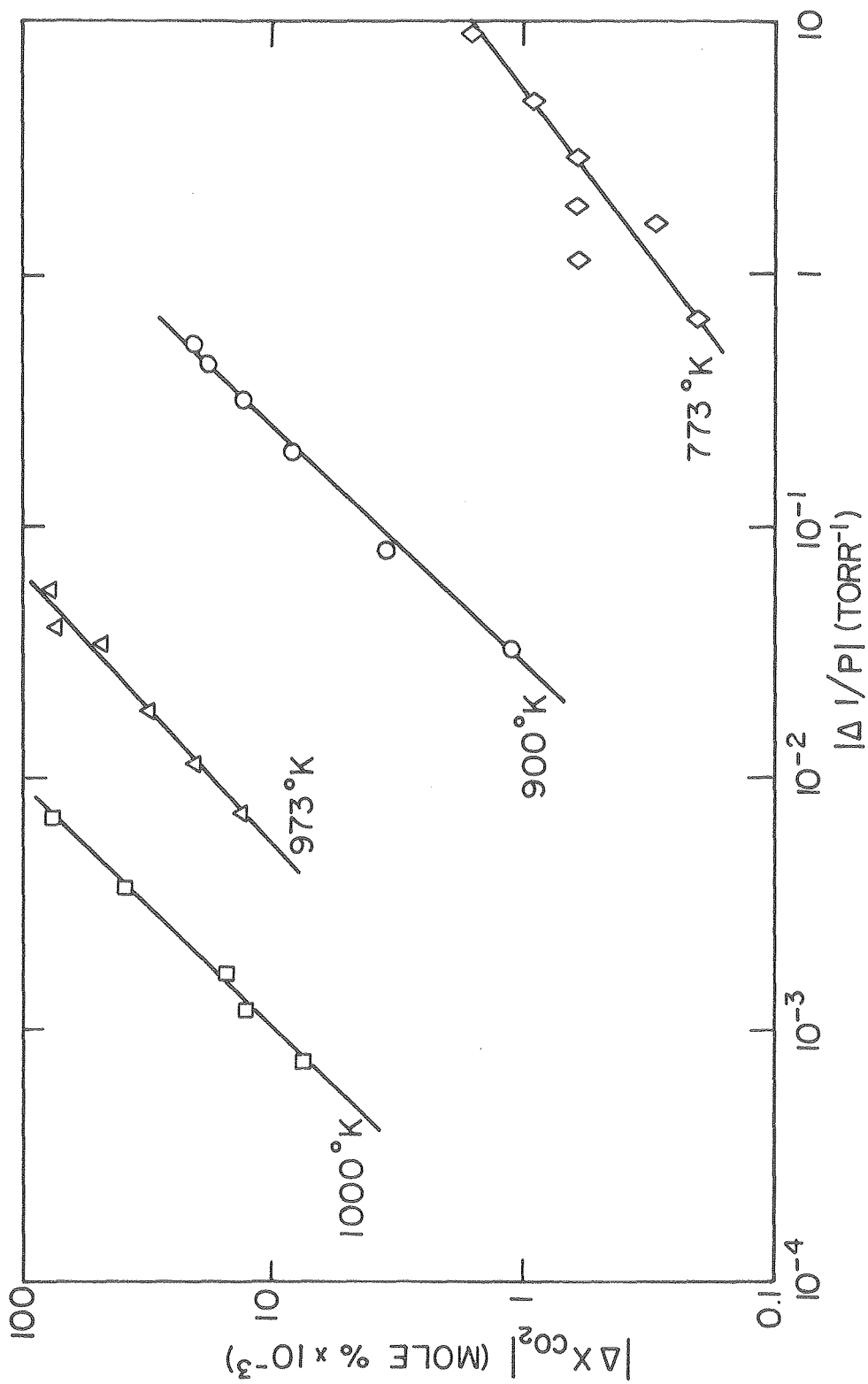
XBL797-6523

Fig. 22



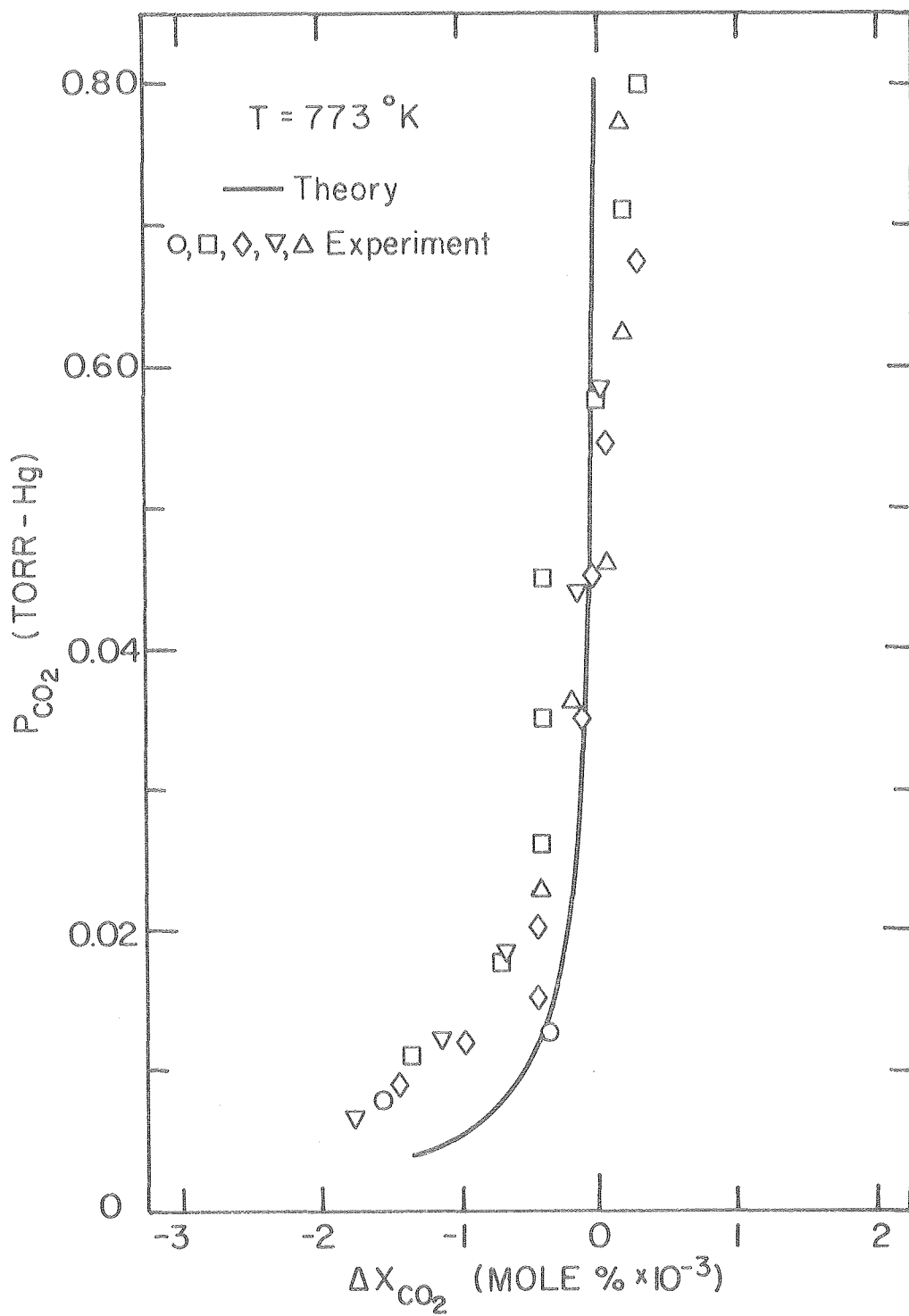
XBL 797-6524

Fig. 23



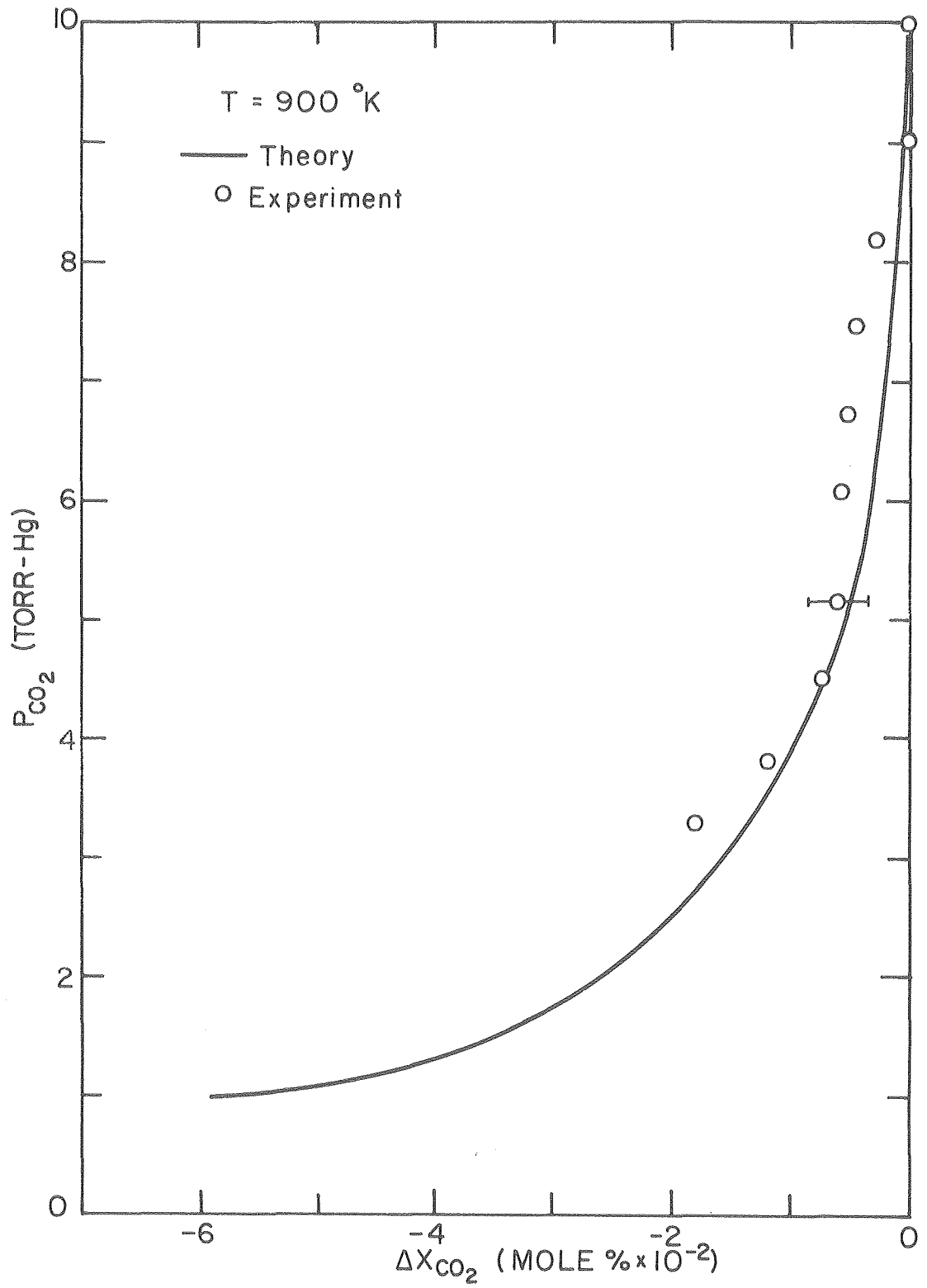
XBL 797-6525

Fig. 24



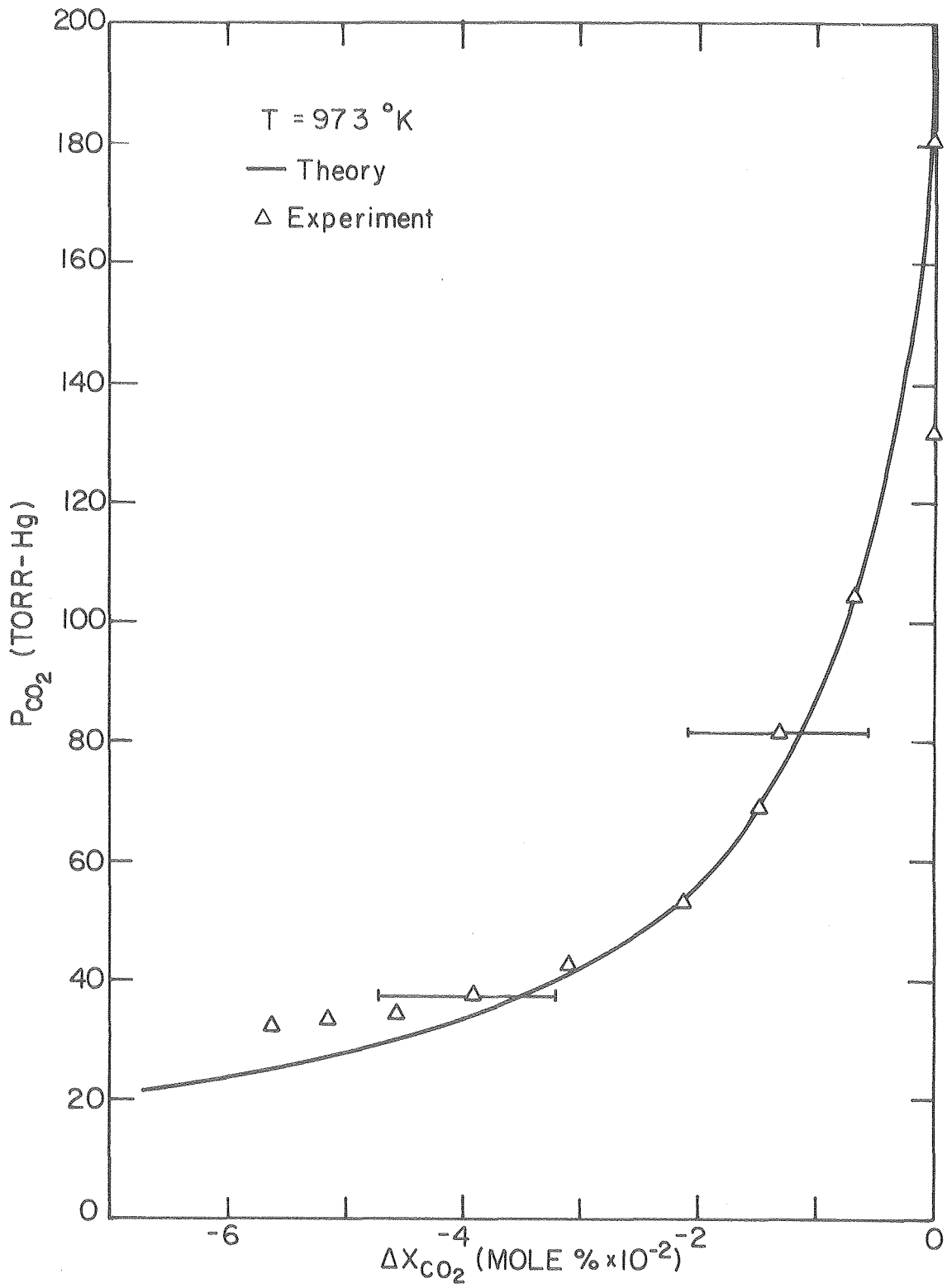
XBL 797-6526

Fig. 25



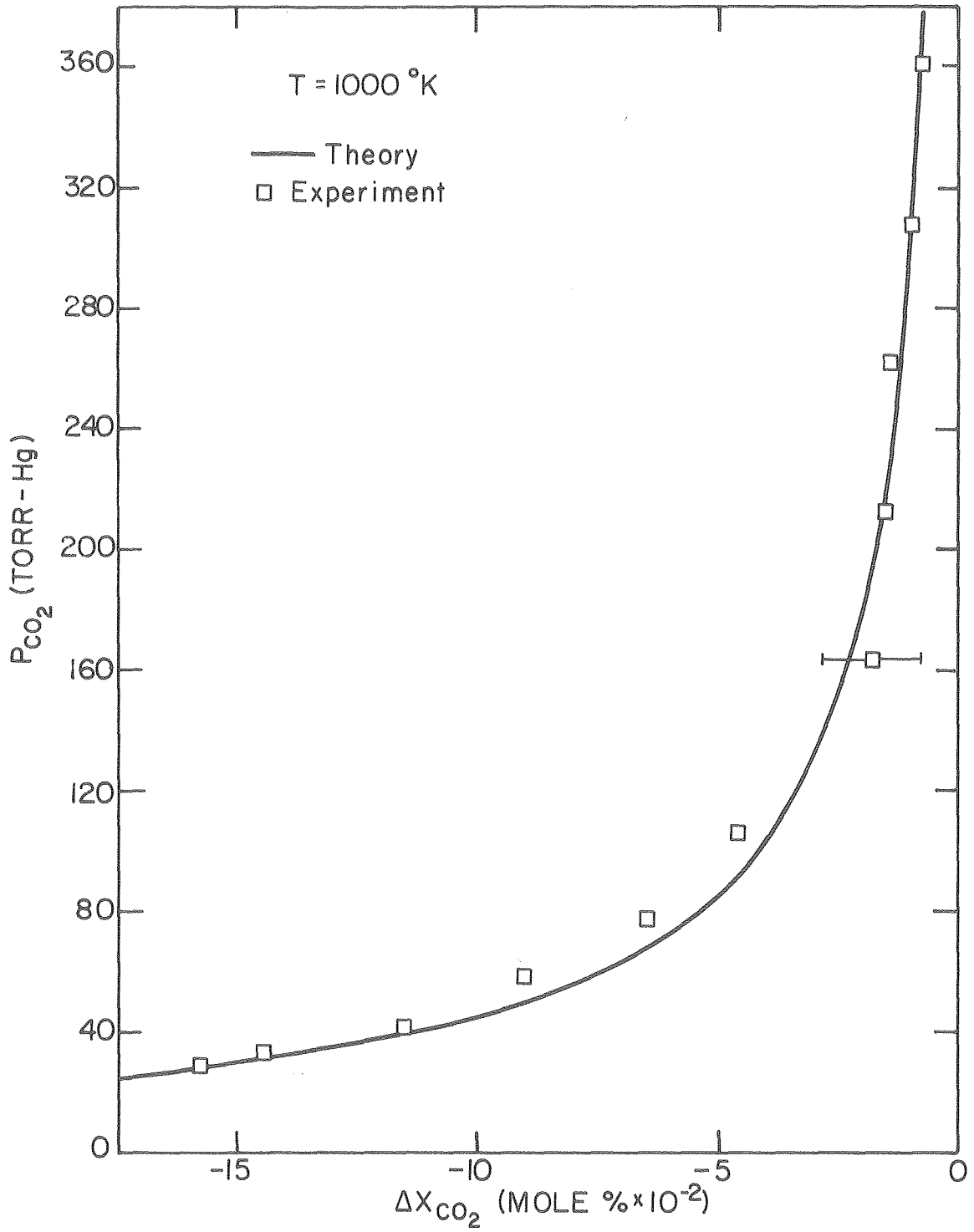
XBL 797-6527

Fig. 26



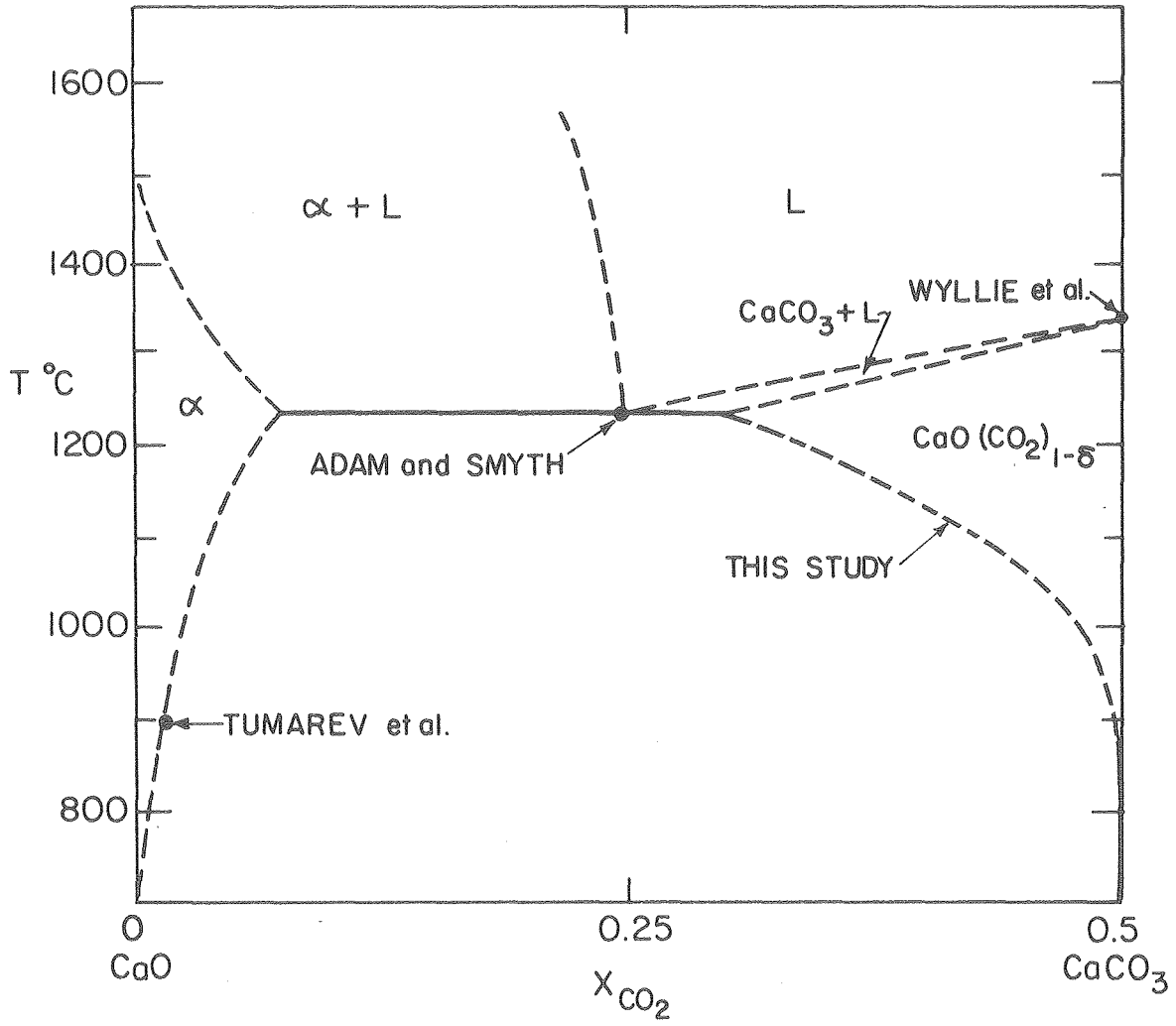
XBL797-6528

Fig. 27



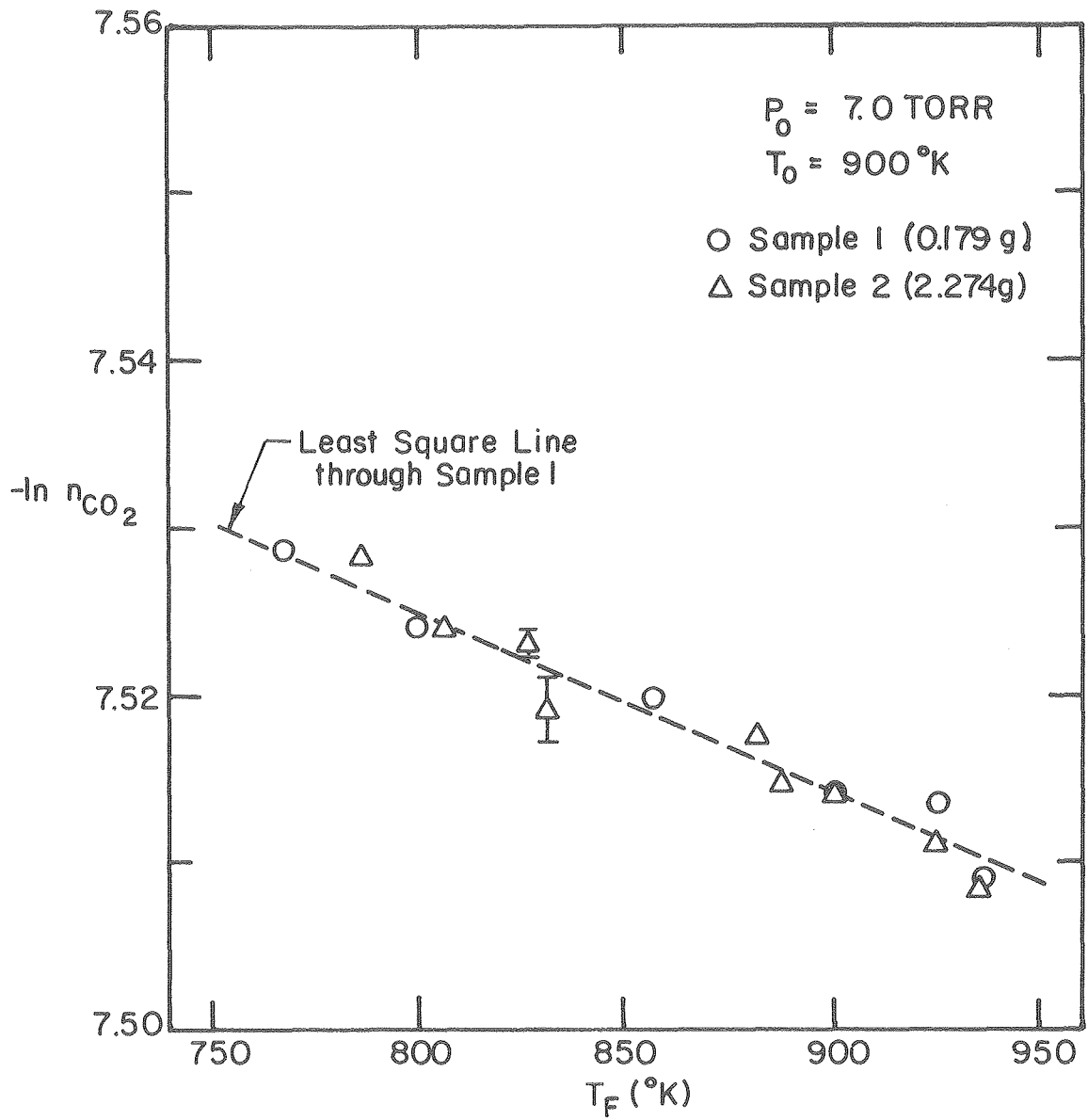
XBL 797 - 6529

Fig. 28



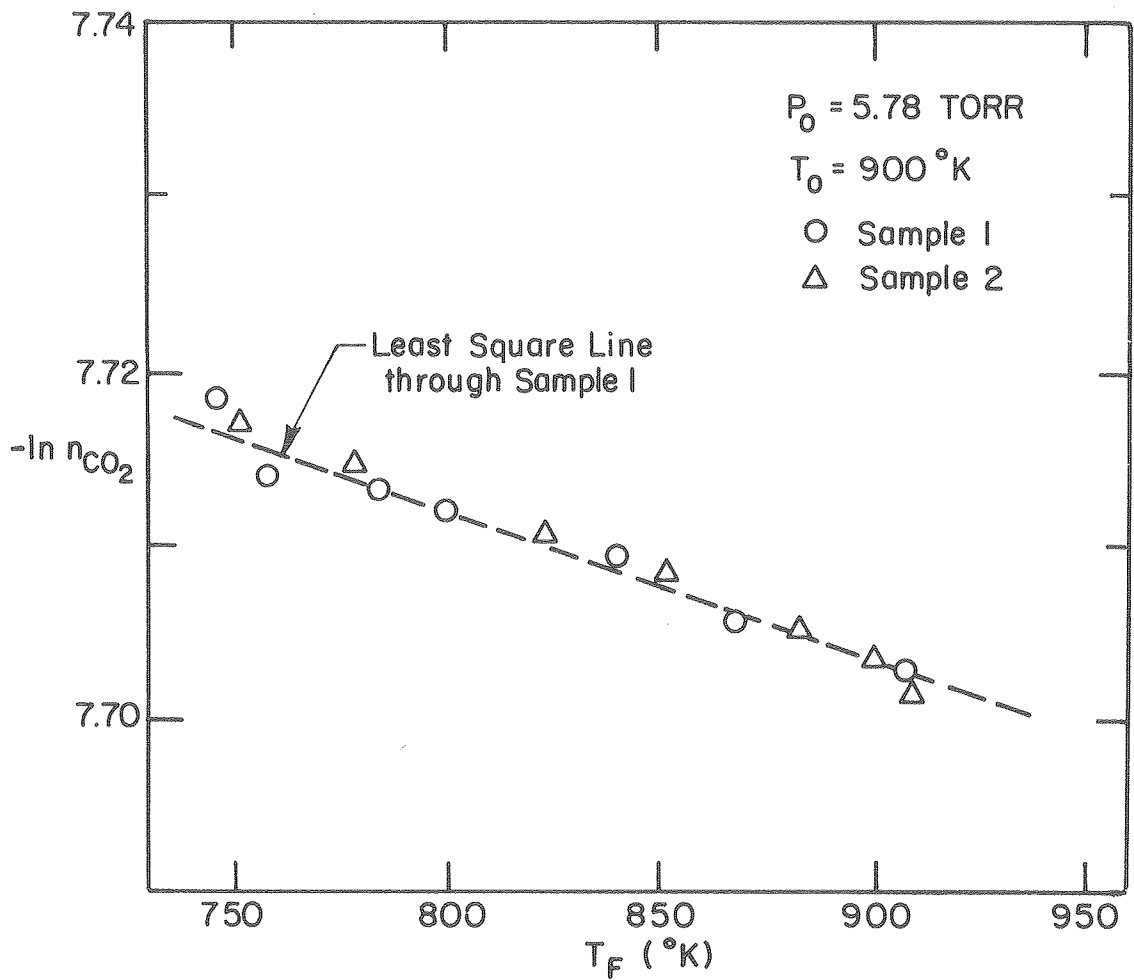
XBL797-6697

Fig. 29



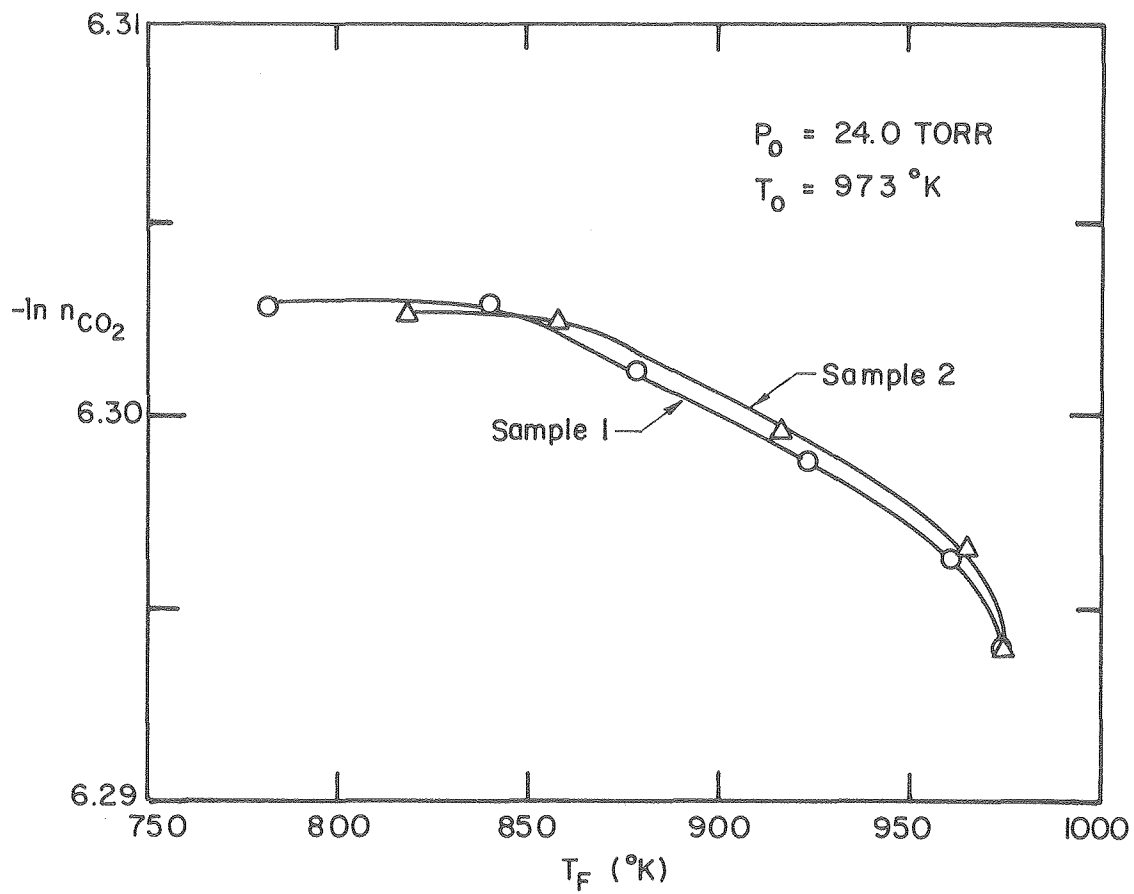
XBL 797-6531

Fig. 30



XBL 797-6532

Fig. 31



XBL 797-6533

Fig. 32

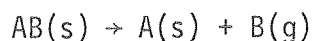
PART II

DECOMPOSITION KINETICS OF CALCITE

I. INTRODUCTION

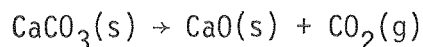
The kinetics of endothermic decomposition reactions are of considerable importance because a large number of industrial processes involve such reactions as key steps in the processing of materials.

Decomposition reactions have the general form,



which is the simplest example of decomposition reactions because, in principle, more than one solid and one gas may be produced in a decomposition process.

A prototype decomposition reaction is the decomposition of calcite (CaCO_3),



This reaction has been a subject of numerous investigations dating as far back as 1777.¹ The literature on CaCO_3 decomposition is rich in experimental data but the effect of pressure of CO_2 on the decomposition rates is still not well established, though the effect of CO_2 pressure is generally to influence not only the decomposition rate but also the product morphology, crystallinity, etc.²⁻⁶

Searcy and Beruto⁷ have recently developed a general theory of those decomposition reactions in which a solid AB decomposes to yield a porous solid A plus a gas B, as shown schematically in Fig. 1. According to their model, the decomposition rates are predicted to decrease linearly with increased pressure of product gas if a chemical step for component B is rate limiting, but to be a constant function of the difference

between the reciprocals of equilibrium decomposition pressure and the product gas pressure, if a step for component A is rate limiting. They also included in their theory, the effect of a porous product barrier and the possibility of a metastable product, on the reaction rates.

Experiments on the pressure dependence of the decomposition rates of CaCO_3 were performed first by Zawadzki, et al.⁸ (1933). They investigated the region of P_{CO_2} very close to P_{eq} , to avoid the influence of nucleation rates, because the authors were primarily interested in the rate law for the CaO growth. They reported that the rates varied linearly with pressure of CO_2 , according to equation

$$v = k(P_{\text{eq}} - P_{\text{CO}_2}) \quad (1)$$

where v is the reaction velocity and k is rate constant. The authors found k to be temperature independent, implying that the process does not require thermal activation.

The earliest theoretical investigation of the influence of P_{CO_2} on decomposition rate of CaCO_3 was made by Hyatt, et al.⁹ (1958), who found the rates of decomposition of single crystals to be proportional to $1/P_{\text{CO}_2}$ and proposed a model to explain the rather unexpected pressure dependence. However, their experimental data (obtained in the temperature range 800-950°C) has large scatter, which makes their fit to the rate expression questionable.

Cremer and Nitsch¹⁰ (1962) found a similar pressure dependence and provided their own model to explain their experimental data. However, their experimental pressures cover a range of $P_{\text{CO}_2}/P_{\text{eq}}$ from only about 0.3 to 0.6, in the temperature range of 800-900°C.

The validity of the theoretical expressions derived by various workers to explain the influence of P_{CO_2} on the rate of CaCO_3 decomposition should be tested against the data collected over a wider range of non-equilibrium conditions. The measurement of pressure dependence so far available were all made at temperatures above 800°C and for $P_{\text{CO}_2}/P_{\text{eq}}$ between 0.3 and 0.6. Decomposition rates in vacuum over a wide temperature range are also available.¹¹

The tensi-volumetric apparatus discussed in Part I is ideally suited for a study of decomposition rates as a function of pressure, and accordingly, the decomposition rates have been measured at values of $P_{\text{CO}_2}/P_{\text{eq}}$ ranging from as low as 0.01 to close to unity and at temperatures of 580°C to 660°C .

II. EXPERIMENTAL METHOD

The apparatus used in this study has already been described in Part I of the thesis. In a typical experiment, a CaCO_3 sample was placed in the Pt-boat and baked in vacuum at 300°C for about 24 hours. The system was then isolated by closing off the valve to the vacuum pump. CO_2 was added from the gas burette to reach $P_{\text{CO}_2} > P_{\text{eq}}$ for the test temperature. The temperature was then raised to the test temperature (580°C - 660°C). After isothermal conditions were achieved, the valve to the vacuum pump was opened for about 30 seconds, which caused the pressure of CO_2 to drop to less than 0.1 torr-Hg. The vacuum pump valve was then closed to isolate the system. The pressure, which rose rapidly as the decomposition ensued, was recorded continuously on a strip-charge recorder. At pressures close to the equilibrium decomposition pressure, the rate of pressure rise became negligible (typically, this happened at $P_{\text{CO}_2} \approx 0.8 P_{\text{eq}}$). The valve to the vacuum pump was then reopened and the whole cycle of decomposition was repeated as many times as desired. The total amount of CaCO_3 decomposed in any cycle was generally less than 3% by weight, so decomposition cycles could be repeated many times without an appreciable depletion of the starting material. To determine whether the time that the system was opened to the vacuum pump was important or not, the valve was left open for various lengths of time (1-3 minutes). In some experiments, the pressure was changed discontinuously while the decomposition was in progress by using the gas burette to add or subtract CO_2 .

Experiments were done at four different temperatures ranging from 580°C to 660°C . Because particle size and powder bed depth are likely to influence the decomposition rates, measurements were made with (a)

'Baker analyzed', low in alkali, CaCO_3 powder (of about 2-5 μm average dimensions, (b) Iceland Spar single crystals, which typically had dimensions of 1 cm x 1 cm x .5 cm and (c) CaCO_3 granular particles of Iceland Spar of mesh size 14, with average linear dimensions of about 0.2 cm. All of these samples were from the batches for which analyses were reported in Part I of this thesis. Sample weights used were in the range of 1-7 gms. The surface area of powder and granular samples were measured by methods discussed in Part I of the thesis. The surface areas of single crystals were calculated by measuring their linear dimensions with a travelling microscope.

Since details regarding sample particle size, decomposition cycle and pressure changes are important, a brief summary with special reference to any exceptional procedures is reported below. In the following, t_0 represents the time during which sample was exposed to vacuum and T is the temperature of dissociation:

- Run #1: $t_0 = 20$ secs., $T = 900^\circ\text{K}$, powder sample I, I cycle
- Run #2: $t_0 = 25$ secs., $T = 900^\circ\text{K}$, powder sample I, II cycle
- Run #3: $t_0 = 25$ secs., $T = 900^\circ\text{K}$, powder sample I, III cycle
- Run #4: $t_0 = 20$ secs., $T = 900^\circ\text{K}$, powder sample I, IV cycle
- Run #5: $t_0 = 40$ secs., $T = 900^\circ\text{K}$, powder sample I, V cycle
- Run #6: $t_0 = 25$ secs., $T = 900^\circ\text{K}$, powder sample I, VI cycle
- Run #7: $t_0 = 20$ secs., $T = 900^\circ\text{K}$, single crystal sample, I cycle
- Run #8: $t_0 = 30$ secs., $T = 900^\circ\text{K}$, single crystal sample, II cycle
- Run #9-11: $t_0 = 40$ secs., $T = 900^\circ\text{K}$, single crystal sample, III, IV and V cycles
- Run #12: $t_0 = 30$ secs., $T = 900^\circ\text{K}$, powder sample II, I cycle

- Run #13: $t_0 = 30$ secs., $T = 900^\circ\text{K}$, powder sample II, II cycle
Run #14: $t_0 = 30$ secs., $T = 900^\circ\text{K}$, powder sample II, III cycle
Run #15: $t_0 = 30$ secs., $T = 930^\circ\text{K}$, powder sample II, IV cycle
Run #16: $t_0 = 30$ secs., $T = 930^\circ\text{K}$, powder sample II, V cycle
Run #17: $t_0 = 30$ secs., $T = 873^\circ\text{K}$, powder sample II, VI cycle
Run #18: $t_0 = 30$ secs., $T = 873^\circ\text{K}$, powder sample II, VII cycle
Run #19: $t_0 = 30$ secs., $T = 900^\circ\text{K}$, granular sample I, I cycle
Run #20: $t_0 = 45$ secs., $T = 900^\circ\text{K}$, granular sample I, II cycle
P changed discontinuously from $P = 1.250$ torr-Hg to
 $P = 1.580$ torr-Hg.
Run #21: $t_0 = 5$ secs., $T = 900^\circ\text{K}$, granular sample I, III cycle,
initial $P_{\text{CO}_2} = 0.100$ torr-Hg
Run #22: $T = 900^\circ\text{K}$, granular sample I, IV cycle, initial $P_{\text{CO}_2} = 1.5$
torr-Hg
Run #23,24: $t_0 = 50$ secs., $T = 873^\circ\text{K}$, granular sample II, I and II cycles
Run #25: $t_0 = 40$ secs., $T = 933^\circ\text{K}$, granular sample II, III cycle
Run #26: $t_0 = 45$ secs., $T = 901^\circ\text{K}$, granular sample II, IV cycle
Run #27,28: $t_0 = 50$ secs., $T = 853^\circ\text{K}$, granular sample II, V and VI cycles
Run numbers 1-6, 7-11, 12-18, 19-22, and 23-28 are reported in Figs. 2, 3,
4, 5 and 6, respectively. For the purpose of these figures, decomposition fluxes, j , in units of $\text{gms sec}^{-1}/\text{cm}^2$ of actual sample surface, as distinct from cross-sectional areas of the boat, were calculated according to the equation

$$j(P,T) = \left(\frac{dP}{dt}\right) \cdot \frac{V_A}{RT_A} \cdot \frac{M_{\text{CO}_2}}{\sigma\omega} \quad (2)$$

where dP/dt is the rate of pressure rise at pressure P , V_A is the ambient, calibrated volume of the apparatus (see Part I of thesis), T_A is the ambient (room) temperature, M_{CO_2} is the molecular weight of CO_2 , σ is the specific surface area of the sample and w is the weight of sample used. Typical values for σ were $\sigma_{\text{powder}} = .67 \text{ m}^2 \text{ g}^{-1}$, $\sigma_{\text{granular}} = 10^{-3} \text{ m}^2 \text{ g}^{-1}$ and $\sigma_{\text{single crystal}} = 10^{-4} \text{ m}^2 \text{ g}^{-1}$.

III. RESULTS AND DISCUSSION

Figures 2-6 show values of $\log j$ as a function of activity of CO_2 ($= P/P_{\text{eq}}$), taking P_{eq} as the standard state. Choosing the activity of CO_2 to be unity at the equilibrium decomposition pressure essentially normalizes the representation of decomposition flux j vs. P_{CO_2} curves. Various features which are noticeable in these plots, and their significance will be discussed below:

- (i) Shape of $\ln j$ vs. P/P_{eq} plots: An examination of Figs. 2-6 shows that all samples have the same general dependence of $\log j$ on P/P_{eq} , the curves have sigmoid shapes. In general, j approaches a maximum value as P_{CO_2} goes to zero, and it approaches zero ($\ln j \rightarrow -\infty$) as P_{CO_2} approaches the equilibrium pressure, as expected.
- (ii) Effect of cycling on j : From Fig. 2 it is seen that for CaCO_3 powder, the value of j at a given value of P/P_{eq} increased during the first three cycles after which the rates became independent of cycling. This result suggests that the initial decomposition rate depends upon the sample history. The discrepancy seems to be maximum for the intermediate values of P/P_{eq} . The high reproducibility of variation of j with P/P_{eq} in the last four cycles shows that the transport of CO_2 through porous product layer does not limit the rate of decomposition, for values of P/P_{eq} as high as 0.9. This is an important conclusion because it need not be true but was assumed without explicit experimental proof in the theoretical rate expressions derived by Hyatt, et al., and by Cremer and Nitsch. The extent of decomposition was about 2% in each cycle. Thus, the rate of decomposition is not affected by amounts of decomposition as high as 12% in the sixth cycle in Fig. 2.

For single crystals, the effect of cycling on decomposition rates is almost negligible at all pressures studied (Fig. 3). Beruto and Searcy¹¹ had shown earlier that rates of decomposition in vacuum ($P/P_{eq} < 0.001$) are independent of the extent of reaction up to 80% of the maximum possible weight loss of a single crystal. It therefore seems probable that decomposition rates for single crystals are independent of the thickness of the porous product layer for all values of P/P_{eq} .

A CO_2 pressure build up in the powder bed during decomposition might be responsible for the low steady state fluxes and even lower initial fluxes from the powder bed, as compared to decomposition fluxes for single crystals. To test these possibilities, fluxes were measured for a boat loaded with about 5 gms of sample (Fig. 4). The weight of powder used in obtaining the data for Fig. 2 was about 2 gms.

Figure 7 shows a composite plot of the values of $\ln j$ vs. P/P_{eq} at $900^\circ K$ for the final cycles made with the two powder samples mentioned previously. It is seen that the decomposition rate for the 5 g sample is lower than for the 2 g sample by almost an order of magnitude at low values of P/P_{eq} . At higher pressures, the two curves approach each other.

This result indicates that the powder decomposition kinetics are influenced by the powder bed depth. The effect of bed depth is greatest at the low background pressures, where the high decomposition fluxes themselves create a significant pressure gradient in the sample. But the initial rates of decomposition found for the larger powder sample differed from the steady state rate (obtained after three cycles) less than found for the smaller sample. No convincing explanation for the initial changes in rate of decomposition on cycling has yet been found.

(iii) Effect of discontinuous change in pressure: In obtaining data for Figs. 2 to 5, the number of times that the samples were exposed to vacuum were different for different cycles, which have been described earlier in the summary of different runs. No detectable difference was observed in the rates, showing that the initial time of vacuum decomposition does not affect the decomposition fluxes at higher pressures. This implies that the initial nucleation rate, and the number of CaO nuclei generated under vacuum decomposition conditions do not decide the overall rate at subsequent higher pressures.

The discontinuous rise in pressure brought upon by addition of CO_2 from an external source to the reaction chamber also did not affect the behavior of j vs. P/P_{eq} , as shown in Fig. 5 (granular calcite, cycles II and III).

In the same figure, cycle III was started at $P/P_{\text{eq}} = 0.23$, while cycles I and II were started at $P/P_{\text{eq}} = 0.1$. No difference in the subsequent decomposition rates for the three cycles is seen. This result implies that the behavior of j vs. P/P_{eq} is not affected by the initial vacuum conditions or background pressures. However, cycle IV, which was started at $P/P_{\text{eq}} = 0.32$ showed distinctly lower rates of decomposition j , which approached the steady state curves (cycles I-III) at higher pressures. This suggests that an induction period occurs if decomposition is carried out at higher pressures, in agreement with the observation of Cremer and Nitsch.¹⁰

(iv) Effect of particle size on decomposition rates: Figure 8 is a composite plot of j vs. P/P_{eq} under steady state conditions for various samples. It is seen from this plot that decomposition rates for powders

are lower by 2 to 3 orders of magnitude than rates for the granular and single crystal samples. The data for the latter two are in close agreement.

The maximum flux that can leave a powder sample in vacuum is set by the flux calculated by substituting the equilibrium decomposition pressure in the Hertz-Knudsen-Langmuir equation with the projected geometrical area of the outer surface of the powder bed replacing the BET total surface area of the powder in that equation.¹² It is therefore of interest to calculate the flux per unit cross-sectional area of the sample boat to determine whether this maximum flux is achieved - indicating equilibrium pressures are reached in the bed - or not.

Figure 9 shows the fluxes recalculated on the above basis for powder samples as well as the fluxes for single crystals (calculated for the total geometrical area of samples). It is seen that the flux density for the powder bed, in this representation, is about an order of magnitude higher than that for a single crystal, but it is about a factor of 10^4 lower than the maximum possible flux. This result means that the decomposition reaction is highly irreversible in this CO_2 pressure range, as it is in vacuum.¹¹

(v) Comparison with existing theories: Various models proposed for CaCO_3 decomposition lead to the following predicted dependence of decomposition flux on P_{CO_2} :

$$(i) \quad j = (1 - P/P_{\text{eq}})/(BP + C) \quad (\text{Hyatt, et al.}) \quad (3)$$

$$(ii) \quad j = k_1 \left[\frac{1}{\bar{p}} - \frac{1}{p_{\text{eq}}} \right] \quad (\text{Cremer \& Nitsch}) \quad (4)$$

$$(iii) \quad j = k_2 \left[\frac{1}{P} - \frac{1}{P_{eq}^m} \right] \quad (5)$$

$$\text{or } j = k_3 [P_{eq}^m - P] \quad (6)$$

(Searcy and Beruto)

In these equations, B, C, k_1 , k_2 and k_3 are temperature dependent constants, P is the pressure of CO_2 during decomposition and P_{eq} is the equilibrium decomposition pressure, P_{eq}^m is the equilibrium decomposition pressure when the CaO product may be metastable.^{4,11} If it is stable, equation (4) becomes formally equivalent to (3).

Experimental j vs. P/P_{eq} curves obtained in this work failed to follow any one of these equations over the whole range of pressures. This is illustrated below by use of the single crystals decomposition data of Fig. 6.

(1) j vs. P curve

Figure 10 is a plot of j vs. P/P_{eq} , which should be linear, if equation (6) is obeyed. It is seen that in the pressure range studied, equation (6) does not describe the pressure dependence satisfactorily.

(2) j vs. $(1/P - 1/P_{eq})$ curves

In Fig. 11, values of j have been plotted with respect to $(1/P - 1/P_{eq})$ on a log-log plot. If j were directly proportional to $(1/P - 1/P_{eq})$, as predicted by equation (4) (or equation (5) when the stable form of CaO is produced), the plot in Fig. 11 would be linear with a slope of unity. The plot is non-linear.

The curves approach linearity at high values of P (lower j values), but the slopes have an average exponent of 0.3, showing that $j \propto (1/P - 1/P_{eq})^n$, $n \cong 3.3$, instead of 1, as predicted by equations (4) and (5).

Only equation (3) remains to be tested. In that equation, B is temperature dependent parameter, while C is the reciprocal of the maximum value of j in vacuum, i.e., C corresponds to Langmuir flux,¹¹ denoted at j_m . Since B and j_m are not obtainable directly from the data, the following analysis was done to test the validity of equation (3).

Differentiating it with respect to $1/P$, at constant temperature, we get

$$\frac{\partial j}{\partial V P} \bigg|_T = \frac{B'}{(B + C/P)^2} \quad (7)$$

where $B' = B + C/P_{eq}$

Using the data of run numbers 7 to 11 (at 900°K), values of $(\partial j / \partial 1/P)_T$ were obtained by the finite difference approximation using small intervals, i.e.,

$$(\partial j / \partial 1/P)_{T,i} = \frac{J_{i+1} - J_i}{1/P_{i+1} - 1/P_i} \quad (8)$$

where J_i and J_{i+1} are the values of j at pressures P_i , P_{i+1} respectively, which were taken to be two neighboring experimental points on the j vs. P/P_{eq} curves (Fig. 3).

Figure 12 is a schematic plot of $(\partial j / \partial V P)_T$ vs. $1/P$, as predicted by equation (7), on which experimental values have been superimposed according to equation (8). It is seen that fit to the equation of Hyatt, et al. is also unsatisfactory.

(3) j vs. 1/P curves

It has been reported by Cremer and Nitsch that the decomposition flux j varies linearly with $1/P_{CO_2}$. Even though previous discussion showed that

j is not proportional to $(1/P - 1/P_{eq})$, it could still be proportional to $1/P$ according to data of Cremer and Nitsch. To test this, values of j for steady state fluxes for granular and single crystal samples have been plotted in Figs. 13 and 14. It is seen that for $P/P_{eq} > 0.03$ ($P_{eq}/P < 30$), the plots approximate a linear behavior in limited regions though the slopes are different for different samples. This linearity is misleading, however, as shown in Figs. 15 and 16, which are similar plots but with greatly expanded scale to test the linearity of j with $1/P$ at pressures close to equilibrium. It is seen that these plots are non-linear on this expanded scale. Earlier observation of Cremer and Nitsch of linear dependence of j with $1/P$ is thus a consequence of their use of data in a relatively narrow range of pressures.

(v) Activation energy of decomposition

It seems reasonable to suppose that reaction rates are functions of the activity of CO_2 , which is equal to P/P_{eq} , denoted as θ henceforth. The temperature dependence of the rates of decomposition at constant activity of CO_2 can be obtained from the data as follows:

Values of $\ln j$ calculated for various fixed values of θ at different temperatures were plotted against $1/T$. For powders data for θ values ranging from 0.05 to 0.9 were used (Fig. 17) and for the granular samples, θ values ranging from 0.025 to 0.7 were used (Fig. 18). A least squares fit was obtained for the Arrhenius plots of these two figures for various values of θ .

The apparent activation enthalpies, ΔH^* , determined in this way are plotted as a function of θ in Fig. 19. It is seen that for the granular samples, the apparent activation enthalpy ΔH^* is approximately constant at $49.2 \pm 1.2 \text{ k Cal/s mole}^{-1}$, for values of $\theta \leq 0.1$. This value agrees

very well with the activation enthalpy for single crystal decomposition in vacuum,¹¹ 49 K Cals mole⁻¹. For $\theta > 0.1$, ΔH^* rises to a new value averaging 61.8 ± 1.8 K Cals mole⁻¹. Cremer and Nitsch¹⁰ using data collected at least 150°C higher than in this study obtained $\Delta H^* = 60$ K Cals mole⁻¹ for θ ranging from 0.3 to 0.6.

It therefore seems very likely that decomposition of CaCO_3 follows two different mechanisms with different activation enthalpies, the transition occurring in the neighborhood of θ values of 0.1. This conclusion is consistent with the earlier observations that the decomposition flux is practically pressure independent up to about $\theta = 0.1$ to 0.2, but decreases with pressures in the range $\theta = 0.1$ to 0.8.

The values of ΔH^* calculated as a function of θ for powders do not show such a simple behavior (Fig. 19). For powders, calculated values of ΔH^* are relatively constant in the low θ regime, but increase linearly as θ increases beyond $\theta = 0.2$. As noted earlier, decomposition rates in powder beds seem to depend upon the bed depth. Powder decomposition kinetics, therefore, cannot be interpreted until the effects of particle size and bed depth are quantitatively measured.

IV. CONCLUSIONS

The rates of decomposition of single crystals and powders measured under CO_2 pressures from $0.05 P_{\text{eq}}$ to $0.8 P_{\text{eq}}$ differ by 2 to 3 orders of magnitude. Isothermal decomposition rates of CaCO_3 do not show a simple pressure dependence.

Single crystal decomposition kinetics seem to follow at least two distinct mechanisms. The reaction rates at low values of P/P_{eq} (≤ 0.1) have an apparent activation enthalpy of $49.2 \pm 1.2 \text{ K Cals mole}^{-1}$, while at higher values of P/P_{eq} , the apparent activation enthalpy is about $61.8 \pm 1.8 \text{ K Cals mole}^{-1}$.

Decomposition rates of CaCO_3 powders depend upon powder bed depth and on the pressure of CO_2 . The apparent activation enthalpy for powders does not remain constant over a range of values of P/P_{eq} .

REFERENCES

1. Oliver Bowles, "The Lime Industry," U.S. Bur. Mines Info. Circ. No. 7651, 43 pp, (1952).
2. H. C. Fischer, Jour. Am. Cer. Soc., 38, No. 7, 245 (1955).
3. D. R. Glasson, J. Appl. Chem., 11 June, 1961.
4. S. J. Gregg, Jour. Chem. Soc., 3940, (1953).
5. D. Beruto and A. W. Searcy, Nature, 263, 221 (1976).
6. K. H. Obst, et al., Zement-Kalk-Gips, No. 8, (1978).
7. D. Beruto and A. W. Searcy, Jour. Phys. Chem., 82, 163 (1978).
8. J. Zawadzki and S. Bretsnajder, Trans. Faraday Soc., 34, 951 (1938).
9. E. P. Hyatt, et al., J. Am. Cer. Soc., 41, 70 (1958).
10. E. Cremer and W. Nitsch, Z. Elektrochem. Ber. Bun. Phys. Chem., 66, 697 (1962).
11. D. Beruto and A. W. Searcy, J. Chem. Soc., Faraday Trans., I, 70, 2145 (1974).
12. G. M. Rosenblatt, in Treatise on Solid State Chem., V. 6A, B. Hannay (ed.), Chapter 3, (1976).

FIGURE CAPTIONS

- Fig. 1. Schematic model of decomposition of AB leading to porous product A, evolution of gas B; and various fluxes of A and B involved in decomposition.
- Fig. 2. Plot of log decomposition flux vs. P_{CO_2}/P_{eq} for calcite powder at 900°K.
- Fig. 3. Plot of log decomposition flux vs. P_{CO_2}/P_{eq} at 900°K for single crystal calcite.
- Fig. 4. Plot of log decomposition fluxes vs. P_{CO_2}/P_{eq} at 873°K, 900°K and 930°K for calcite powder.
- Fig. 5. Plot of log decomposition flux vs. P_{CO_2}/P_{eq} at 900°K for granular calcite.
- Fig. 6. Plot of log decomposition fluxes vs. P_{CO_2}/P_{eq} at 853°K, 873°K, 901°K and 933°K for granular calcite.
- Fig. 7. Plot of log decomposition flux vs. P_{CO_2}/P_{eq} at 900°K for two samples of different powder-bed depths.
- Fig. 8. Plot of log decomposition flux vs. P_{CO_2}/P_{eq} at 900°K for calcite of three different particle sizes.
- Fig. 9. Plot of log decomposition fluxes vs. P_{CO_2}/P_{eq} at 900°K as calculated using total sample surface area and cross-sectional area of sample holder for samples of different particle sizes.
- Fig. 10. Decomposition flux vs. P_{CO_2}/P_{eq} at 933°K for granular calcite.
- Fig. 11. Plot of $\log[1/P_{CO_2} - 1/P_{eq}]$ vs. log decomposition flux at different temperatures for granular calcite.
- Fig. 12. Plot of $(\partial j/\partial 1/P)_{900^\circ K}$ vs. P_{CO_2}/P_{eq} obtained experimentally and as predicted by equation 3 in text.

Figs. 13- Plots of decomposition flux vs. $P_{\text{eq}}/P_{\text{CO}_2}$ for granular, single

15. crystal and powder calcite at 900°K.

Fig. 16. Plot of decomposition flux vs. $P_{\text{eq}}/P_{\text{CO}_2}$ for granular calcite

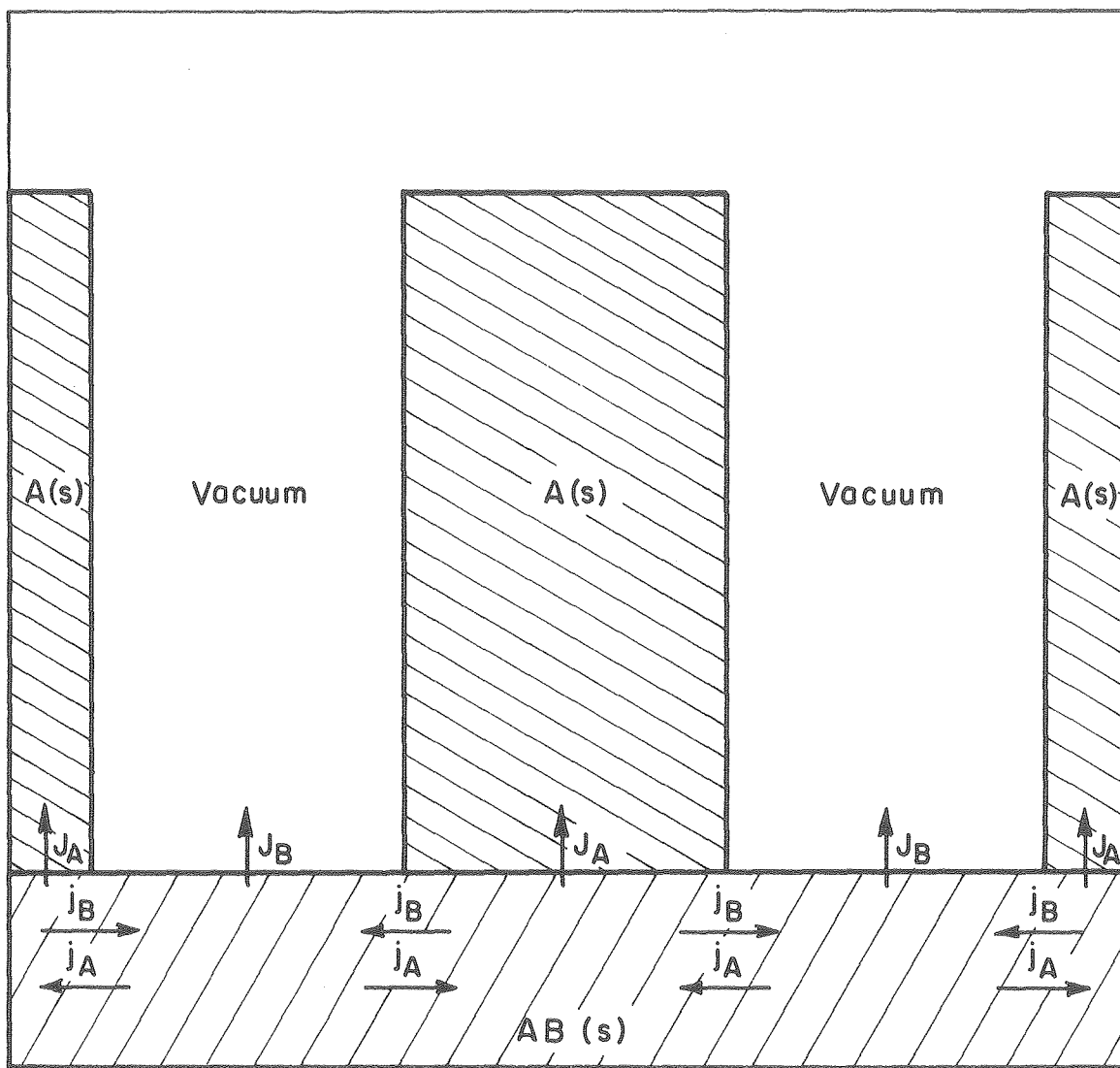
at 900°K, in the region very close to equilibrium.

Figs. 17- Arrhenius plots of $\ln j$ vs. $1/T$ for powder and granular samples

18. at different values of $\theta (= P_{\text{CO}_2}/P_{\text{eq}})$.

Fig. 19. Plot of enthalpy of activation for decomposition vs. CO_2

activity for both powder and single crystal samples.



XBL 748-6867

Fig. 1

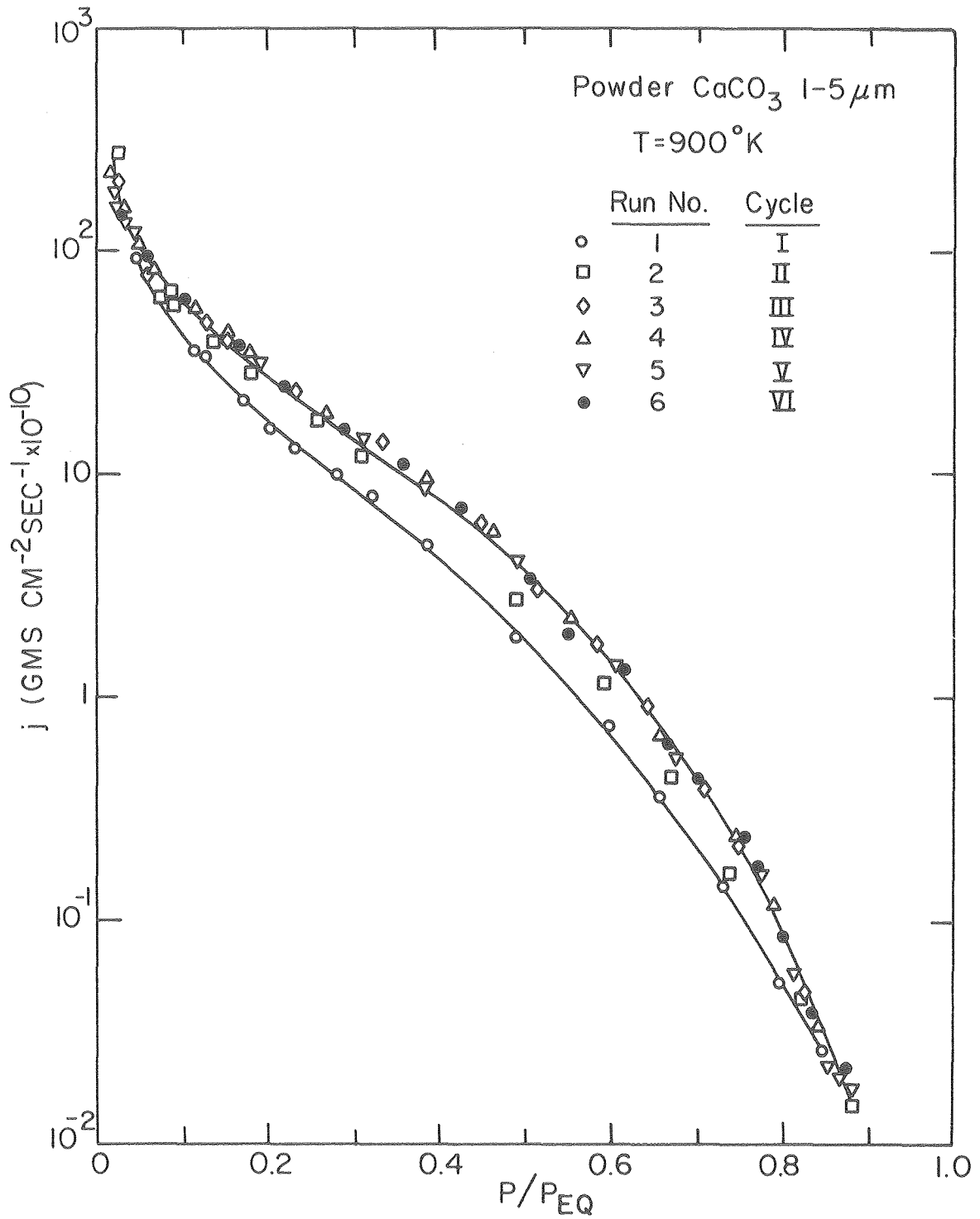
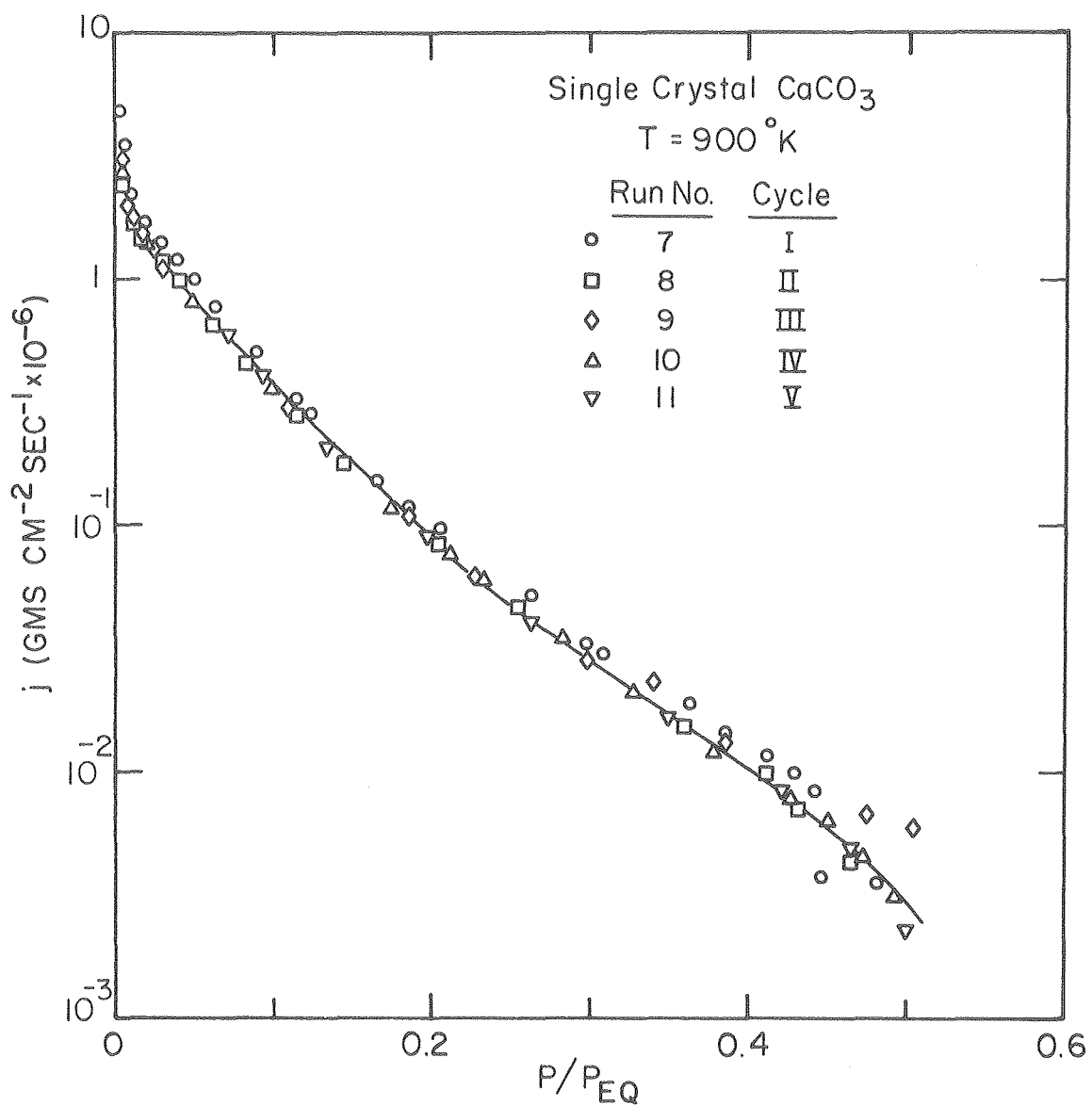
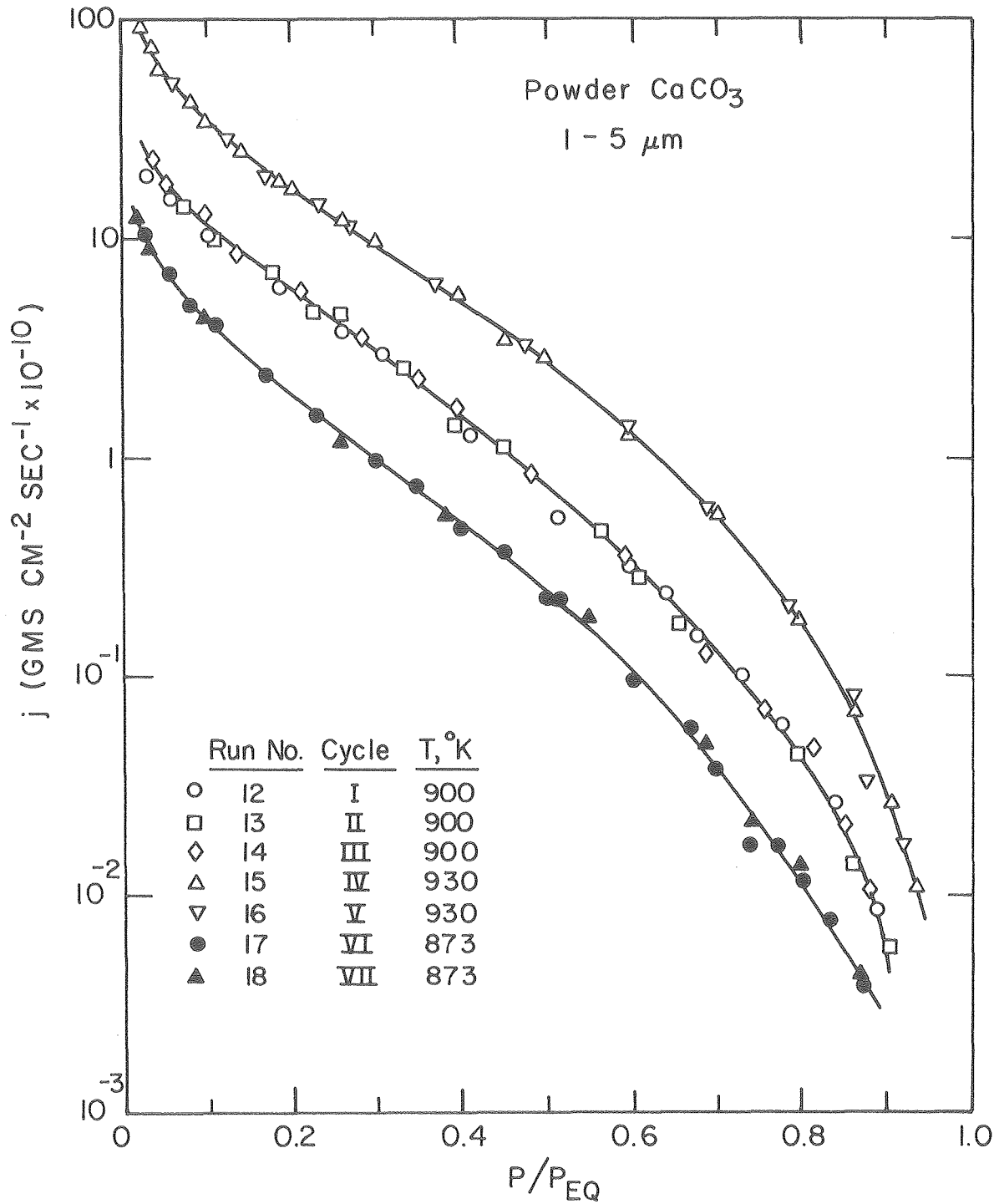


Fig. 2



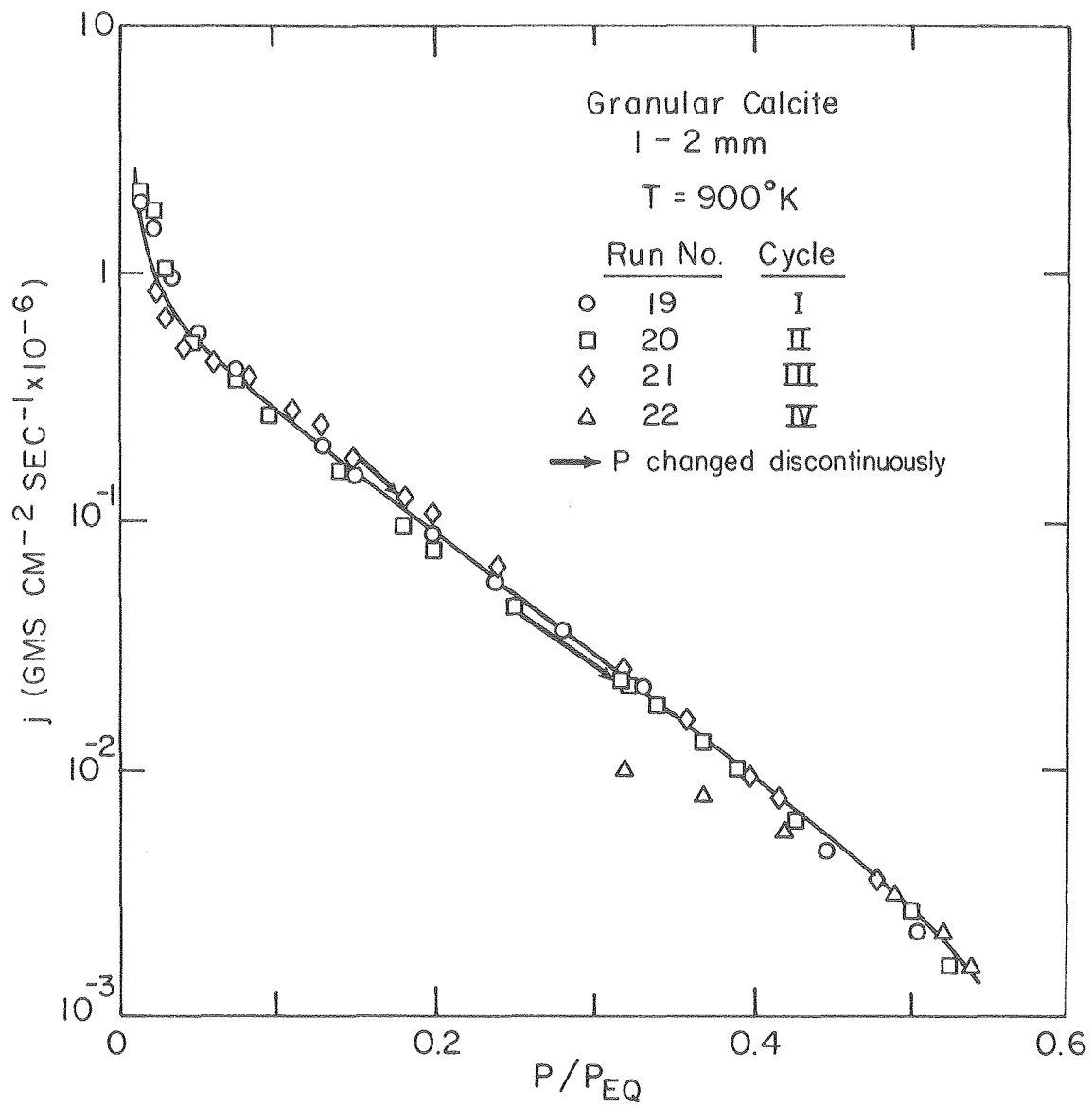
XBL 797-6677

Fig. 3



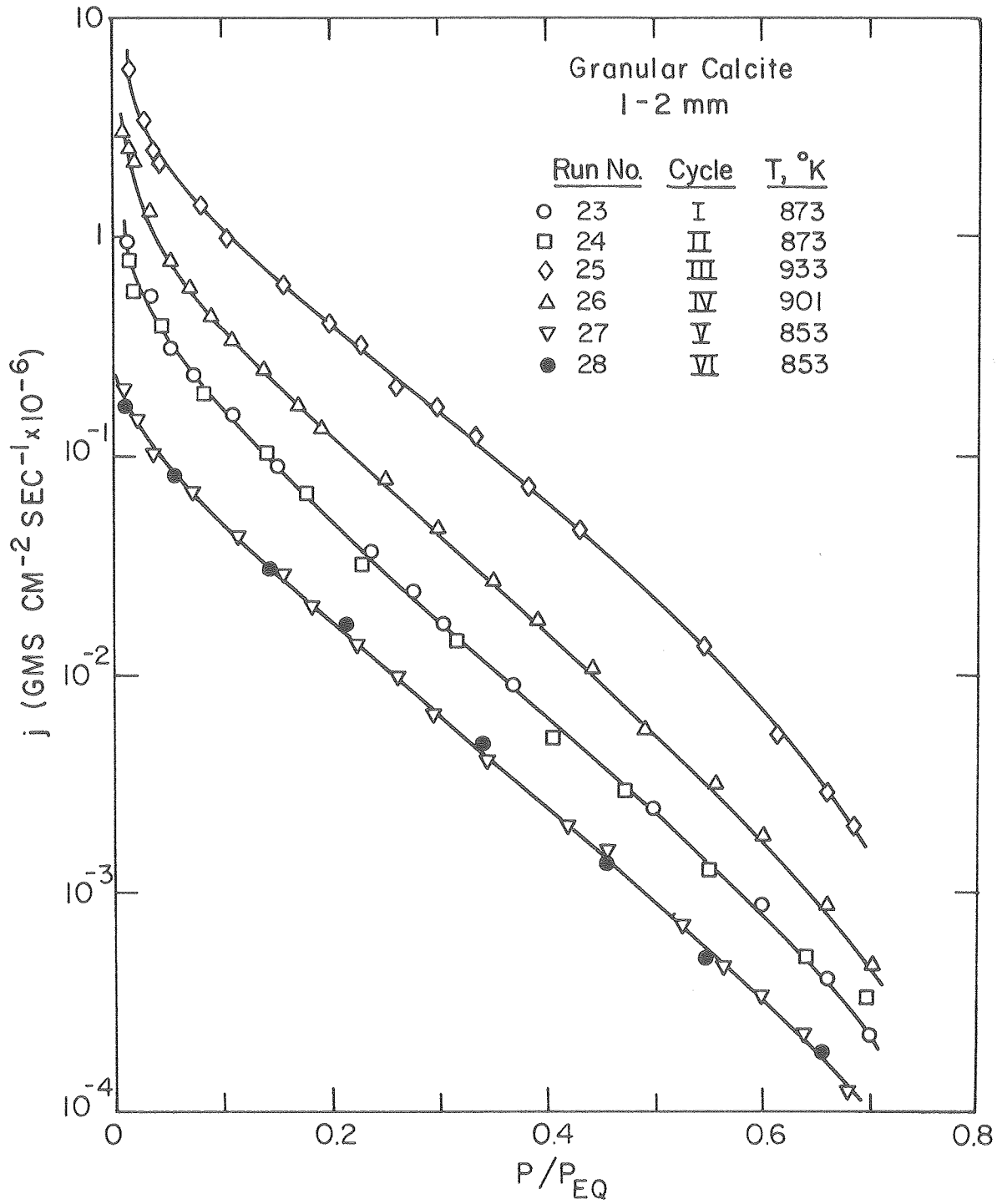
XBL 797-6678

Fig. 4



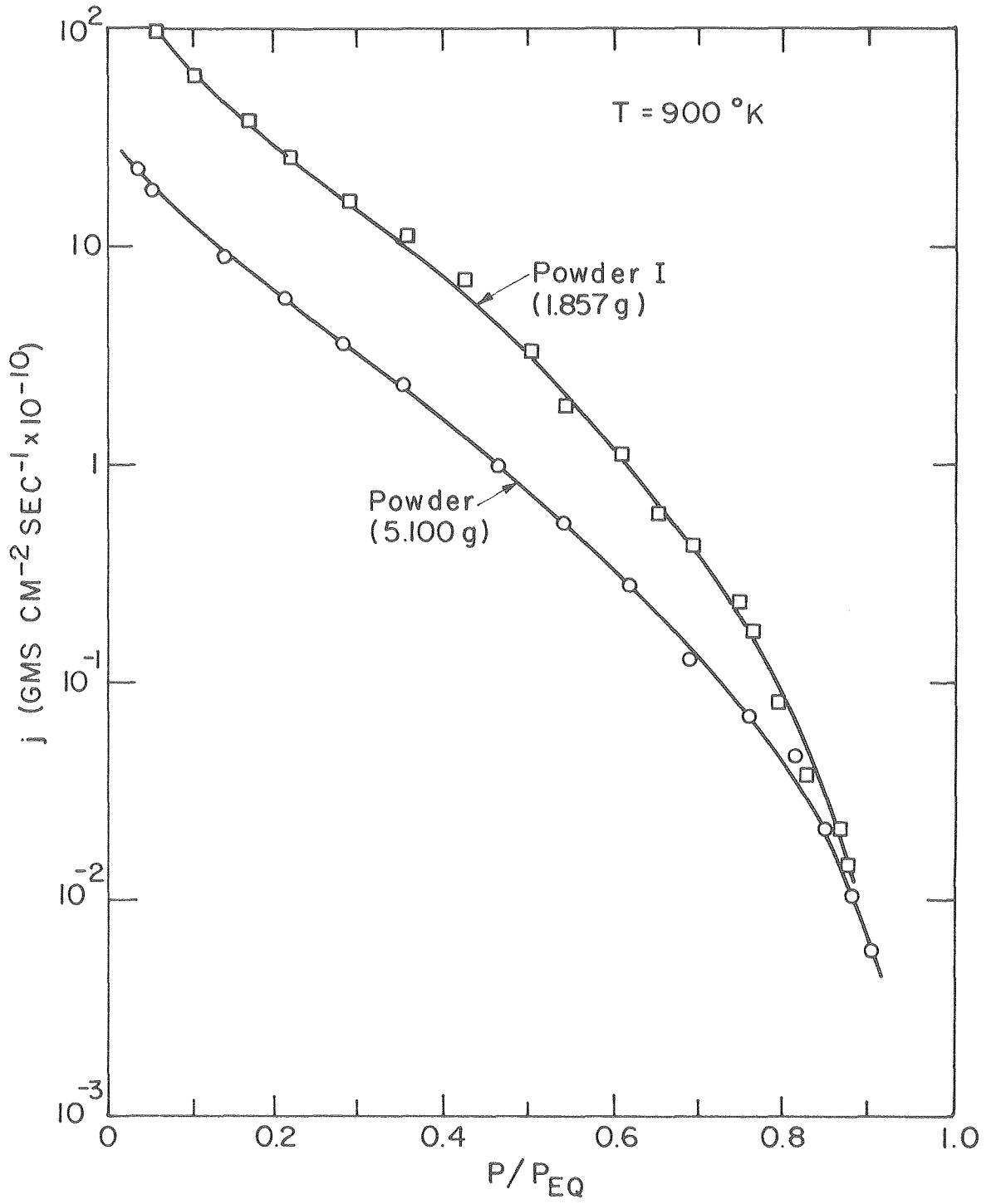
XBL797-6679

Fig. 5



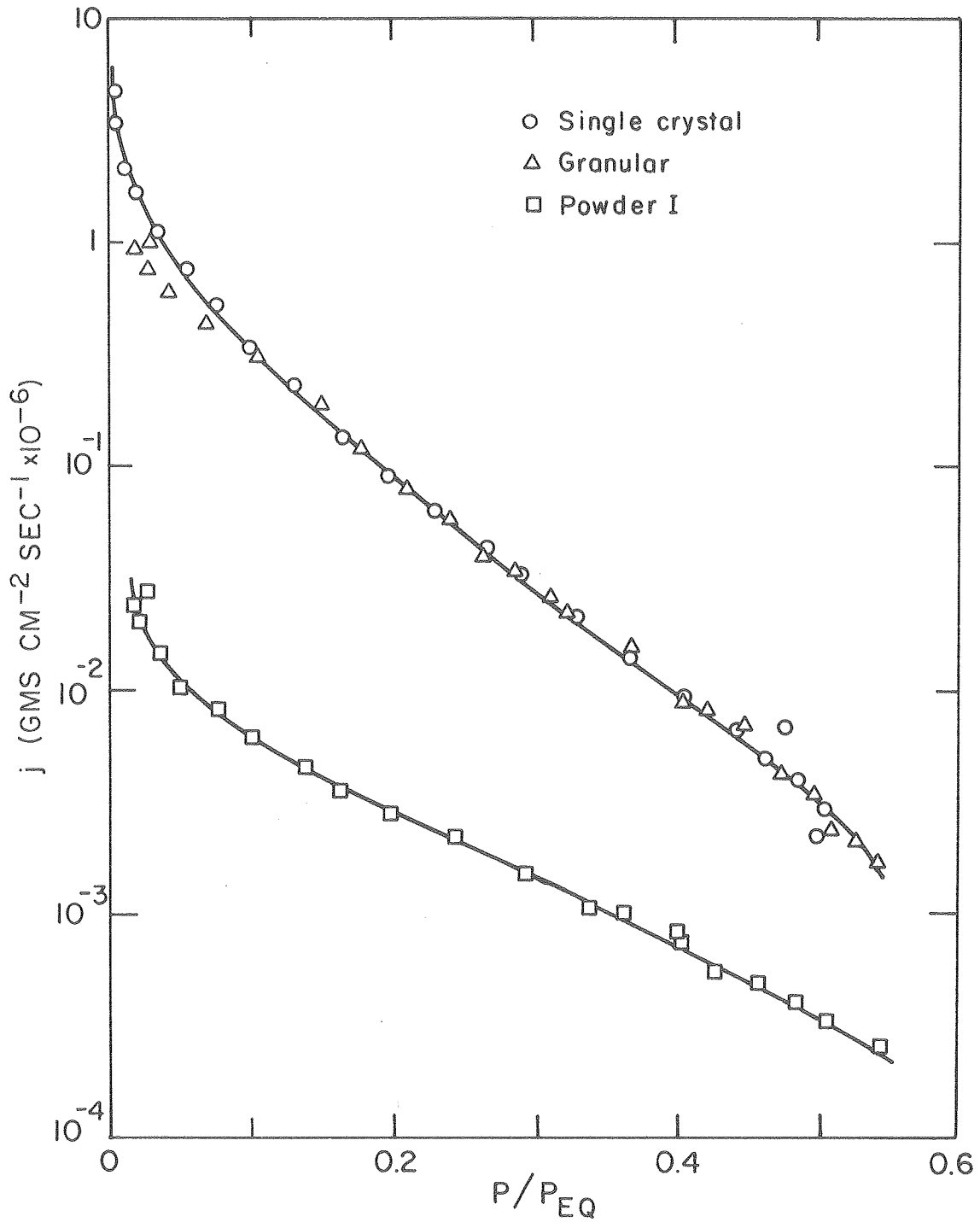
XBL 797-6680

Fig. 6



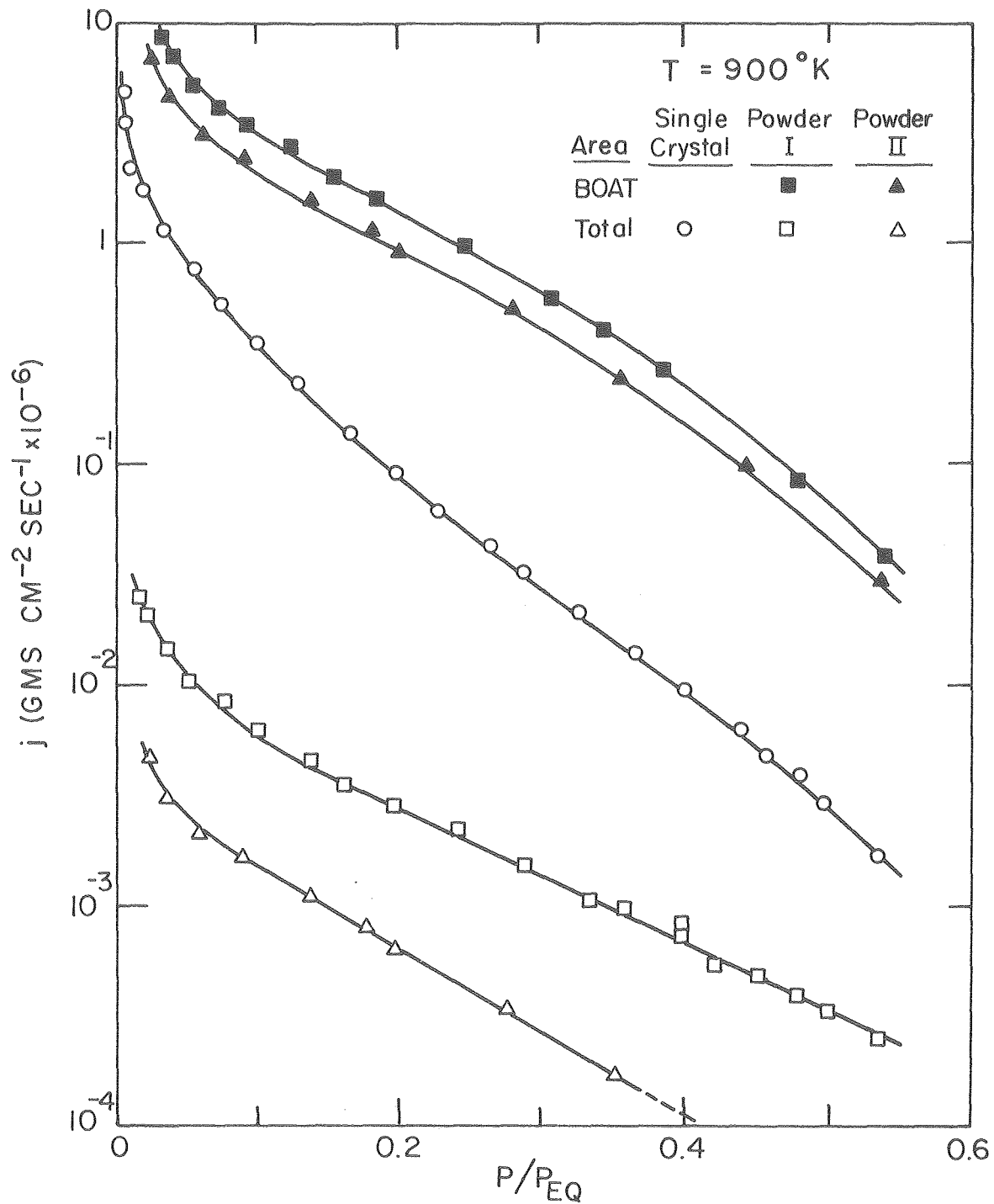
XBL797-6681

Fig. 7



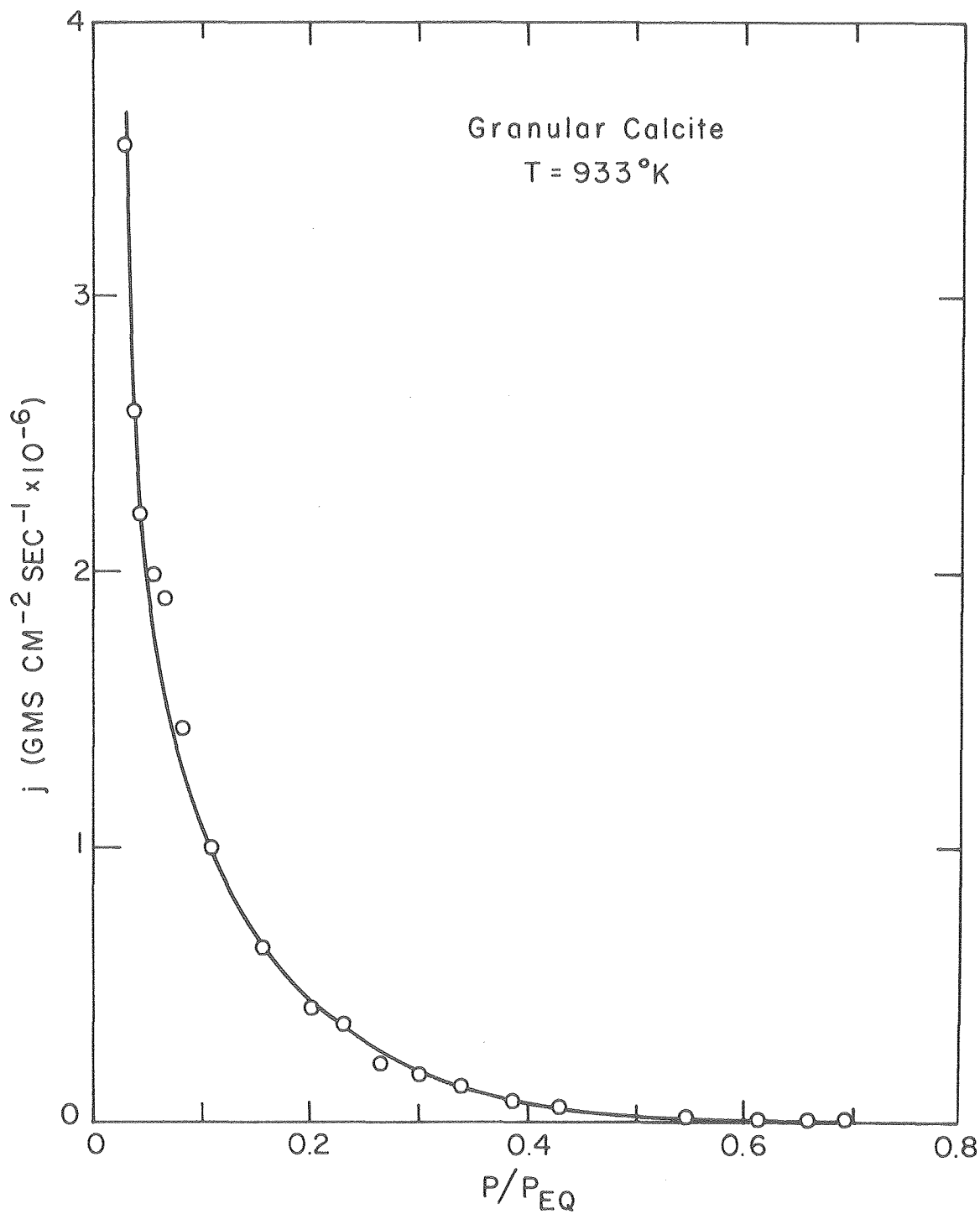
XBL 797-6682

Fig. 8



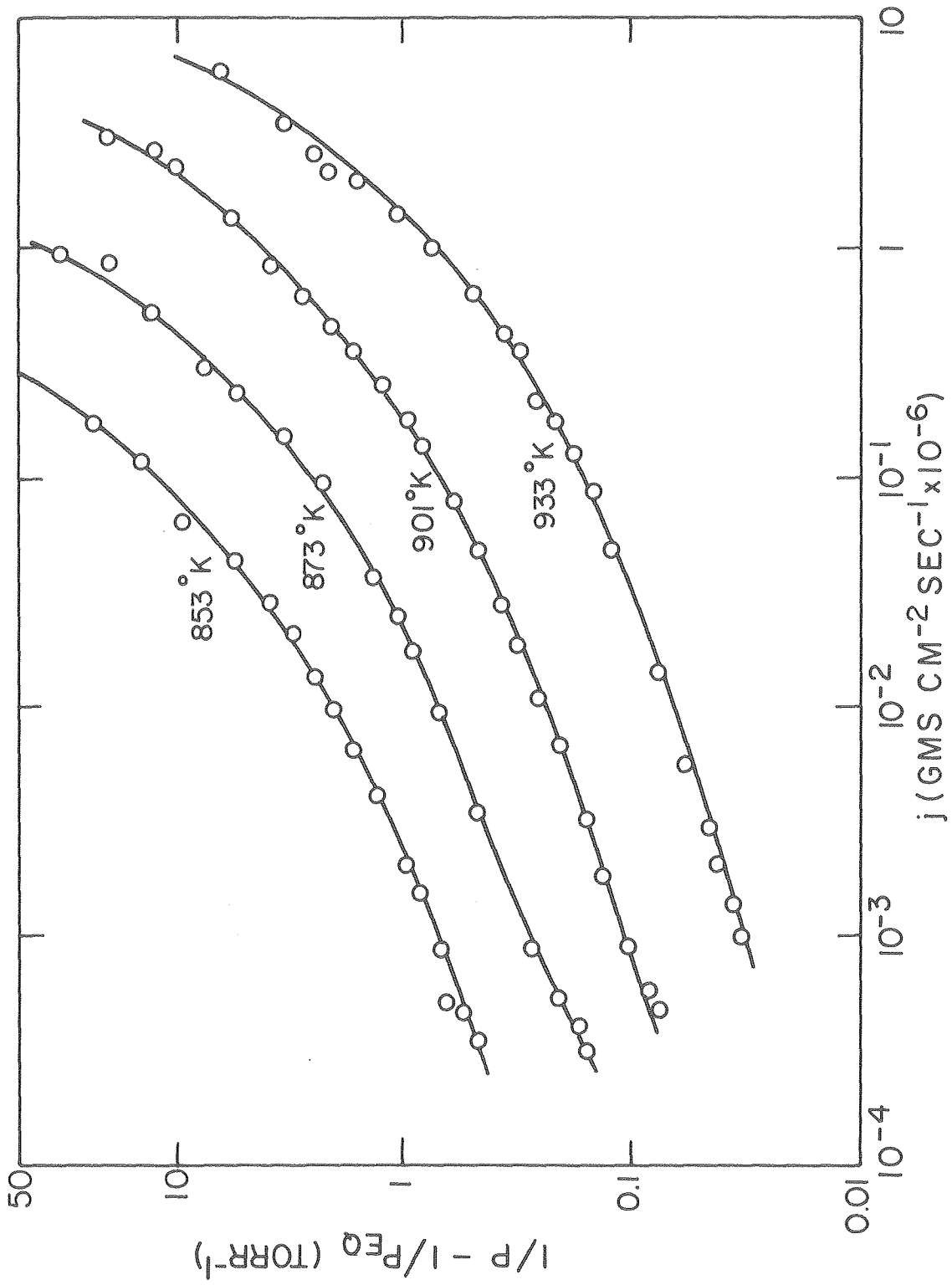
XBL 797-6693

Fig. 9



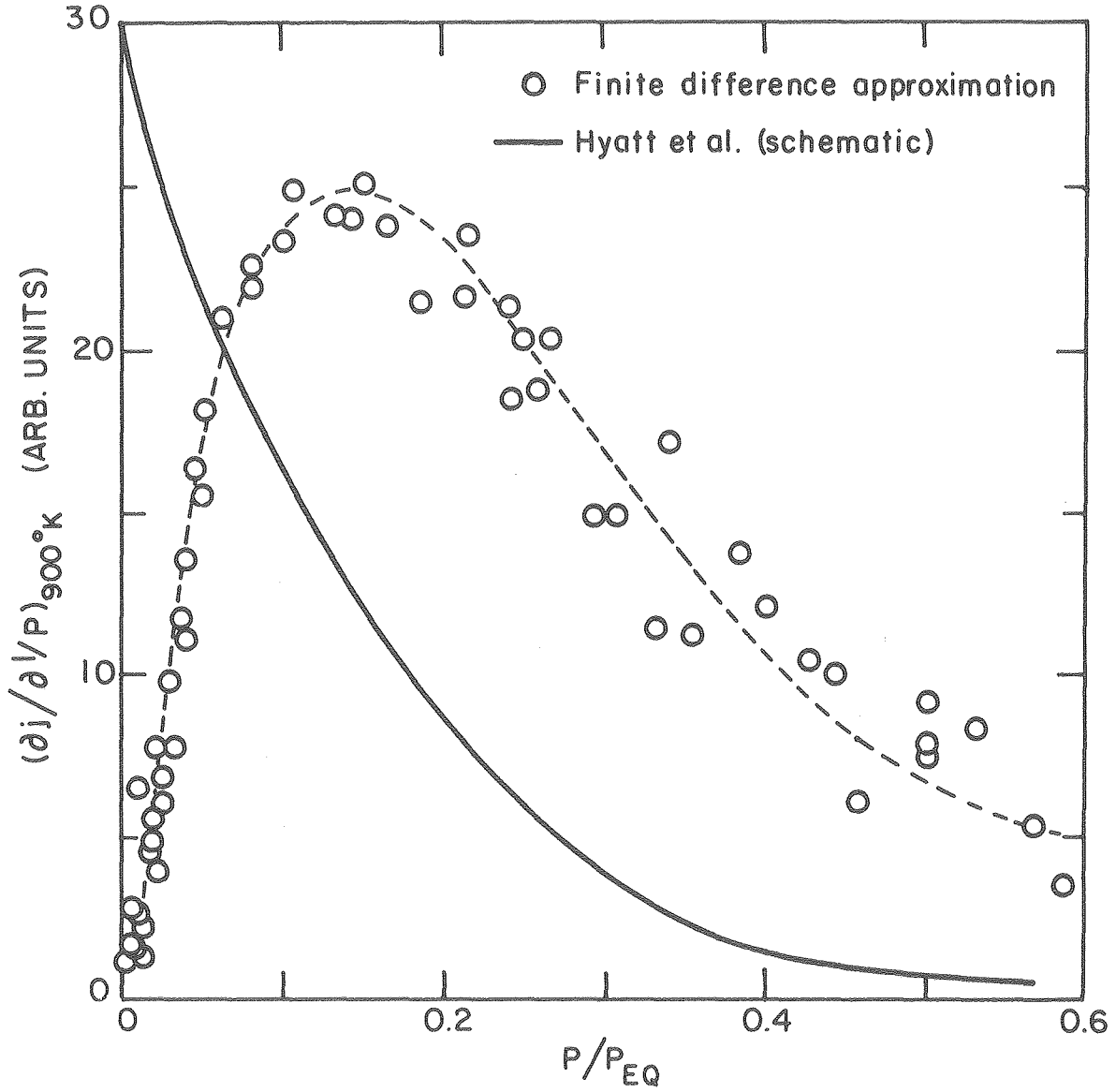
XBL 797-6683

Fig. 10



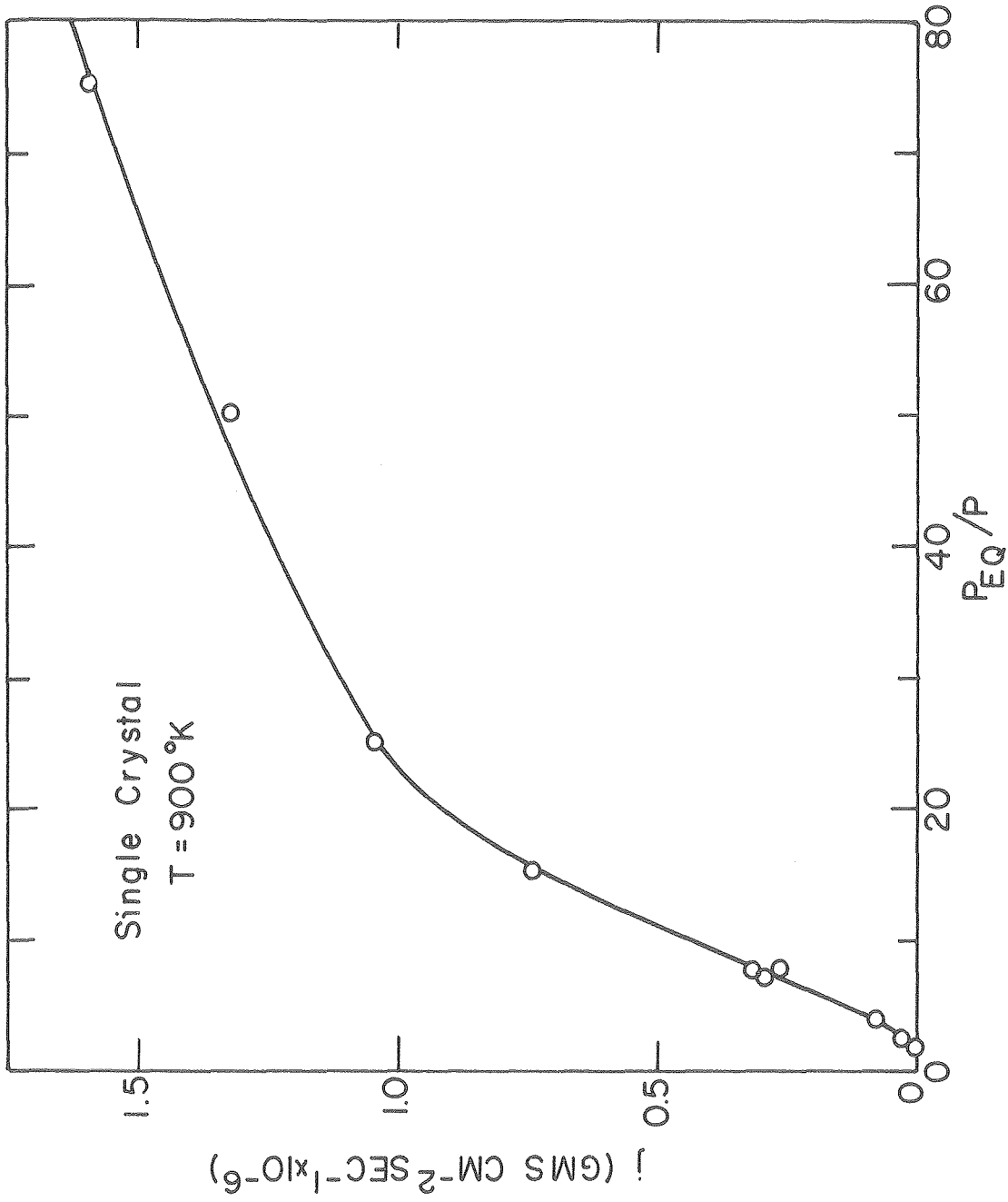
XBL797-6684

Fig. 11



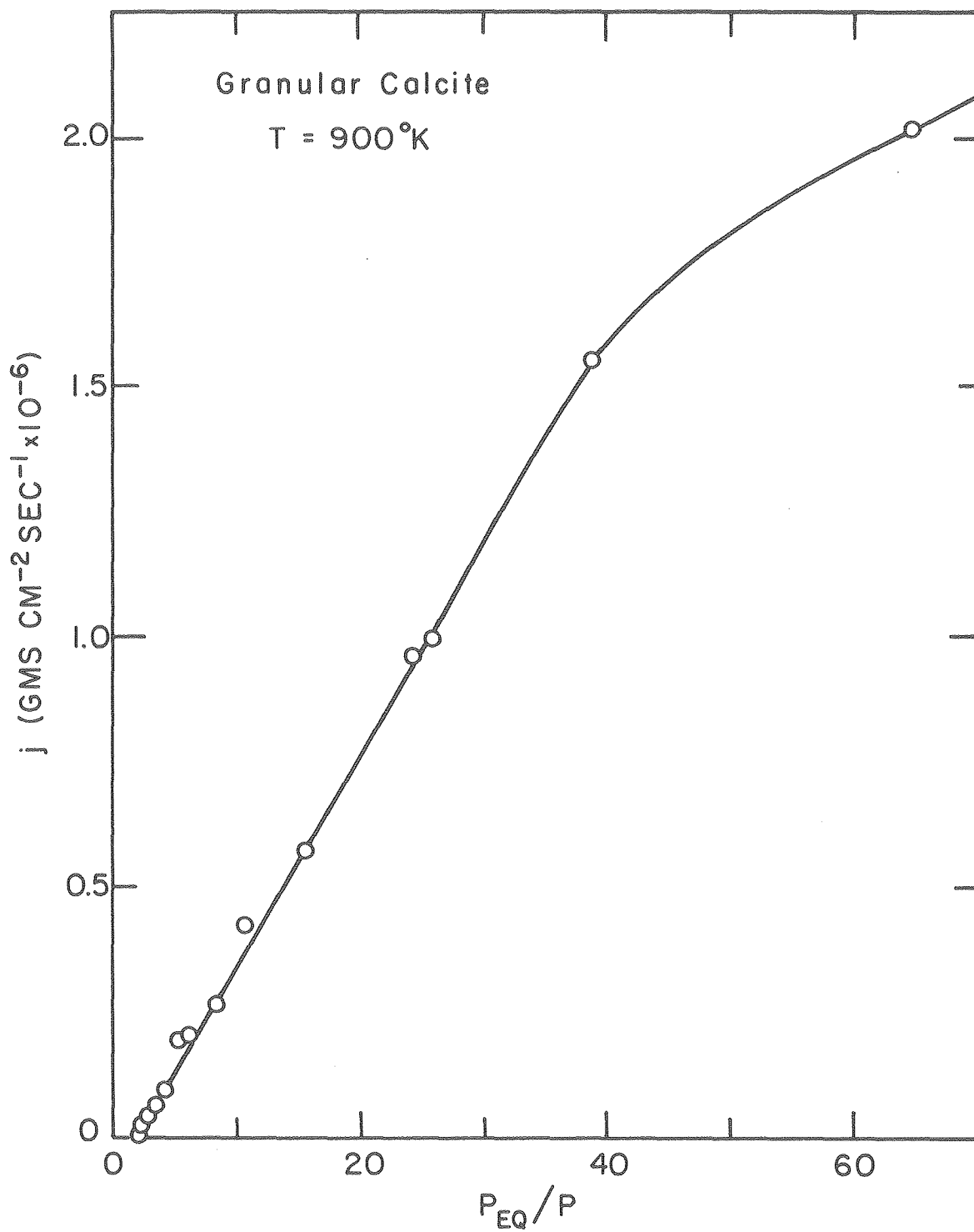
XBL797-6685

Fig. 12



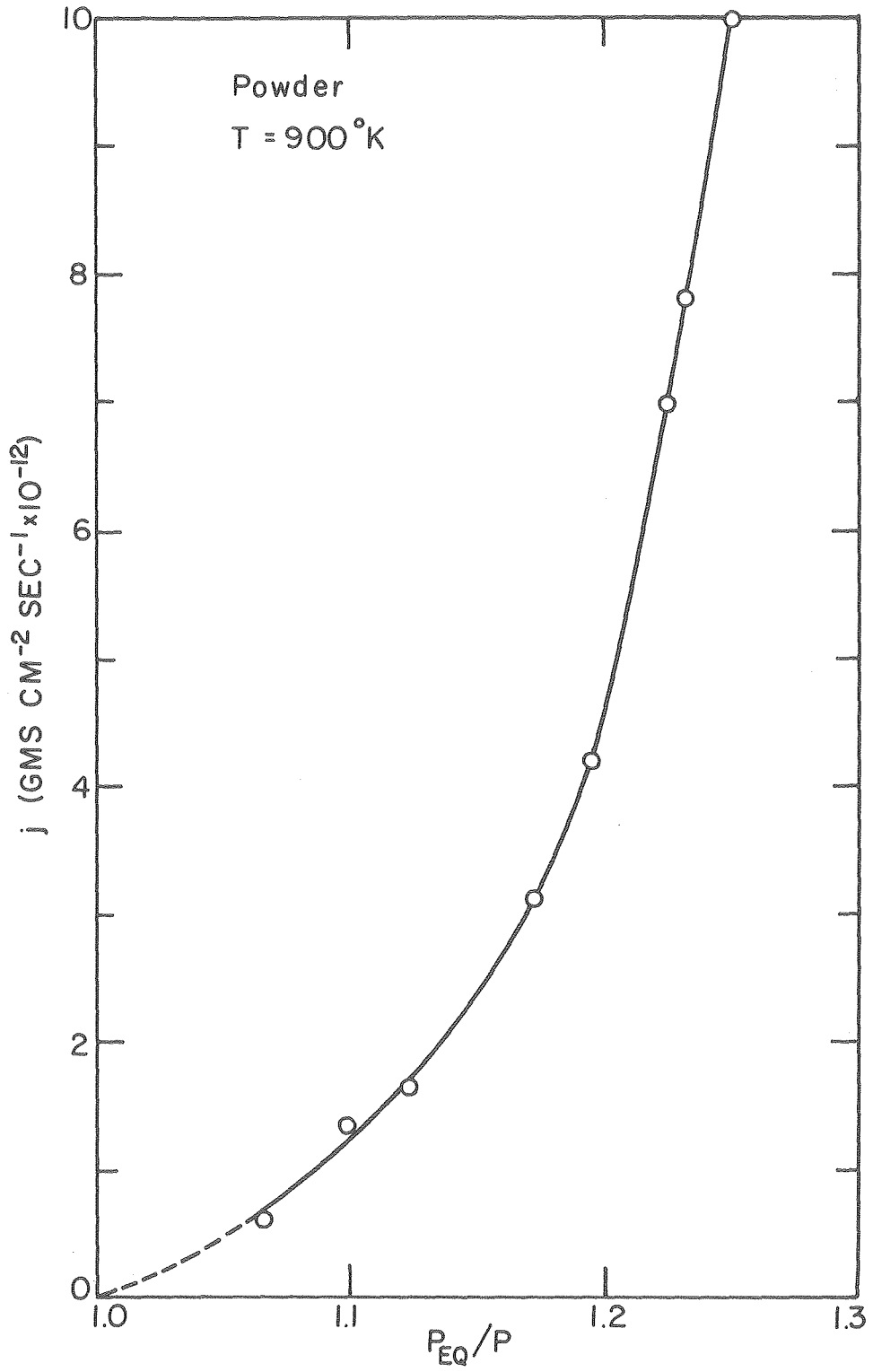
XBL 797-6692

Fig. 13



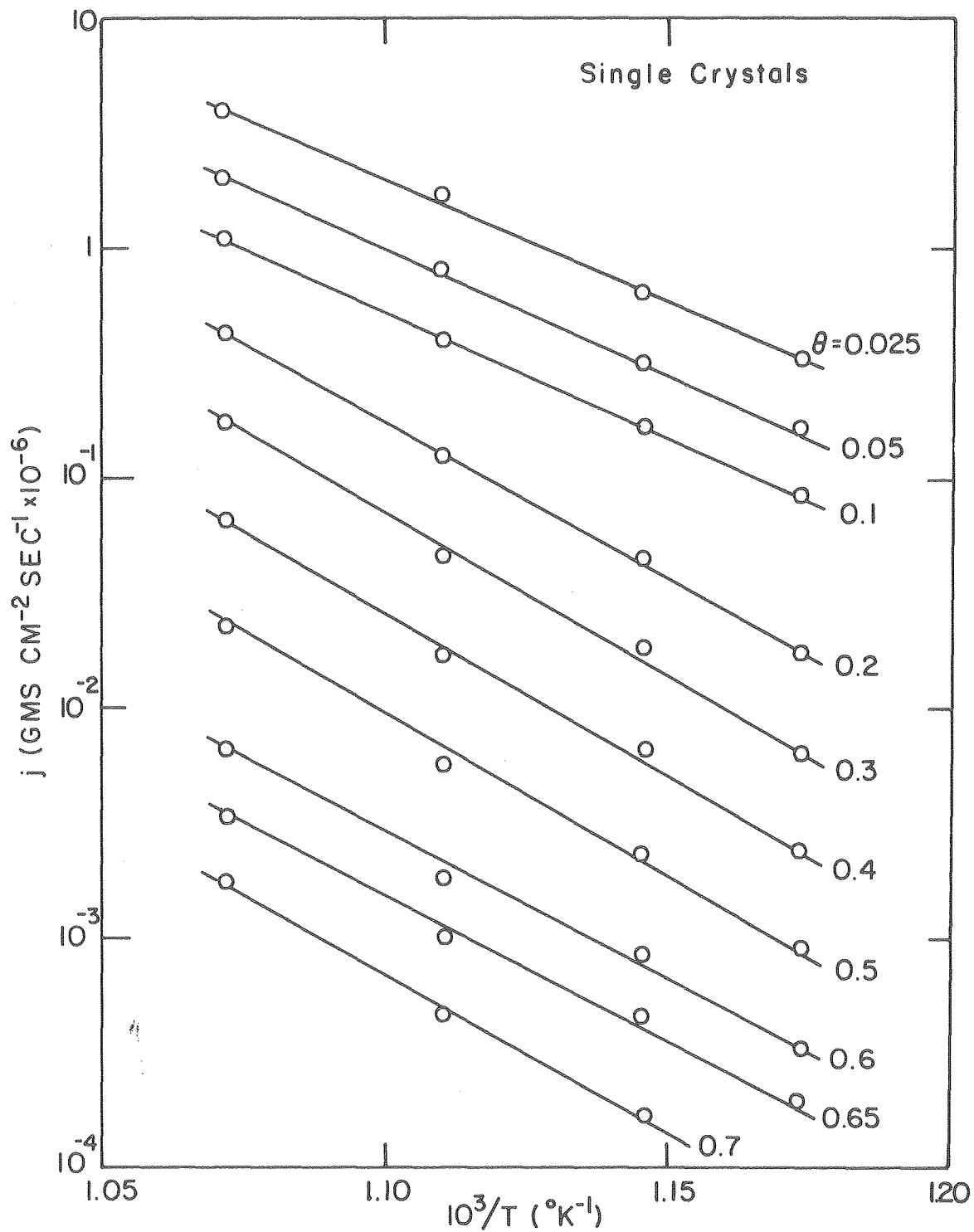
X BL 7 97-6690

Fig. 14



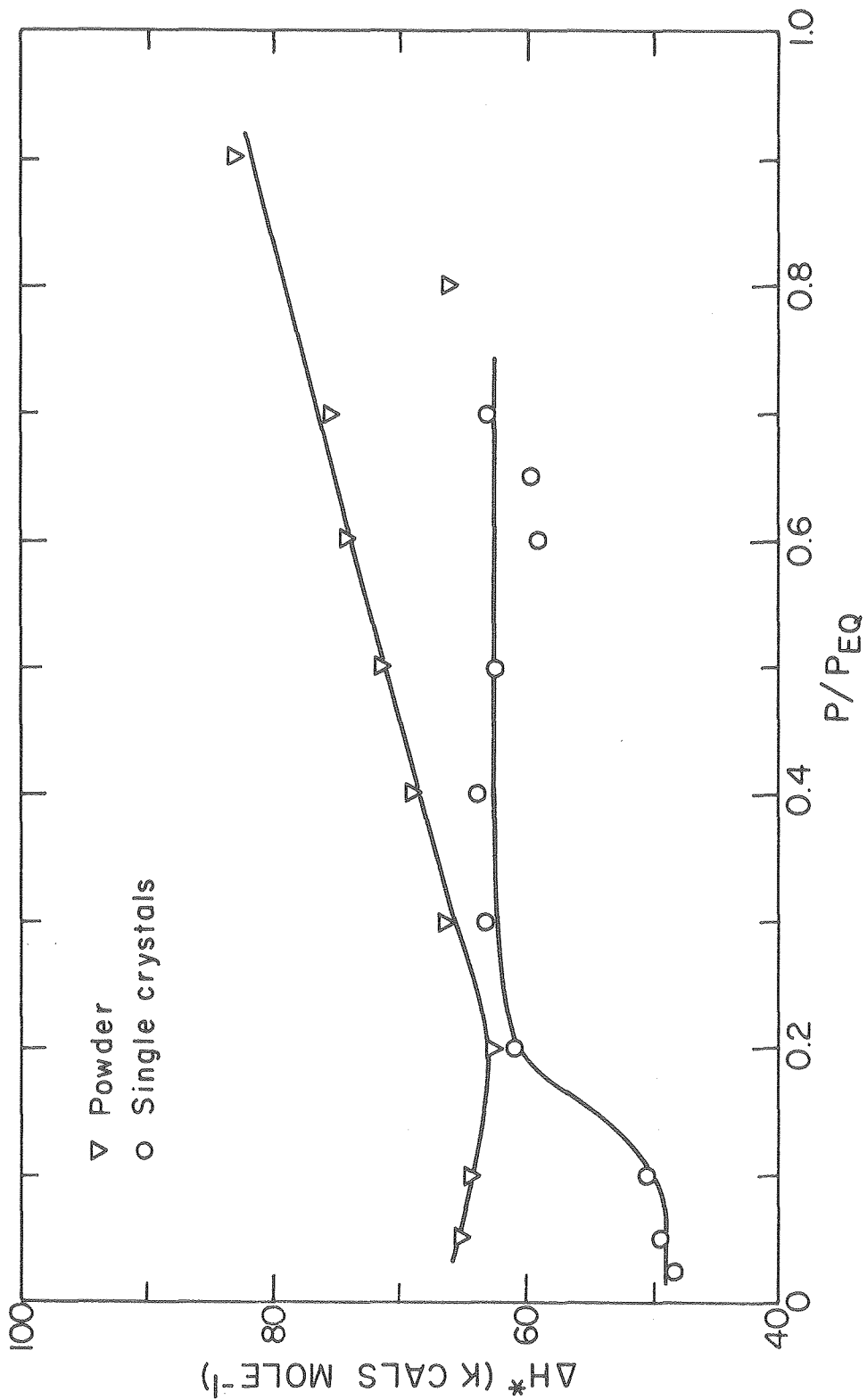
XBL 797-6691

Fig. 15



XBL 797-6687

Fig. 18



XBL797-6688

Fig. 19

ACKNOWLEDGMENT

I wish to express my deepest gratitude to Professor Alan W. Searcy, a true scholar and gentleman, for his continuous guidance throughout this work. Working with Dr. Searcy has been a very satisfying and great learning experience.

I also wish to express sincere appreciation to Dr. David Meschi and Dr. Jim Roberts, whose mentorial advice and lively discussions made the working environment truly rewarding.

Thanks are also due to Dr. Dario Beruto and Dr. Bob Powell for providing many helpful suggestions.

Special thanks are due to my research colleagues, Messrs. G. Knutsen, N. Jacobson, S. Roche, D. Davis, J. Ewing and E. Powell for providing a harmonious, friendly atmosphere which made my study in Berkeley a memorable experience.

I also salute the MMRD staff — E. Kozak, G. Baum and R. Lindberg for providing valuable technical support and help. It is with deep appreciation that I thank Gay Brazil for typing the manuscript, working through the intricate quagmire of subscripts and superscripts.

Dr. R. Wenk kindly supplied some of the minerals used in this work.

This work was supported by the Division of Materials Sciences, Office of Basic Energy Sciences, U.S. Department of Energy under contract No. W-7405-Eng-48.

This report was done with support from the Department of Energy. Any conclusions or opinions expressed in this report represent solely those of the author(s) and not necessarily those of The Regents of the University of California, the Lawrence Berkeley Laboratory or the Department of Energy.

Reference to a company or product name does not imply approval or recommendation of the product by the University of California or the U.S. Department of Energy to the exclusion of others that may be suitable.

TECHNICAL INFORMATION DEPARTMENT
LAWRENCE BERKELEY LABORATORY
UNIVERSITY OF CALIFORNIA
BERKELEY, CALIFORNIA 94720